Structure and interactions of biological helices

Alexei A. Kornyshev*

Department of Chemistry, Faculty of Natural Sciences, Imperial College London, SW7 2AZ London, United Kingdom

Dominic J. Lee†

Department of Chemistry, Faculty of Natural Sciences, Imperial College London, SW7 2AZ London, United Kingdom

Sergey Leikin‡

Section of Physical Biochemistry, National Institute of Child Health and Human Development, National Institutes of Health, DHHS, Bethesda, Maryland 20892, USA

Aaron Wynveen§

Department of Chemistry, Faculty of Natural Sciences, Imperial College London, SW7 2AZ London, United Kingdom

(Published 6 August 2007)

Helices are essential building blocks of living organisms, be they molecular fragments of proteins (α-helices), macromolecules (DNA and collagen), or multimolecular assemblies (microtubules and viruses). Their interactions are involved in packing of meters of genetic material within cells and phage heads, recognition of homologous genes in recombination and DNA repair, stability of tissues, and many other processes. Helical molecules form a variety of mesophases *in vivo* and *in vitro*. Recent structural studies, direct measurements of intermolecular forces, single-molecule manipulations, and other experiments have accumulated a wealth of information and revealed many puzzling physical phenomena. It is becoming increasingly clear that in many cases the physics of biological helices cannot be described by theories that treat them as simple, unstructured polyelectrolytes. The present article focuses on the most important and interesting aspects of the physics of *structured* macromolecules, highlighting various manifestations of the helical motif in their structure, elasticity, interactions with counterions, aggregation, and poly- and mesomorphic transitions.

DOI: 10.1103/RevModPhys.79.943 PACS number(s): 87.15.−v

CONTENTS

*Electronic address: a.kornyshev@imperial.ac.uk
†Electronic address: dj.lee@imperial.ac.uk
‡Electronic address: leikins@mail.nih.gov
§Electronic address: a.wynveen@imperial.ac.uk

I. INTRODUCTION

Genetic recombination, packaging of DNA in cells and viruses, folding of proteins, and assembly of the organic matrix of bone are just a few of the many fundamental biological reactions that involve interactions between helical macromolecules. Some of these reactions, such as self-assembly of collagen fibers, can be reproduced in a test tube without the complex biological machinery. Other reactions, like condensation and decondensation of chromosome material, are controlled by multiple factors in cells. But even the latter reactions ultimately depend on the underlying physics of helix-helix interactions.

The physics of interactions between biological helices is surprisingly rich and often counterintuitive. Collagen self-assembles into highly ordered fibers at elevated temperature instead of denaturing. DNA forms a variety of liquid crystalline phases. In the presence of Mn^{2+} (but not Ca^{2+} or Mg^{2+}), DNA liquid crystals self-assemble from solution upon heating, just like collagen fibers. A variety of polyamines and basic polypeptides also induce "condensation" of DNA from solution into liquid crystals, but the temperature does not play an important role in this case.

In low-density, highly hydrated liquid crystals, DNA packing is generally cholesteric. The average orientation of the molecules is perpendicular to the cholesteric axis and rotates around this axis with a period equal to the cholesteric pitch (usually several microns). The cholesteric packing is caused by chiral interactions between the helices. One would expect such interactions to strengthen with increasing density of the molecules, resulting in a monotonically decreasing cholesteric pitch. Instead, the cholesteric pitch goes through a minimum and begins to increase again. A further increase in the density causes a transition from the cholesteric to the columnar (hexagonal) or line-hexatic phase even though the molecules are still separated by more than a nanometer of water. When almost all water is squeezed out, a conformational transition from the *B* into the *A* structure of DNA takes place. Electrostatic interactions between DNA at such densities become very strong, but the charge density of DNA upon the transition into the *A* conformation does not decrease. Instead, it increases by almost 30%.

Studies of liquid crystalline phases of DNA, collagen, α-helices, helical viruses, and so on, as well as measurements of the chemical potential vs separation between molecules within them, revealed many more surprising phenomena and produced a wealth of experimental data. But our understanding of the underlying physics is clearly lagging behind these experiments. For instance, the possible physical mechanisms of DNA condensation into liquid crystals by counterions and the nature of the short-range exponential forces between DNA molecules observed in these liquid crystals are still debated in the literature. At least in these debates, the problem is one of choice between different models. The lack of understanding is more severe, for example, for the cholesteric to hexagonal phase transition, for which a few speculative ideas but no molecular models have been proposed.

Recent advances in theory and simulations suggest that the key to the physics of these phenomena might be in understanding the relationships between intermolecular interactions and the structure of the molecules (and/or counterions adsorbed onto them). In retrospect, this might seem obvious; for instance, the chirality of DNA liquid crystals is a direct consequence of the chiral structure of the double helix. Nevertheless, even now some of the most popular models represent DNA by a homogeneously charged cylinder.

This review is an attempt to analyze these recent advances within a general theoretical framework that incorporates models proposed by different authors as special cases (including the cylinder-based models). Our goal is to elucidate the most productive ideas through a systematic comparison of the corresponding predictions with all relevant empirical knowledge (rather than hand picking a few measurements that fit the best). We focus on electrostatic interactions since much more work has been done in this area, and at least some consensus appears to be emerging. We only briefly discuss other interactions (hard core, van der Waals and hydration), but we point out their potential contributions whenever necessary. DNA is the central object of the review, because its analysis is more amenable to rigorous theory and because most of the empirical information was accumulated for it. Nevertheless, we do discuss models and experimental observations for other biological helices (α-helices, collagen, and guanosine) as well.

The general theoretical framework employed here is based on the formalism of helical structure factors developed by Crick over 50 years ago (Cochran, Crick, and Vand, 1952; Crick, 1953a, 1953b; Klug *et al.*, 1958). The Crick theory converted the art and magic of model building into an exact science for rigorous analysis of x-ray diffraction from noncrystalline aggregates of heli-

ces. It allowed Watson and Crick (1953) to decipher the structure of DNA from the x-ray data reported by Franklin and Gosling (1953) and Wilkins *et al.* (1953). This theory laid the foundation for the revolution in modern biology and medicine, but it did not find its way into the physics of helices until the last decade.

The review is structured as follows. In Sec. II, we introduce the Crick structure factors and generalize them for nonideal helices. We briefly discuss the discovery of the DNA structure and point out some features of the Franklin and Gosling diffraction pattern that were not noticed at the time, although they contain important information about intermolecular interactions. In Sec. IV, we focus on the electrostatics of an isolated helix, relate modern theories of counterion condensation to counterion structure factors, and discuss available experimental data. We address different models of pair interaction potentials and phenomena related to the interaction between just two helices in Sec. V. In Sec. VI, we analyze models of multimolecular, liquid crystalline assemblies for which most of the experimental observations were reported. We reconsider the interpretation of the classical DNA diffraction patterns and provide a detailed comparison of the predictions of different models with measured intermolecular forces. We also briefly describe advances in the statistical mechanics of such assemblies, which might present some additional interest due to the unusual, frustrated form of the underlying interaction potentials. In Sec. VII, we concentrate on a critical comparison of different proposed mechanisms of counterion-induced DNA condensation. We briefly depart from the main theme in Sec. III to introduce the elasticity theory of helical macromolecules. This area of research has been rapidly pushed forward by recent advances in single-molecule manipulation techniques. For interested readers we provide several references to some of the latter studies, but we describe only those aspects of helix elasticity that are essential for understanding the physics discussed in subsequent sections.

In an effort to keep the analysis self-contained, whenever practical we provide the derivations in the main text of the review. However, to simplify the task for readers more interested in the physics than mathematical details of the theory, the derivations and formulas that are too cumbersome or elaborate are described in supplementary material (refer to the EPAPS Document at the end of the Reference section).

II. STRUCTURE

A. Biological helices

Many biological macromolecules and their structural domains consist of one or several interwoven helical chains of atoms (helical strands). Examples of some of the most common *molecular* helices are shown in Fig. 1.

The connected chain of polypeptide backbone atoms forms a single, right-handed helical line in a polypeptide α-helix [Fig. 1(a)]. Polyaminoacids and polypeptides may have a pure α-helical conformation. More commonly, however, shorter α-helices form the building blocks of proteins.

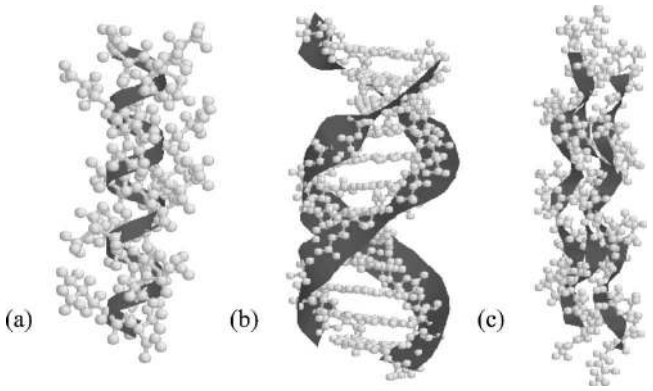

FIG. 1. Atomic structure of (a) a sample polypeptide α-helix, (b) a double-stranded helix of *B*-DNA, and (c) triple-helix collagen. The gray ribbons are guides to the eye showing the protein or DNA helical backbones. The two grooves separating the sugar-phosphate backbone strands (ribbons) in DNA are often referred to as minor and major grooves based on their size in the *B* form of DNA.

Two sugar-phosphate chains form the backbone of DNA, the macromolecular carrier of the genetic information [Fig. 1(b)]. The two strands are connected together via hydrogen bonds between the nucleotide "side chains." The hydrogen-bonded pairs of nucleotides (base pairs) are stacked, forming the inner core of the molecule [Fig. 1(b)]. Depending on its environment and mechanical strain, the DNA double helix may have several different helical forms, of which the most common are right-handed *A*- and *B*-DNA, and the most peculiar is the left-handed *Z*-DNA. Several different helical conformations of DNA may even coexist as domains of the same long molecule (Ha *et al.*, 2005).

Collagen [Fig. 1(c)] is a triple helix formed by three interwoven, left-handed polypeptide chains connected together through hydrogen bonds between backbone amide and carbonyl groups. Collagen triple helices self-assemble into fibers which form tendons, ligaments, and the organic scaffold of bone, skin matrix, and other structures of connective tissues.

More complex supramolecular helices are formed upon self-assembly of small molecules. For instance, self-assembly of guanosine-phosphate nucleotides produces a four-stranded guanosine helix, which mimics the structure of chromosome telomeres. Some proteins self-assemble into multimolecular helices such as microtubules and actin filaments in cytoskeleton. Some viral particles [e.g., tobacco mosaic virus (TMV)] are also multimolecular helices formed by self-assembly of several different proteins, encapsulating a nucleic acid in the viral particle core.

B. Helical structure factors

A rigorous description of helical macromolecules in terms of their structure factors in reciprocal space was

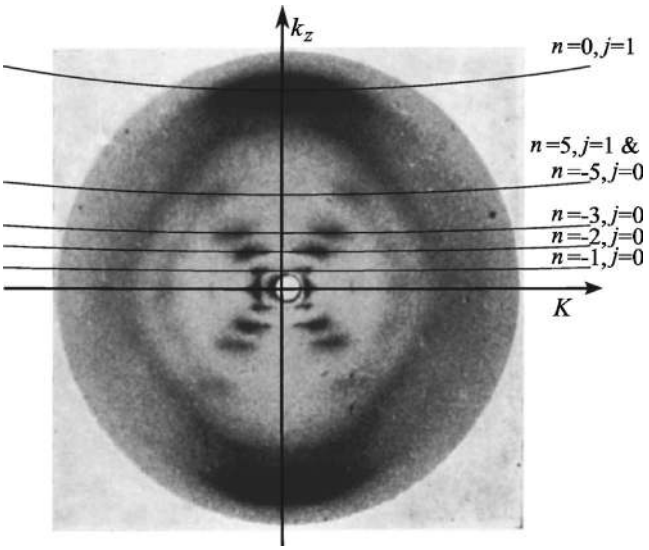

FIG. 2. X-ray-diffraction pattern from calf thymus *B*-DNA (Franklin and Gosling, 1953) showing the location of layer lines, Eq. (9), on the scattering wave-vector axis. The lines of constant k_z (thin solid lines) are slightly curved due to the specific geometry of x-ray film mounting. From Franklin and Gosling, 1953.

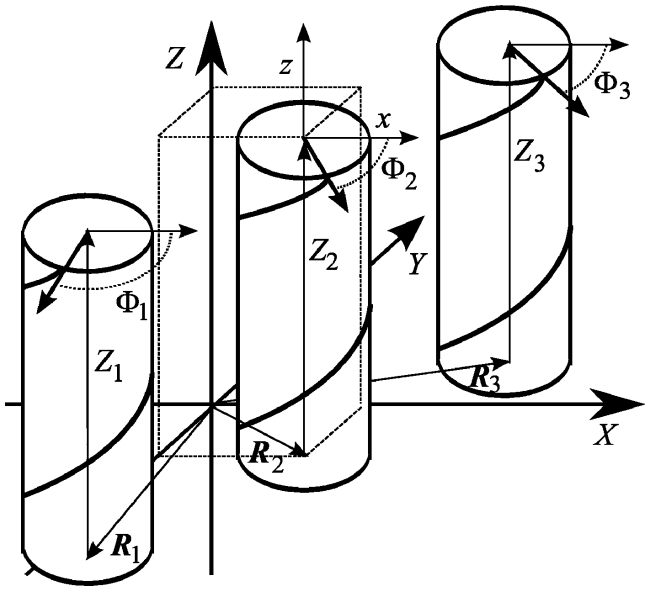

FIG. 3. Convention used for x-ray analysis of helical molecules. The location of each molecule is given by the lateral ($\mathbf{R}_\nu$) and axial coordinates (Z_ν) in the laboratory frame (X,Y,Z). The local (r,z,ϕ) coordinates of the atomic scattering centers in the molecule ν have their origin at the location ($\mathbf{R}_\nu, Z_\nu$). The molecular azimuthal orientation Φ_ν of a helix is determined by a cut through molecular origin ($\mathbf{R}_\nu, Z_\nu$) parallel to the XY plane.

proposed by Cochran, Crick, and Vand (1952) to describe x-ray scattering from α-helical polypeptides. It was crucial for the discovery of the DNA structure by Watson and Crick (1953) and formed the basis of modern crystallography of helical macromolecules.

In this section we describe the helical structure factors in the context of a generalized form of the Cochran-Crick-Vand (CCV) theory for x-ray scattering from helical macromolecules. In Secs. IV and V we utilize the same expressions in a different context and demonstrate that these structure factors and structural parameters also determine structure-dependent physical properties and interactions between macromolecules.

The x-ray scattering intensity of an ensemble of macromolecules is given by

$$I(\mathbf{k}) = \sum_{\nu,\mu} \sum_{i,j} f_i f_j \langle F_i^\nu(\mathbf{k}) F_j^\mu(-\mathbf{k})\rangle, \tag{1}$$

where $\mathbf{k} \equiv (k_z, \mathbf{K})$, is the scattering vector (Fig. 2), f_i is the scattering amplitude for each type of scattering center, and

$$F_i^\nu(\mathbf{k}) = \frac{1}{(2\pi)^{3/2}} \int n_i^\nu(\mathbf{r}) \exp(i\mathbf{k}\cdot\mathbf{r}) d^3\mathbf{r} \tag{2}$$

is the Fourier transform of the density $n_i^\nu(\mathbf{r})$ of scattering centers i on the molecule ν. Hereafter we refer to $F_i^\nu(\mathbf{k})$ as the *structure amplitude* and to $\langle F_i^\nu(\mathbf{k}) F_j^\mu(-\mathbf{k})\rangle$ as the average *structure factor*, although some authors reserve the latter term for $\Sigma_i f_i F_i^\nu(\mathbf{k})$. The structure factor is averaged over both time and volume inside the x-ray beam, to account for dynamic (thermal) fluctuations and static, quenched disorder (e.g., due to sequence-dependent variations in molecular structure, discussed in Sec. II.E and throughout the review).

For helical macromolecules, it is convenient to describe the density of scattering centers within each molecule ν in cylindrical coordinates (r,z,ϕ), which are coaxial with the main axis of this molecule and associated with a selected point of origin ($Z_\nu, \mathbf{R}_\nu$), which defines the lateral ($\mathbf{R}_\nu$) and axial (Z_ν) coordinates of the molecule (Fig. 3). It is also convenient to separate scattering centers into subhelices i, which are distinguished not only by the kind of centers they are composed of (e.g., phosphate, carbon, oxygen, and other atoms) but also by their radii a_i,

$$\tilde{n}_i^\nu(r,z,\phi) \equiv n_i^\nu(\mathbf{r}) \propto \delta(r - a_i), \tag{3}$$

where $\delta(x)$ is the Dirac δ function.

For straight, helical macromolecules, the structure factors are given by CCV as

$$\langle F_i^\nu(\mathbf{k}) F_j^\mu(-\mathbf{k})\rangle = \frac{1}{2\pi} \sum_{n,m} i^{n-m} s_{i,j}^{\nu,\mu}(k_z,n,m) J_n(Ka_i) J_m(Ka_j) \times \langle e^{-in\Phi_\nu + im\Phi_\mu} e^{ik_z(Z_\nu - Z_\mu)} e^{i\mathbf{K}(\mathbf{R}_\nu - \mathbf{R}_\mu)}\rangle. \tag{4}$$

Here $K \equiv |\mathbf{K}|$, $J_n(x)$ is the cylindrical Bessel function of order n, Φ_ν is the azimuthal orientation of each molecule at the point of origin (Fig. 3), and we introduced the *molecular structure factors*

$$s_{i,j}^{\nu,\mu}(q,n,m) = \langle v_i^\nu(q,n) v_j^\mu(-q,-m)\rangle, \tag{5}$$

based on the Fourier transforms in local coordinates associated with each molecule,

$$v_i^{\nu}(q,n) = \frac{1}{2\pi}\int_0^{2\pi} d\phi \int_{-\infty}^{\infty} dz \int_0^{\infty} r\, dr\, \tilde{n}_i^{\nu}(r,z,\phi) e^{in\phi} e^{iqz}. \tag{6}$$

The advantage of utilizing the latter factors is that they are independent of the locations and orientations of the molecules and are determined only by the molecular structure.

C. Ideal helices

The structure factors for ideal helical chains of atoms have a fairly simple form. Consider, e.g., a two-stranded, right-handed helix formed by regularly spaced points, which mimics the pattern of phosphates on DNA [Figs. 1(b) and 7],

$$n_p(\mathbf{r}) = \sum_l \left[\delta\left(\phi - \tilde{\phi}_s - \frac{2\pi z}{H}\right) + \delta\left(\phi + \tilde{\phi}_s - \frac{2\pi z}{H}\right)\right] \times \frac{\delta(r-a)}{a}\delta(z - lh), \tag{7}$$

where l is the running index numbering the phosphates, $2\tilde{\phi}_s$ is the azimuthal angle between the strands, H is the pitch of the helix, h is the axial rise per residue, and a is the helix radius. The molecular structure factor of this helix is given by

$$s_{p,p}^{\nu,\mu}(k_z,n,m) = \frac{N_p^2}{\pi^2}\cos(n\tilde{\phi}_s)\cos(m\tilde{\phi}_s) \times \sum_{j,J=-\infty}^{\infty} \delta_{k_z,Gj-gn}\delta_{m,n+JG/g}, \tag{8}$$

where N_p is the total number of phosphates on each strand, $G=2\pi/h$, $g=2\pi/H$, and $\delta_{x,y}$ is the Kronecker delta ($\delta_{x,y}=1$ at $x=y$ and $\delta_{x,y}=0$ at $x\neq y$).

Because of the helical symmetry, the structure factor is not zero only along the layer lines (Cochran, Crick, and Vand, 1952),

$$k_z = jG - ng, \tag{9}$$

whose separation is determined by the helical pitch and the axial rise per residue. In fact, the same symmetry rule also determines important properties of interactions between helical macromolecules (see Sec. V).

D. Discovery of DNA structure

Soon after the CCV theory of helical structure factors was published, high-quality fiber diffraction patterns of DNA were reported by Franklin and Gosling (1953) (see Fig. 2) and by Wilkins *et al.* (1953). Interpretation of these patterns based on the CCV theory allowed Watson and Crick to decipher the structure of DNA (Watson and Crick, 1953).

The classical interpretation of the DNA fiber diffraction pattern shown in Fig. 2 is based on the assumption most clearly formulated by Franklin and Gosling: "It therefore seems reasonable to suppose that in structure B the structural units (DNA) are relatively free from the influence of neighboring molecules, each unit being shielded by a sheath of water" (Franklin and Gosling, 1953). Indeed, assuming uncorrelated molecular rotations we find

$$\langle e^{-in\Phi_\nu + im\Phi_\mu} e^{ik_z(Z_\nu - Z_\mu)} e^{i\mathbf{K}\cdot(\mathbf{R}_\nu - \mathbf{R}_\mu)}\rangle = \delta_{\nu,\mu}\delta_{n,m} + (1-\delta_{\nu,\mu})\delta_{k_z,0}\delta_{n,0}\delta_{m,0}\langle e^{i\mathbf{K}\cdot(\mathbf{R}_\nu - \mathbf{R}_\mu)}\rangle. \tag{10}$$

Taking into account that the scattering amplitude of phosphates is much larger than those of other atoms or molecules, the contribution of the latter to the diffraction pattern from noncrystalline fibers can be neglected and (Klug *et al.*, 1958)

$$I(\mathbf{k}) \propto N \sum_{n,j=-\infty}^{\infty} \delta_{k_z,ng-jG}\cos^2(n\tilde{\phi}_s)J_n^2(Ka) + \delta_{k_z,0}J_0^2(Ka)\sum_{\nu\neq\mu}\langle e^{i\mathbf{K}\cdot(\mathbf{R}_\nu - \mathbf{R}_\mu)}\rangle, \tag{11}$$

where N is the number of DNA molecules in the x-ray beam. The first and second terms in Eq. (11) describe intramolecular and intermolecular scattering, respectively.

The two strong spots on the equator ($k_z=0$) in the diffraction pattern shown in Fig. 2 correspond to the first order of intermolecular Bragg scattering on a hexagonally packed fiber described by the second term in Eq. (11). They correspond to the smallest K at which $\mathbf{K}\cdot(\mathbf{R}_\nu - \mathbf{R}_\mu) = 2\pi M$ ($M=0,\pm1,\pm2,\ldots$) and are related to the interaxial spacing d_{int} between the nearest neighbors as $K=4\pi/\sqrt{3}d_{\text{int}}$. Higher-order diffraction peaks cannot be seen clearly because of imperfect hexagonal packing and the relatively small number of molecules in the fiber.

The nonequatorial ($n\neq0$ and/or $j\neq0$) diffraction spots originate from intramolecular scattering described by the first term in Eq. (11). The cross formed by the diffraction spots on the $n=\pm1,\pm2,\pm3,\pm5$; $j=0$ layer lines is in good agreement with the maxima of the corresponding Bessel functions $J_n(Ka)$, assuming that the radius of DNA is $a\approx10$ Å. The distance between these layer lines $2\pi/H$ reveals the helical pitch of the molecule, $H\approx34$ Å. The notable absence of diffraction spots at $n=\pm4$, $j=0$ suggests that $\cos(4\tilde{\phi}_s)\approx0$ or $\tilde{\phi}_s \approx 0.38\pi$. The two darkest spots on the meridian correspond to $n=0$, $j=\pm1$, $k_z=2\pi/h$ and reveal the axial rise per base pair, $h\approx3.4$ Å. Their smearing toward the center of the pattern is related to imperfect orientation of the molecules in the fiber, imperfections of the helical structure, thermal motions, and overlap with adjacent diffraction spots ($n=\pm1,\pm2; j=\pm1$).

E. Nonideal helices: Helical coherence length

At the time of the discovery of DNA structure the ideal helix approximation seemed reasonable, and no further structural details were known. Later, atomic-resolution structures of DNA oligomers (short, 10–20

base pair fragments) were obtained by x-ray diffraction from crystals (Dickerson and Drew, 1981; Dickerson, 1992). They revealed significant deviations from the ideal helix due to sequence dependence of the structural parameters. It was argued that such nonideality of the DNA structure is important for its function (Gorin *et al.*, 1995; Rozenberg *et al.*, 1998).

To illustrate possible effects of deviations from the ideal helix on the structure factors, we first modify the DNA model discussed above by incorporating a realistic sequence-dependent twist between adjacent base pairs. In the ideal helical conformation described by Eq. (7), the twist angle between the adjacent base pairs,

$$\Omega(z) \equiv \phi(z+h) - \phi(z), \tag{12}$$

was assumed to be constant. In contrast, real DNA has ten distinct combinations of adjacent base pairs, all of which have different preferred values of Ω. The axial pattern of this intrinsic twist angle $\Omega_l \equiv \Omega(z=lh)$ is a unique, sequence-dependent "fingerprint" of DNA structure.

We now take into account that Ω_l have different values and that real DNA sequences have no long-range correlations in Ω_l (Stanley *et al.*, 1999). The deviation from the average twist angle $\langle\Omega\rangle$,

$$\omega_l = \Omega_l - \langle\Omega\rangle, \tag{13}$$

is relatively small $[\sqrt{\langle\omega_l^2\rangle} \equiv \Delta\Omega \approx 4^\circ - 6^\circ$, $\langle\Omega\rangle \approx 34^\circ$ (Kabsch *et al.*, 1982; Gorin *et al.*, 1995; Olson *et al.*, 1998), and $\langle\rangle$ denotes an ensemble average over all possible $\Omega_l]$. Nevertheless, this nonideality has important implications. In particular, it leads to a deviation of $\phi(lh)$ from the value expected for an ideal helix $[\phi(0)+\langle\Omega\rangle l]$,

$$\delta\phi(lh) = \phi(lh) - \phi(0) - \langle\Omega\rangle l, \tag{14}$$

which follows the simple law of a random walk,

$$\langle[\delta\phi(lh) - \delta\phi(l'h)]^2\rangle = |l-l'|h/\lambda_c, \tag{15}$$

at a large number of steps ($|l-l'| \gg 1$), where $\lambda_c = h/\Sigma_i\langle\omega_l\,\omega_{l+i}\rangle$ may be referred to as the *helical coherence length* (Kornyshev and Leikin, 2001; Cherstvy *et al.*, 2004).

For such helices, the molecular structure factor has only diagonal components $n=m$ but its general form is rather cumbersome (Inouye, 1994; Mu *et al.*, 1997). For typical parameters of DNA, the dominant term in this expression is given by

$$s_{p,p}^{\nu,\mu}(k_z,n,m) \approx \frac{N_p\delta_{n,m}}{\pi^2}(\cos n\tilde{\phi}_s)^2 \times \sum_j \frac{n^2/\lambda_c h}{(k_z+ng-jG)^2 + n^4/4\lambda_c^2}. \tag{16}$$

Similar to ideal helices, Eq. (16) has the maxima at k_z given by Eq. (9). However, the intensity of the maxima decreases as n^{-2} and their width increases as n^2 (Egelman *et al.*, 1982; Egelman and DeRosier, 1982; Barakat, 1987). It follows from Eq. (16) that the ideal helix approximation for the structure factor is valid only when

$$n^2 \ll 4\pi\lambda_c/H. \tag{17}$$

Not only the twist but the base pair tilt, roll, and axial rise depend on the sequence (Bolshoy *et al.*, 1991). These, as well as thermally induced structural variations, may contribute to further deviations from the ideal helix. However, such variations still exhibit the simple random-walk behavior described by Eq. (15) at large distance scales. As a result, the deviation of the average structure factor from an ideal helix can generally be described by Eq. (16) with the single parameter of the helical coherence length λ_c. Different independent contributions $\lambda_c^{(i)}$ into the helical coherence length simply add up as (Lee, Wynveen, and Kornyshev, 2004)

$$\lambda_c^{-1} = \sum_i 1/\lambda_c^{(i)}, \tag{18}$$

reducing the total helical coherence length λ_c.

An estimate of the helical coherence length of DNA based on the known average structural parameters and elasticity constants (Kabsch *et al.*, 1982; Hagerman, 1988; Dickerson, 1992; Gorin *et al.*, 1995; Olson *et al.*, 1998) and from direct analysis of known NMR structures of *B*-DNA fragments in solution yields $\lambda_c \sim 100-300$ Å and $4\pi\lambda_c/H \sim 30-100$ or smaller. The diffraction pattern calculated from Eq. (16) shows a noticeable deviation from the ideal helix approximation at $n=3$ and strong smearing and almost complete disappearance of the diffraction peaks at $n=5$. In contrast, the $n=5$ peaks in the observed diffraction patterns (Fig. 2) are still quite sharp and consistent with the ideal helix model.

F. Effect of assembly on DNA structure

Around the time Franklin and Gosling photographed the diffraction pattern shown in Fig. 2, the imperfectness of the helical structure of DNA was not known. It is the present knowledge of the sequence-dependent structure variations that makes the ideal appearance of the double helix in their pictures surprising. It suggests that long, natural DNA molecules in hydrated aggregates are closer to ideal helices than DNA in solution and short oligomers in crystals.

In fact, the first indication that DNA molecules become more uniform and closer to ideal helices when packed into aggregates was obtained several decades ago. A significant variation in the twist angle per base pair (bp) with the average near 10.5 bp per helical turn was observed in solution (Wang, 1979; Rhodes and Klug, 1980), while nearly perfect, integral 10.0 bp/turn helices were observed in hydrated fibers regardless of packing density (Zimmerman and Pheiffer, 1979; Rhodes and Klug, 1980).

In Sec. VI we detail further, direct evidence demonstrating that the simplifying assumption about DNA being "free from the influence of neighboring molecules" was incorrect. A more general interpretation of the classical diffraction patterns without this assumption turns out to be in better agreement with the established Watson and Crick model. The interactions between neigh-

boring molecules are strong enough not only to affect their alignment but even to change their structure.

Significantly, the variation of structural parameters of synthetic DNA oligomers in crystals is closer to that in natural DNA in solution than in hydrated fibers (Dickerson, 1992), suggesting that interactions between fragments with *identical sequences* in crystals are different from interactions between long DNA with uncorrelated sequences in fibers. In other words, intermolecular interactions between DNA depend not only on overall structure of the double helix, but also on the sequence of base pairs. In Sec. V we give a clear interpretation of this phenomenon.

G. Bent and supercoiled helices

In nature, DNA and other biological helices rarely exist as straight rods. Most of the time they bend, winding around other molecules and around each other. For instance, eukaryotic DNA is wound around a protein core in nucleosomes. The three left-handed helical chains of collagen triple helix are wound together in a right-handed helical supercoil. The two α-helical chains in myosin filaments coil around each other forming an extended coiled coil. (The latter term is typically used for α-helices while supercoil is a part of DNA terminology, but otherwise they have similar meaning.) Circular DNA fragments form a variety of supercoiled structures with the help of specialized enzymes (topoisomerases). A schematic picture of a supercoil made by two molecules is shown in Fig. 4.

Various aspects of the studies of such structures have been described in numerous reviews [see, e.g., Vologodskii and Cozzarelli (1994) and Mason and Arndt (2004)]. Surprisingly little attention, however, has been paid to the physics of the interactions governing the structural hierarchy in these objects. For instance, we still do not know how the pitch of the molecular helix affects the energy and the structure of the supercoil formed by two such helices tightly wound around each other.

We return to a more detailed discussion of this issue in Sec. IV. Here, we point out that the first step toward a rigorous solution of this problem would be the calculation of the structure factor of a coiled coil. Such a calculation was actually reported by Crick (1953a, 1953b).

The density of atoms in a cross section $\mathbf{r}=(\mathbf{R},z)$ of the strand j of a coiled coil with a large supercoli pitch P can be approximated as

$$n_j(\mathbf{R},z) \approx \int n_s^j(\mathbf{R}'-\mathbf{R},z) n_0^j(\mathbf{R}',z) d^2\mathbf{R}', \tag{19}$$

which is the convolution of the continuous helix formed by the centerline $[x=x_j(z),\ y=y_j(z)]$ of the strand,

$$n_s^j(x,y,z) = \delta(x - b_j \cos(Qz - \psi_j))\delta(y - b_j \sin(Qz - \psi_j)), \tag{20}$$

and the density of atoms $n_0^j(\mathbf{R},z)$ in the z cross section of the strand in the coordinate frame coaxial with its center. Here, in Eq. (20), b_j, $Q=2\pi/P$, and ψ_j are the radius of the helix formed by the central line, the supercoil twist, and the supercoil azimuthal phase, respectively. We can think of $n_0^j(\mathbf{R},z)$ as the density of atoms in the *straightened* strand j in a coaxial coordinate frame. In the simplest case, when each strand of the coiled coil is a single-chain helix with pitch H and equal axial spacing h between the atoms, $n_0^j(\mathbf{R},z)=n_p(\mathbf{r},\tilde{\phi}_s=0)/2$, where $n_p(\mathbf{r},\tilde{\phi}_s)$ is defined by Eq. (7). A straightforward calculation of the Fourier transform of $n_j(\mathbf{R},z)$ yields

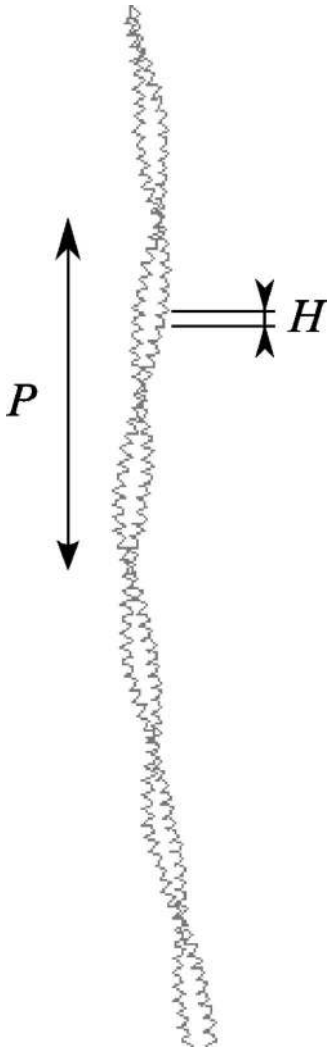

FIG. 4. Sketch of a supercoil (coiled coil) formed by two helical molecules (strands).

$$F_j^{\nu}(\mathbf{k}) \approx \frac{N}{(2\pi)^{3/2}} \sum_{l,n,m=-\infty}^{\infty} J_n(Ka_j) J_m(Kb_j) \delta_{k_z,Gl-gn-Qm} \times e^{i(m+n)(\phi_{\mathbf{k}}+\pi/2)-im\psi_j-in\phi_j}, \tag{21}$$

where as well as b_j and ψ_j we have a_j and ϕ_j, which are the radius and the azimuthal phase of each helical strand, respectively. This approximation for the structure amplitude corresponds to Crick's result (Crick, 1953a, 1953b), generalized to the case of several strands, when $2\pi b_j/P \ll 1$. The latter is often the case for supercoiled biological helices.

In Sec. IV we show how this structure amplitude can be used to calculate the electrostatic energy of a coiled coil. More general expressions for the structure amplitudes may contain distortions of the helical structure, as discussed above, various details about the discrete molecular structure of the helices, and so on. This awaits further development.

H. Summary and comments

We see that the rigorous description of ideal and nonideal helices and even such complex objects as coiled coils is conceptually and mathematically quite simple, despite the somewhat meticulous algebra and the traditionally cumbersome notation. The corresponding language of molecular structure factors has so far been confined primarily to crystallography texts. However, learning it is well worth the effort for physicists interested in biological macromolecules. Not only was this language crucial for unlocking the secrets of DNA and protein structures, but, as discussed in the forthcoming sections, we argue that it may hold the key to understanding relationships between molecular structure and interactions and to unraveling the complex physics of assemblies of biological helices.

III. ELASTICITY

Since intermolecular interactions affect the structure of biological helices (Sec. II.F), part of the work of bringing two or more helices together is expended toward the elastic cost of changing their structure. In this section we discuss the simplest continuum model of molecular elasticity, which allows one to account for these effects. The theory and measurements of elasticity of helical macromolecules, particularly DNA, have attracted so much interest in recent years that it is not practical here to provide a more comprehensive review. For an in-depth study we refer an interested reader to several recent reviews (Hagerman, 1988; Schlick, 1995; Olson and Zhurkin, 2000; Travers, 2004; Benham and Mielke, 2005; and references therein).

A. Elastic rod theory

The continuum description of the mechanics of long, rodlike macromolecules is based on macroscopic elastic rod theory, sometimes referred to as Kirchhoff and sometimes as Cosserat theory [for a formulation and brief history of its development, see, e.g., Antman (2005)]. The elastic energy of a rodlike macromolecule is described by

$$E = \frac{1}{2}\int_0^L \left[B_1(c_1 - c_1^0)^2 + B_2(c_2 - c_2^0)^2 + C_t\left(\frac{d\phi}{ds} - g_0\right)^2 + C_s\left(\frac{ds}{ds_0} - 1\right)^2\right] ds, \tag{22}$$

where L is the length of the molecule and s is the coordinate along its centerline. The first two terms in the integrand give the bending energy; c_1 and c_2 are the two principal curvatures, B_1 and B_2 are the corresponding bending rigidities, and c_1^0 and c_2^0 are the intrinsic curvatures in an undeformed state. The third term is the torsional energy, ϕ is the azimuthal orientation (twist angle) of the rod, $d\phi/ds$ is the torsional strain (twist per unit length), C_t is the torsional rigidity, and g_0 is the intrinsic twist (e.g., the intrinsic twist of an ideal helix with pith H is $g_0 = 2\pi/H$). The last term is the energy associated with the axial strain $(ds/ds_0 - 1)$ caused by displacement of material from the centerline position s_0 to s upon stretching; C_s is the corresponding stretching elasticity. Because of molecular heterogeneity, for example, sequence variation in DNA, the intrinsic curvatures, twist, and all elastic constants might explicitly depend on s (Manning *et al.*, 1996). Shearing of macromolecular helices is usually neglected.

In general, bending, twist, and stretching are coupled to each other. The pitch H and therefore g_0 are affected by the stretching of the centerline. The directions of the principal curvatures are determined by the molecular structure and depend on the twist angle ϕ at each point s. The latter dependence results in a tradeoff between bending and twist and has a significant effect on the local equilibrium shape in molecules with anisotropic bending rigidity $(B_1 \neq B_2)$ such as DNA [see, e.g., Balaeff *et al.* (2006), and references therein]. Explicit twist-bend (Marko and Siggia, 1994) and twist-stretch (O'Hern *et al.*, 1998) coupling energies can also be introduced.

In many cases, however, the expression for the elastic energy can be significantly simplified. In particular, the centerline is frequently not stretched and its bending occurs on much larger distance scales than twist $(c_1 H, c_2 H \ll 1)$. Such gradual bending becomes decoupled from the twist and can be described by an isotropic bending rigidity B and zero intrinsic curvature (Kehrbaum and Maddocks, 2000; Rey and Maddocks, 2000). Small variations in local intrinsic curvatures and bending rigidities (e.g., due to sequence dependence in DNA) result in renormalization of the effective value of B at larger distance scales where bending becomes isotropic and sequence independent (Trifonov *et al.*, 1987; Nelson, 1998). The elastic energy of an inextensible rod without sharp kinks can therefore be rewritten as

$$E = \frac{1}{2}\int_0^L \left[B\left(\frac{d^2\mathbf{r}(s)}{ds^2}\right)^2 + C_t(s)\left(\frac{d\phi(s)}{ds} - g_0(s)\right)^2\right] ds, \tag{23}$$

where $\mathbf{r}(s)$ is the coordinate of each point s on the centerline and $d^2\mathbf{r}(s)/ds^2$ is the curvature of the centerline. While the effective torsional rigidity and intrinsic twist are also often assumed to be constant, Eq. (23) underscores that their explicit dependence on s in highly twisted biological helices (e.g., $g_0 h \sim 1$ in DNA) might become important.

Continuum models based on Eqs. (22) and (23) have been successfully applied to explain many phenomena, from the complex shapes and topologies of supercoiled[1] DNA (Benham, 1983; LeBret, 1984; Tanaka and Takahashi, 1985; Tsuru and Wadati, 1986; Jülicher, 1994; Schlick, 1995; Coleman and Swigon, 2004) to switching between right- and left-handed helical conformations in bacterial flagella (Goldstein *et al.*, 2000). Note, however, that a different approach was utilized to describe helical tubules and ribbonlike helices formed upon self-assembly of chiral amphiphilic membranes [see, e.g., Chung *et al.* (1993), Schnur (1993), Selinger *et al.* (1996), Zastavker *et al.* (1999); Smith *et al.* (2001), Zastavker *et al.* (2005), and references therein].

Remarkably, treating DNA as a simple elastic rod not only captures the qualitative physics but often provides an accurate quantitative description of elastic strains and stresses in biological helices, as demonstrated by numerous studies of DNA discussed below (Sec. III.C).

B. Thermal motions

In addition to elastic deformations in response to external stresses, long semi-flexible helices undergo "wormlike" thermal motions. Most often these motions are described within the simplest wormlike-chain model (Kratky and Porod, 1949; Fixman and Kovac, 1973; Kovac and Crabb, 1982; Odijk, 1995; Ha and Thirumalai, 1996), which incorporates only the isotropic bending energy given by Eq. (23) and the entropy of chain configurations. However, various extensions of this model have also been developed to account for elongation of the molecules in conjunction with electrostatic effects (Odijk, 1977; Skolnick and Fixman, 1977; Barrat and Joanny, 1993; Marko and Siggia, 1995; Hansen *et al.*, 1999; Podgornik *et al.*, 2000) twisting (Kamien *et al.*, 1997; Marko, 1997a, 1997b), and supercoiling of the molecules under special circumstances (Bouchiat and Mézard, 1997, 2000; Moroz and Nelson, 1998).

For instance, without a stretching force the mean square distance between the ends of a long, inextensible, untwisted wormlike-chain is given by (Kratky and Porod, 1949; Harris and Hearst, 1969)

$$\langle[\mathbf{r}(L)-\mathbf{r}(0)]^2\rangle = 2\lambda_p^2(L/\lambda_p - 1 + e^{-L/\lambda_p}) \tag{24}$$

while $\langle \mathbf{r}(L)-\mathbf{r}(0)\rangle = 0$. Here $\lambda_p = B/k_BT$ is the persistence length of the molecule and k_BT is the thermal energy. The stretching force f needed to hold the ends of such a chain at the average distance $\langle z\rangle$ (in the projection of the direction of the force) can be approximated by (Marko and Siggia, 1995)

$$\frac{f\lambda_p}{k_BT} \approx \frac{1}{4}\left(\frac{1}{(1-\langle z\rangle/L)^2} - 1\right) + \frac{\langle z\rangle}{L}. \tag{25}$$

This expression, derived as an interpolation formula between $f\lambda_p/k_BT \ll 1$ and $f\lambda_p/k_BT \gg 1$ (Marko and Siggia, 1995), fits the results of the force-extension measurements on single DNA molecules over several orders of magnitude (Bustamante *et al.*, 1994).

C. DNA elasticity

Measurements of the effective size of stretched and unstretched chains and the probabilities of the two ends of a DNA fragment joining together to form a circle were used in numerous experimental studies of DNA flexibility. In most cases the wormlike-inextensible-chain model with isotropic bending elasticity was found to work extremely well. The same effective bending rigidity of $B \approx 2\times10^{-19}$ erg cm ($\lambda_p \approx 50$ nm) was deduced from single-DNA-molecule stretching experiments, electric birefringence, electron microscopy, hydrodynamic stretching, ligase-catalyzed DNA ring closure, and other techniques (Hagerman, 1988; Crothers *et al.*, 1992; Smith *et al.*, 1992; Bustamante *et al.*, 1994; Bednar *et al.*, 1995; Perkins *et al.*, 1995; Cluzel *et al.*, 1996; Wenner *et al.*, 2002). The bending rigidity weakly depends on salt concentration above 50 mM, but increases almost twofold between 10 and 1 mM (Hagerman, 1988; Wenner *et al.*, 2002). Surprisingly, the values of the bending rigidity obtained for small, ~100 bp, circles of DNA with significant curvature ($cH \sim 0.6$) were also similar (Du *et al.*, 2005), suggesting that anisotropy and sequence dependence of the rigidity become important only at higher curvatures or smaller length scales.

In single-molecule experiments with large stretching forces it becomes important to account for the stretching elasticity of DNA (Smith *et al.*, 1996). It was argued that similar strong stretching of DNA might also be induced by proteins *in vivo* and might play an important role in biological processes [see, e.g., Kosikov *et al.* (1999), and references therein]. The value of the stretching elasticity modulus estimated from single-molecule stretching experiments was found to be $C_s \sim 1\times10^{-4}$ dyn [see, e.g., Smith *et al.* (1996), Wenner *et al.* (2002), and references therein]. It appears to be only weakly dependent on salt concentration from 2 mM to 1M NaCl (Wenner *et al.*, 2002), as predicted by Podgornik *et al.* (2000).

There is less agreement on the torsional rigidity modulus of DNA. Values from $\sim 1\times10^{-19}$ to $\sim 5\times10^{-19}$ erg cm have been reported based on measurements of the distribution of different topoisomers in supercoiled DNA loops, the probability of ligase-catalyzed DNA ring closure, and fluorescence polarization anisotropy of fluorophores bound to DNA (Allison and Schurr, 1979; Barkley and Zimm, 1979; Millar *et al.*, 1980; Shore and Baldwin, 1983; Horowitz and Wang, 1984; Taylor and Hagerman, 1990; Crothers *et al.*, 1992). As opposed to the case of bending rigidity, all of these measurements require more extensive theoretical mod-

[1]Note that supercoiling of closed DNA loops is topologically constrained. In particular, the number of times each strand wraps around the central axis of the molecule is a topological invariant (the linking number). Since such deformations are not discussed in present review, we refer the reader to Vologodskii and Cozzarelli (1994) and Bloomfield *et al.* (2000).

eling for interpretation of the results, which was discussed as one possible reason for the lack of good agreement (Bryant *et al.*, 2003). However, the most recent, refined data from such experiments (Heath *et al.*, 1996) and more direct measurements based on the twisting of single molecules (Allemand *et al.*, 1998; Strick *et al.*, 1999; Bryant *et al.*, 2003; Smith *et al.*, 2003) yield approximately the same torsional rigidity value, $C_t \approx 3 \times 10^{-19} - 4 \times 10^{-19}$ erg cm.

A thornier and still debated issue is the local elastic response of DNA to deformations at distance scales on the order of the pitch or smaller. One interesting controversy associated with local elastic constants was raised by measurements suggesting lower rigidity of DNA at smaller distance scales (Akiyama and Hogan, 1997; Zuccheri *et al.*, 2001; Cloutier and Widom, 2004), in contrast to the opposite theoretical expectation (Nelson, 1998), although some of these measurements have been questioned (Du *et al.*, 2005).

At small distance scales, the sequence, discreteness, and anisotropy of the molecule are likely to become important (Calladine and Drew, 1986). The corresponding discrete models of DNA as elastically connected base-pair stacks [see, e.g., Bolshoy *et al.* (1991), Olson *et al.* (1993), Coleman *et al.* (2003), and references therein] as well as continuous models with sequence-dependent intrinsic twist, curvatures, and local elastic constants [see, e.g., Manning *et al.* (1996), Vaillant *et al.* (2003), Balaeff *et al.* (2006), and references therein] have been considered. In Secs. V and VI we discuss how the latter approach can be used in evaluation of sequence-dependent effects in interactions between DNA molecules. It is important to keep in mind, however, that all such approaches suffer from the classical (yet rarely mentioned) problem of utilizing inherently macroscopic approximations (e.g., thermal equilibrium and ergodicity) at a mesoscopic level (Laughlin *et al.*, 2000). While one might expect to capture much of the qualitative physics, the quantitative accuracy of these approximations is not well defined.

D. Summary and comments

Deformations of a molecular helix over distance scales much larger than its pitch appear to be well described by the simple model of a continuous elastic rod with bending, torsional, and stretching rigidity. For DNA, this model has been extensively tested and confirmed experimentally, and the effective values of the corresponding elastic constants have been determined reasonably well. As discussed further, the cost of such deformations plays an important role in the energetics of assemblies of biological helices.

IV. ELECTROSTATICS

All biological helices produce strong electric fields near their surfaces, whether they are highly charged like DNA or zwitterionic like α-helices or collagen. These fields are important for biological function. Activation of chromosomes for genetic transcription is controlled through enzymatic modification of histone tail charges that neutralize DNA wound on nucleosomes. Interaction between α-helices (usually misinterpreted as dipolar, Sec. IV.A) is an important force in protein folding. Electrostatics contributes to proper alignment of collagen helices in fibers, forming tendons and the organic matrix of bone.

Most often, electric fields and electrostatic interactions of helices are described at two extremes. In simplified models the helical structure is neglected and the molecule is approximated by a charged line or cylinder. All-atom computer simulations account for the structure, but they are usually applied to quantify local events, for example, binding of counterions or ligands. Both of these approaches have been well reviewed (Frank-Kamenetskii *et al.*, 1987; Jayaram and Beveridge, 1996). Here we try to fill the void in the middle. We focus on recent advances in models that relate helical charge patterns to the physics of such collective phenomena as interactions between long helices, supercoiling, mesomorphic and polymorphic transitions in aggregates, and so on.

A. Zwitterionic helix in a nonpolar dielectric medium

Consider the simplest example of an exact solution for the electric field created by a zwitterionic helix, a net neutral arrangement of positive and negative charges, embedded in a nonpolar dielectric medium. We assume that the latter has the same dielectric constant ε as the helix core. In reciprocal space, the electrostatic potential of such a helix is

$$\tilde{\varphi}(\mathbf{k}) = \sum_i eq_i F_i(\mathbf{k}) G(\mathbf{k}), \tag{26}$$

where e is the elementary charge, eq_i is the actual (fractional) charge of each subset i of charged centers on the helix (e.g., negatively charged carbonyls or positively charged amides on the α-helix backbone), $F_i(\mathbf{k})$ is the corresponding structure amplitude defined in Sec. II [where the $n_i(\mathbf{r})$ in Eq. (2) are the number densities of the charged centers], and $G(\mathbf{k}) = 4\pi/\varepsilon k^2$ is the Coulombic Green's function for a uniform dielectric medium.

Because the $F_i(\mathbf{k})$ factors for most helical charge patterns have a fairly simple form (Sec. II), the inverse Fourier transforms can usually be performed analytically and the calculation of the electrostatic potential $\varphi(\mathbf{r})$ in real space is straightforward. However, some important conclusions about this potential can be made directly from Eq. (26) without any calculations.

First of all, $F_i(\mathbf{k})$ is nonzero only at the values of $\mathbf{k}$ corresponding to the x-ray-diffraction maxima. Hence the x-ray-diffraction pattern of a helix can often be used to deduce information about the spatial dependence of the electrostatic potential created by this helix (Kornyshev and Leikin, 1998a).

Second, for zwitterionic helices $\Sigma_i eq_i F_i(0) = 0$. Moreover, whenever the charge pattern follows the helical

symmetry of the long molecule, $\Sigma_i e z_i F_i(\mathbf{k})=0$ for $k_z<g$, $g=2\pi/H$. As a result, the electric field near such a helix varies periodically along its surface and decays *exponentially* away from the surface with a characteristic length less than $H/2\pi$ (Kornyshev and Leikin, 1997, 1998a).

Any long α-helix satisfies these criteria, and the electric field near its surface does not resemble the field created by a dipole. The notion of a large α-helix dipole perpetuated by many biochemistry and biophysics textbooks [see, e.g., Voet and Voet (1995)] is at best misleading. In general, the electric field of a helical (or any other) periodic array of parallel dipoles becomes reminiscent of the electric field of a single dipole only at distances larger than the overall size of this array. At such distances the field is usually so weak that it becomes irrelevant. Although an α-helix does respond to a slowly varying *external* field (at the scale of its size) as if it were a large dipole, it is incorrect to speak of molecular interactions involving α-helices as dipolarlike interactions.

In reality, the electric field created by a long, straight, ideal α-helix in a nonpolar medium or inside a protein can be calculated from Eq. (26) exactly. Except in the immediate vicinity of the ends of the helix, this potential is given by

$$e\varphi(\mathbf{r})/k_BT \approx (8l_B/l_c)K_1(gr)I_1(ga)\cos(gz-\phi), \tag{27}$$

where again, now for the α-helix, $g=2\pi/H$. Here

$$l_B = e^2/\varepsilon k_B T \tag{28}$$

is the Bjerrum length in the dielectric (e.g., $l_B \approx 300$ Å when $\varepsilon \approx 2$), $a \approx 2.3$ Å is the helix radius, $H \approx 5.4$ Å is the α-helix pitch, K_1 and I_1 are the modified first-order Bessel functions, and l_c is a length defined by $l_c = h/|q_\alpha|$ with h the axial rise per carbonyl or amide group. In the expression for l_c, $q_\alpha \approx \pm 0.5$ are the fractional charges on backbone carbonyl (−0.5) and amide (+0.5) groups, and the axial rise is $h \approx H/3.7$. The coil of carbonyls is shifted axially from the coil of amides by $\approx H/2$ (Pauling and Corey, 1951; Chothia *et al.*, 1981). The cylindrical coordinates (r, z, ϕ) are coaxial with the helix axis and the point $(r=a, z=0, \phi=0)$ is selected to coincide with one of the positive charges. Although the field decays with the characteristic length $H/2\pi \approx 0.86$ Å, it remains significant ($e\varphi > 1\ k_BT$) up to $r-a \approx 3.8$ Å away from the helix surface, suggesting that it should be an important force in protein folding.

B. Charged cylinders in an electrolyte solution

Poisson-Boltzmann (PB) and strong-coupling (SC) theories. The electrostatics of highly charged molecules in an electrolyte solution is more complicated. Even for homogeneously charged cylinders, pertinent models of charge screening are still debated in the literature. The most conceptually simple and therefore popular approach used to calculate the electrostatic potential $\varphi(\mathbf{r})$ inside an electrolyte solution is based on the PB equation

$$\nabla^2\varphi(\mathbf{r}) = -4\pi\frac{\rho_{\text{ext}}(\mathbf{r})}{\varepsilon} - 4\pi\frac{e}{\varepsilon}\sum_i n_i q_i \exp\left(-\frac{eq_i\varphi(\mathbf{r})}{k_BT}\right), \tag{29}$$

where $\rho_{\text{ext}}(\mathbf{r})$ is the density of fixed, external charges and eq_i and n_i are the charge and average number density of electrolyte ions of each kind, respectively.

The PB theory is a mean-field theory in which the density of electrolyte ions depends on the mean-field potential $\varphi(\mathbf{r})$ through the Boltzmann exponent. Its application is therefore limited to cases when fluctuations of electrolyte ion density and ion-ion correlations are not important (Kirkwood, 1934). For instance, it has long been argued that the PB theory should not be used for the calculation of the free energy of a small, spherical ion in an electrolyte solution, which is determined predominantly by ion-ion correlations. The PB theory is not entirely self-consistent in this context (Onsager, 1933; Bockris and Reddy, 1970; Oldman and Myland, 1994; Schmickler, 1996; Kornyshev, Spohr *et al.*, 2002). Nevertheless, it is widely used in biophysics literature exactly for this purpose (e.g., to calculate the electrostatic energies of ionic groups on protein surfaces) (Yang *et al.*, 1993; Gallagher and Sharp, 1998; Misra *et al.*, 1998; Murray *et al.*, 1999). Reasonable agreement of such calculations with explicit computer simulations of water and electrolyte ions near biomolecules is often attributed to fortuitous cancellation of multiple factors [for a review, see, e.g., Sharp and Honig (1990)].

A better understanding and justification of the PB theory were developed in its application to the counterion distribution and the resulting electrostatic potential near flat, charged surfaces (Guldbrand *et al.*, 1984; Kjellander and Marčelja, 1984, 1986; Borukhov *et al.*, 2000a, 2000b; Netz and Orland, 2000; Moreira and Netz, 2001, 2002; Naji and Netz, 2004; Naji *et al.*, 2005). Empirically, the PB theory (corrected for finite ion size, e.g., via introduction of a dense surface layer of water and ions) was found to work very well near metal electrodes up to fairly high surface charge densities and concentrations of 1:1 electrolytes. [A recent review of various models correcting the PB theory for ion size, ion/water size, images of electrolyte ions, etc., can be found, e.g., in Volkov *et al.* (1998)]. Theoretical arguments suggest that the PB theory works so well because counterion-surface correlations, in the case of ions with low valence, are more important than correlations between electrolyte ions (Guldbrand *et al.*, 1984; Kjellander and Marčelja, 1984, 1986). Recent arguments were obtained using advanced field theoretical methods (Netz and Orland, 2000; Moreira and Netz, 2001, 2002; Naji and Netz, 2004; Naji *et al.*, 2005). The partition function of pointlike counterions near a flat charged surface in a solvent described by a continuous, macroscopic dielectric was calculated where counterion-counterion correlations were handled via perturbation theory. Near a surface with charge density σ, the importance of these correlations was gauged by the magnitude of the coupling parameter Ξ,

$$\Xi = q^2 l_B/l_\sigma, \tag{30}$$

where

$$l_\sigma = e/2\pi l_B|\sigma q| \tag{31}$$

is sometimes referred to as the Gouy-Chapman length. The PB theory was argued to be exact at $\Xi \to 0$, but numerical estimates suggested that it should remain a reasonable approximation up to $\Xi \sim 1$ (Guldbrand *et al.*, 1984; Naji *et al.*, 2005). A solution for the counterion distribution was also obtained in the strong coupling (SC) limit of $\Xi \to \infty$ but not for intermediate values of Ξ (Moreira and Netz, 2001, 2002; Naji *et al.*, 2005).

Computer simulations of counterion distributions near highly charged, rodlike macromolecules like DNA at small electrolyte concentrations demonstrated good agreement with predictions of the PB theory (LeBret and Zimm, 1984a; Das *et al.*, 1997; Deserno *et al.*, 2000; Deserno and Holm, 2002). For such molecules, however, it is worthwhile to exercise a certain degree of caution in applying the PB theory and interpreting the results. Consider, for example, the counterion distribution around DNA in 0.15*M* 1:1 electrolyte solution (hereafter referred to as a physiological solution). The radius of a DNA molecule is ≈9 Å, and its surface charge density is approximately one elementary charge per 100 Å^2, so that $l_\sigma \approx 2.3$ Å and $\Xi \approx 3$ ($l_B \approx 7$ Å in water). Strictly speaking, this value of the coupling parameter might be too large for an accurate description of the counterion distribution within the PB limit and too small for the SC limit (Moreira and Netz, 2001, 2002; Naji and Netz, 2004; Naji *et al.*, 2005). Furthermore, formal application of the PB theory to DNA modeled as a homogeneously charged cylinder suggests that over 50% of counterions are located at distances less than the van der Waals diameter of water (~3 Å). At such atomic distance scales, not only the mean-field approximation for counterion density, but also the assumptions of macroscopic electrostatics built into the PB and the SC theories are likely to break down. In particular, the dielectric response of water is expected to be nonlocal (Kornyshev, 1981, 1985; Bopp *et al.*, 1996, 1998; Medvedev, 2004, and references therein), nonlinear (Ruff and Liszi, 1985), or both (Kornyshev and Sutmann, 1998; Fedorov and Kornyshev, 2007), and it has been observed to behave anomalously in some experimental systems (Mertz and Krishtalik, 2000; Mertz, 2005). Therefore it is difficult to justify utilization of the PB theory with the macroscopic value of solvent dielectric constant to describe the distribution of electrolyte ions within this layer.

However, practical applications of the PB theory usually rely on the electrostatic potential outside rather than inside the dense layer of water and ions at the surface. Effectively, the comparison of PB predictions with computer simulations and experimental measurements of the counterion profile is always done at such distances, suggesting why the PB theory appears to work so well. For instance, the counterion distribution around 25 base pair DNA fragments was recently evaluated by anomalous x-ray scattering (Das *et al.*, 2003) at scattering vectors $|k|/2\pi$ from 0.01 to 0.04 Å^{-1} (which corresponds to a true resolution in real space of $2\pi/|k| > 25$ Å). The authors were able to detect a small difference in the scattering profiles from divalent and monovalent counterions associated with the change of the Debye screening length roughly from 2.9 to 4.9 Å, but this difference was at the limit of the experimental accuracy. Such resolution is clearly not sufficient to probe the counterion distribution within the first few angstroms of a DNA surface. The agreement of the measured scattering profiles with the PB theory (Das *et al.*, 2003) indicates only that the theory does a reasonable job of predicting the tail of the counterion distribution.

Debye-Hückel (DH) and Debye-Hückel-Bjerrum (DHB) theories. Outside the layer where the potential energy of counterions $eq\varphi$ exceeds k_BT (the nonlinear screening layer), the PB equation can be reduced to the simpler DH equation

$$\nabla^2\varphi(\mathbf{r}) = -4\pi\rho_{\text{ext}}(\mathbf{r})/\varepsilon + \kappa_D^2\varphi(\mathbf{r}), \tag{32}$$

where

$$\kappa_D^{-1} \equiv \lambda_D = \left(4\pi l_B \sum_i n_i q_i^2\right)^{-1/2} \tag{33}$$

is the Debye screening length. At physiological salt concentrations, the thickness of the nonlinear layer is often so small that the DH theory is applicable everywhere outside the dense layer of water and ions at the surface. For example, this layer is close to the diameter of charged phosphate groups on DNA and smaller than the roughness of the DNA surface.

The simplicity of the DH theory based on this equation, however, is not its only advantage. With corrections for ion size, the DH theory gives accurate predictions for ion solvation energies and activity coefficients up to physiological concentrations (Harned and Owen, 1950). Its modification accounting for the formation of Bjerrum ion pairs (DHB theory) has been successfully applied in studies of Coulomb criticality (Fisher, 1994) and various problems in colloid science (Medina-Noyola and McQuarrie, 1980; Khan *et al.*, 1987; Löwen *et al.*, 1993; Denton, 1999; van Roij and Hansen, 1999a, 1999b; Likos, 2001). Furthermore, a calculation of electrostatic potentials in a nanosized gap between two electrodes (Kornyshev and Kuznetsov, 2006) demonstrated that limitations on counterion density due to the finite size of ions (Borukhov *et al.*, 2000a, 2000b) almost entirely compensate the nonlinear response of the counterion atmosphere, resulting in a potential distribution that looks very much like the one predicted by the linear DH theory.

Counterion condensation theory. For long, highly charged, rodlike polyelectrolytes in salt solution, the treatment of ions condensed at the surface as part of the renormalized surface charge, as well as a description of the more dilute counterion atmosphere within the DH theory were pioneered by Manning (1969). This description was used later in many applications of polyelectrolyte theory (Oosawa, 1971; Manning 1978, 1984; Frank-Kamenetskii *et al.*, 1987). The idea that a highly charged linear polyelectrolyte retains (condenses) some counterions even at infinite dilution was initially formulated by

Manning based on a simple argument. The potential created by an infinitely long, infinitely thin, straight, charged line in a salt-free medium depends on the distance R from the line as $(2e/\varepsilon l_c)\ln R$, where e/l_c is the absolute value of the linear charge density. As pointed out by Onsager, for $l_c < l_B$ the partition function of a counterion in this potential diverges, suggesting instability and counterion condensation onto this line (Manning, 1969). For a long, charged cylinder of a finite radius a, however, a more rigorous argument is as follows. When a fraction θ of the charge is neutralized by counterions condensed within a narrow region close to the cylinder surface, one can calculate the partition function and obtain the corresponding free energy of confinement for a single ion within the cylinder of radius R. When $R \gg a$, for monovalent counterions, this free energy is given by

$$\mathcal{F}(R) = \mathcal{F}_0 - 2k_B T[1 - (1-\theta)l_B/l_c]\ln(R), \tag{34}$$

where $\mathcal{F}_0$ is independent of R. Additional counterion condensation continues as long as the free energy decreases with decreasing R, until equilibrium is established at

$$\theta_M = 1 - l_c/l_B. \tag{35}$$

Since Eq. (34) only requires R to be much larger than the cylinder radius a and the thickness of the confinement layer, it reveals that condensed counterions are localized somewhere close to the cylinder surface, but it does not specify where. The degree of counterion condensation within this layer may be calculated within the counterion-only PB model (Alfrey *et al.*, 1951; Fuoss *et al.*, 1951; LeBret and Zimm, 1984b). While such a calculation reproduces the result for θ_M, it is less rigorous because it is based on the mean-field approximation.

In dilute electrolyte solutions ($\lambda_D \gg a$), one can still speak of counterion condensation in similar terms. However, in biology and in most practical studies of biological macromolecules, $\lambda_D \sim a$ or smaller. For instance, the Debye screening length in physiological solution ($\lambda_D \approx 7$ Å) is smaller than the radius of the DNA molecule and the average distance between fixed charges on the DNA surface. It is comparable to the size of charged phosphates and the roughness of the surface. Under such conditions the physics of counterion condensation changes. Nevertheless, counterions are still retained at the surface of DNA. But counterions are no longer condensed by the long-ranged, logarithmic tail of the electrostatic potential. Instead, they are located directly at the surface inside deep and narrow potential wells created by exponentially decaying electric fields near discrete, fixed surface charges. In other words, they are adsorbed on the surface. And so the counterion distribution may be separated into a surface layer considered as part of the surface charge and a diffuse layer described within the DH theory.

The latter way of thinking about counterion condensation permits application of many powerful methods developed to describe adsorption, as well as allowing one naturally to account for chemical specificity, which plays a crucial role in biology. For example, monovalent cations exhibit preferential binding to DNA in the following sequence (Bleam *et al.*, 1980; Denisov and Halle, 2000):

$$NH_3^+ > Cs^+ > K^+ > Li^+ > Na^+.$$

This sequence does not correlate with the expected effect of ionic radius on electrostatic interactions or hydration. Instead, it indicates chemical specificity of ionic binding, such as the preferential binding of NH_3^+ with DNA via its ability to form hydrogen bonds with the phosphates. [More detailed discussions of other aspects of counterion condensation, applications of the theory, and its successes and problems can be found, e.g., in Frank-Kamenetskii *et al.*, (1987), and references therein.]

Recent developments in the theory describe correlations between multivalent counterions on a highly charged surface [reviewed by Grosberg *et al.* (2002)]. Briefly, in the strong-coupling limit ($\Xi \sim 3 \times 10^4$ or larger), condensed counterions might form a two-dimensional (2D) Wigner crystal (Rouzina and Bloomfield, 1996; Shklovskii, 1999a, 1999b; Grosberg *et al.*, 2002). For DNA-like surface charge densities, this would require $|q| > 10$. However, it was argued that short-range correlations between counterions might already become significant for $|q| \geq 3$. Condensation of such counterions can lead not only to complete neutralization but also to reversal of the surface charge (Grosberg *et al.*, 2002). On a cautionary note, however, complete charge neutralization and reversal can also be caused by hydrogen bonding or other "chemical" interactions of counterions with the surface. For instance, suspected [2] DNA overscreening (charge reversal) (Pelta, Durand, *et al.*, 1996; Pelta, Livolant, and Sikorav, 1996; Raspaud *et al.*, 1998, 1999; Saminathan *et al.*, 1999) by spermine and spermidine might be caused by their hydrogen bonding to phosphates and bases (see below). The only commonly used DNA counterion that might be subject to the strong-coupling conjecture is $Co[NH_3]_6^{3+}$, but it is also capable of hydrogen bonding and it does exhibit chemical preference for GC base pair binding in the major groove [Fig. 1(b)] of DNA (Deng and Bloomfield, 1999; Ouameur and Tajmir-Riahi, 2004).

C. Counterion condensation and adsorption on DNA

Detailed experimental studies and computer simulations have revealed evidence of specific adsorption at sites determined by the DNA structure and sequence for virtually all cations. Some preference for adsorption in the minor groove [Fig. 1(b)], particularly at AT base pairs, was found even for Na^+, which exhibits the weakest chemical specificity both in experiment (Hud and

[2] An alternative, interpretation of the experimental data that does not involve charge reversal was suggested (Yang and Rau, 2005). For a more detailed discussion see Sec. VII.A.

Feigon, 1997; Shui, McFail-Isom, *et al.*, 1998, Shui, Sinas, *et al.*, 1998; Hud *et al.*, 1999; McFail-Isom *et al.*, 1999; Stellwagen *et al.*, 2001) and in simulation (Beveridge and McConnell, 2000; Hamelberg *et al.*, 2001; Korolev *et al.*, 2002; Rueda *et al.*, 2004). Clear evidence of preferential minor groove binding was obtained for Rb^+ and Cs^+ (Tereshko *et al.*, 1999; Woods *et al.*, 2000). Divalent Ca^{2+} and Mg^{2+} were found to bind directly between phosphates on phosphate strands and in the minor groove (Grzeskowiak *et al.*, 1998; Minasov *et al.*, 1999; Tereshko *et al.*, 1999; Egli, 2002). However, some evidence of their binding to bases in the major groove was also reported (McFail-Isom *et al.*, 1998; Shui, McFail-Isom *et al.*, 1998; Chiu and Dickerson, 2000; Kielkopf *et al.*, 2000). Due to their electron *d* orbitals, transition-metal ions, e.g., Mn^{2+} and Cd^{2+}, exhibit much stronger preference for major groove binding, particularly at the N7 atom of guanine (Clement *et al.*, 1973; van Steenwinkel *et al.*, 1981; Granot and Kearns, 1982; Saenger, 1984; Duguid *et al.*, 1993; Froystein *et al.*, 1993; Moldrheim *et al.*, 1998; Davey and Richmond, 2002). Binding of some transition-metal ions, e.g., Cu^{2+}, in the major groove becomes so strong that they severely distort DNA (Duguid *et al.*, 1993). Trivalent metal ions, e.g., Al^{3+} or Fe^{3+}, might have several oxidation states, catalyze chemical reactions affecting DNA, and/or have such dramatic effects on DNA structure (see, e.g., Karlik *et al.*, 1980) that only large and more inert metal complexes (such as $Co[NH_3]_6^{3+}$ discussed above) are commonly used in DNA studies (Bloomfield *et al.*, 2000).

The DNA charge in cells is neutralized primarily by polycations, including polyamines (e.g., spermine and spermidine are present in cells in millimolar concentrations) and basic polypeptides (e.g., protamine and tails of histone proteins). The distance between charged groups on such cations is usually larger than 5 Å. This is comparable with the DNA radius, the distance between phosphates on the DNA surface, and the Debye length in physiological solution. As a result, polycations cannot be modeled as point charges. Present-day strong-coupling theories clearly cannot be applied to their interaction with DNA. Furthermore, an important feature of their interaction with DNA is that hydrogen bonding exists between their amine groups and oxygen atoms on the phosphates and bases, potentially resulting in a large chemical contribution to the binding energy (Feuerstein *et al.*, 1986, 1990). Yet possible locations of bound polycations have not been firmly resolved. For instance, the majority of experimental and molecular simulations suggest preferential binding of spermine in the major groove (Drew and Dickerson, 1981; Feuerstein *et al.*, 1986, 1990; Shui, McFail-Isom, *et al.*, 1998, Shui, Sines, *et al.* 1998; Ruiz-Chica *et al.*, 2001a; Ouameur and Tajmir-Riahi, 2004), but some evidence of its binding in the minor groove, particularly at high bulk concentrations, has been reported as well (Bryson and Greenall, 2000; Korolev *et al.*, 2001; Ruiz-Chica *et al.*, 2001b).

D. Charged helix in an electrolyte solution

The role of the helical pattern of fixed charges in the electrostatics of a DNA helix in solution was first discussed in application to the Manning theory of counterion condensation (Soumpasis, 1978). It was further investigated by, for example, Wagner *et al.* (1997); and Allahyarov and Löwen (2000), and its contribution into the torsional elasticity of DNA was estimated (Mohammad-Rafiee and Golestanian, 2004).

An exactly solvable, analytical model systematically incorporating structure-dependent patterns of fixed molecular charges and counterions was developed by Kornyshev and Leikin (1997, 1999). Within this model the molecular fixed charges and counterions within the nonlinear screening layer are described explicitly as discrete charges, while the field created by them is analyzed within the DH theory.

Consider, e.g., a highly charged ($l_c < l_B$), long, ideal, right-handed helix with a cylindrical, water-impermeable, dielectric core. In reciprocal space, the electrostatic potential created by such a helix can again be described by Eq. (26) with an effective Debye-Hückel Green's function

$$G(\mathbf{k}) = 4\pi/\varepsilon(k^2 + \kappa_D^2), \tag{36}$$

which accounts for screening by the electrolyte and counterions outside the nonlinear screening layer.[3] We should also use a structure amplitude $F_i^T(\mathbf{k})$ that includes fixed charges, condensed counterions in the nonlinear screening layer (not treated as part of the DH ion atmo-

[3]Although this is not a rigorously justified procedure near interfaces, the permittivity ε in Eq. (36) may also be attributed a k dependence. This dependence accounts for nonlocal dielectric screening and is related to the short-range correlation effects in water. The dielectric function $\varepsilon(k)$ reaches its macroscopic value 80 at $k \to 0$, but it may be quite different at finite k. Unfortunately, $\varepsilon(k)$ has never been directly measured for water or any other liquid. But theoretical calculations, simulations, and indirect neutron-scattering data suggest (cf., e.g., Bopp *et al.*, 1996, 1998: Young *et al.*, 1998; and references therein) that at small and moderate k, $\varepsilon(k)$ of water could be substantially smaller than 80, whereas at higher k it changes sign through a divergence ($\pm\infty$—conditions of thermodynamic stability allow only values of $\varepsilon(k) > 1$ or $\varepsilon(k) < 0$; Dolgov *et al.*, 1981). This leads to an anomalously high but finite value of the response function $\chi(k) = 1 - 1/\varepsilon(k)$ with a maximum (the so-called overscreening resonance) located at $2\pi/3$ Å^{-1}. At $k \to \infty$, the response tends to zero, so $\varepsilon(k) \to 1$. Thus the mode of dielectric response depends on the characteristic wave vectors. This determines whether we deal with macroscopiclike screening, reduced screening, or anomalously large screening. For these systems the wave vectors are smaller than the characteristic wave vectors of the overscreening resonance, so that one might expect a reduction of the effective dielectric constant leading to an enhancement of the interactions (Sec. V). The nonlinear response to the electric field close to the charges, as well as perturbation of water structure by the mere presence of the macromolecules, may, however, complicate the resulting response.

sphere), and image charges induced by the fixed charges and condensed counterions at the surface of the dielectric core. $F_i^T(\mathbf{k})$ is described by Eq. (2) where $n_i^v(\mathbf{r})$ should be replaced with $n_i^T(\mathbf{r})$ so that $eq_i n_i^T(\mathbf{r})$ includes the total charge density from all contributions discussed above.

Provided that the fixed charges and condensed counterions follow the helical symmetry of the molecule, as before, $F_i^T(\mathbf{k})$ is not zero only at the values of k_z and n given by the CCV theory (Sec. II). The $n_i^T(\mathbf{r})$ functions may be determined via a number of methods, such as the PB theory, modified PB theory, functional integrals, and so on. However, no matter how the surface charge pattern is found, the corresponding structural amplitudes can be calculated analytically and substituted into Eq. (26) to determine the spatial dependence of the electrostatic potential.

In the simplest case of a continuous, negatively charged helix (where the helical pitch H is much larger than the distance h between the charge residues on the helix, as is the case for DNA), the average potential is

$$\frac{e\langle\varphi(r,z,\phi)\rangle}{k_BT} = -2(1-\theta)\frac{l_B}{l_c}\frac{K_0(r\kappa_D)}{\kappa_D a K_1(a\kappa_D)} - \frac{4l_B}{l_c}\sum_{n=1}^{\infty}\zeta_n\frac{K_n(\kappa_n r)}{\kappa_n a K_n'(a\kappa_n)}\cos(n\phi - ngz), \tag{37}$$

where a is the radius of the helix, l_c is the length characterizing the axial density (e/l_c) of fixed charges on the helix ($l_c \approx 1.7$ Å for B-DNA), and

$$\kappa_n = \sqrt{\kappa_D^2 + (ng)^2}. \tag{38}$$

Here we assumed that the dielectric constant in the core is much smaller than in the surrounding solvent.

The first term in Eq. (37) describes the potential of a homogeneously charged cylinder. The second term is a sum of the "helical harmonics," the contribution to the potential due to the helical distribution of the charges. The dimensionless coefficients θ and ζ_n are the effective fraction of the helix charge neutralized by condensed counterions (a generalized form of the Manning condensation parameter θ) and the nth-order helical moments of the charge pattern, respectively. These are determined by the pattern of fixed charges and condensed counterions in the nonlinear screening layer. General expressions relating ζ_n to any given distribution $n_i(\mathbf{r})$ of fixed charges and condensed counterions of species i are available in the EPAPS Document (see Reference section).

As an example, for DNA, if all condensed counterions were completely delocalized with no preference for phosphate strands or grooves, ζ_n would be entirely determined by the fixed phosphate charge pattern and given by

$$\zeta_n = -\cos(n\tilde{\phi}_s), \tag{39}$$

where $\tilde{\phi}_s \approx 0.4\pi$ is the azimuthal half-width of the narrow groove, such that $\zeta_1 = 0.31$, $\zeta_2 = -0.81$, and so on. Since the modified Bessel functions K_n decrease exponentially with an increasing argument, in most cases the sum can be truncated after the first one or two helical harmonics. For DNA, the first two harmonics have to be included because of the small value of ζ_1 as compared to that of ζ_2, but all higher harmonics may be neglected.

When ions are assumed to be bound preferentially to certain sites on the DNA surface, ζ_n may be approximated, e.g., by (Kornyshev and Leikin, 1999)

$$\zeta_n = f_1\theta + f_2(-1)^n\theta - (1 - f_3\theta)\cos(n\tilde{\phi}_s), \tag{40}$$

where f_1, f_2, and f_3 are the fractions of adsorbed counterions localized in the minor groove, major groove, and on phosphates, respectively. As $1-f_1-f_2-f_3$ is the fraction of adsorbed counterions that are delocalized on the DNA surface, the limiting case of Eq. (39) is retrieved by putting $f_1=f_2=f_3=0$. Note that this approximation, Eq. (40), assumes that counterions follow the helical lines running through the center of the grooves or phosphate strands in a continuous fashion. This approximation does not take into account discreteness of adsorbed counterions, but it conveniently represents the main classes of adsorption sites. (The finite size of the ions can be easily introduced here through corresponding form factors.) We utilize this simple counterion adsorption model in later sections when discussing specific effects of counterions known to exhibit significant chemical preferences in binding at different locations on the DNA surface.

From Eqs. (37) and (38), the potential of a charged helix is found to conform to that of a homogeneously charged cylinder only when (i) the molecular charge is relatively small ($l_c \geqslant l_B$) so that just a small fraction of it is neutralized by counterions ($\theta \ll 1$) or (ii) the helical pitch of the molecule is small compared to the Debye screening length ($H/2\pi \ll \lambda_D$). For DNA in physiological solution, neither of these two conditions is satisfied. The helical harmonics in the potential of DNA can be neglected only at very large distances. When the DNA charge is completely neutralized (e.g., due to chemisorption of such counterions as spermine or spermidine), the helical harmonics entirely determine the potential at any distance.

E. Summary and comments

At distances smaller than or comparable to the helical pitch H, the electrostatic potential created not only by zwitterionic helices but also by highly charged helices is very different from that of a charged line or a charged cylinder. The pitch is one of the natural length scales of the charge distributions on these objects. The other pertinent length scale is the axial rise per unit charge l_c. The latter determines the extent of counterion condensation but not the profile of the potential created by the mol-

ecule. The difference is crucial. For instance, $H=34$ Å while $l_c=1.7$ Å for DNA. Because l_c is so small ($\ll l_B$), most of the DNA charge is always neutralized by condensed or adsorbed counterions within a very thin surface layer. But, because H is so large, the electrostatic potential created by DNA is significantly different from that of a charged cylinder at almost all distances relevant for the biology or the physics of DNA aggregates. Ignoring the structure of DNA, one can study some important phenomena, such as Manning condensation, but one may miss physics that is equally as or even more important for understanding a number of properties of DNA.

V. PAIR INTERACTIONS

The interaction between rodlike macromolecules is experimentally studied primarily in multimolecular assemblies (Secs. VI and VII). However, the theory of pair interactions is the first crucial step to understanding the physics of assemblies. Significant efforts have been made to develop such a theory by utilizing different theoretical and computational approaches. In retrospect, it is not surprising that the main differences in the different results reported can be traced to different approximations and assumptions made to describe the patterns of fixed charges and condensed counterions at molecular surfaces. Because the structural approach sketched in Secs. IV.A and IV.D does not need necessarily *a priori* assumptions about these patterns, it is probably best suited to systematically analyze the reported results and understand them within a universal theoretical framework.

We first summarize the ideas behind this approach and outline their application to the calculation of pair interaction potentials. The energy of electrostatic interaction E between two rods ν,μ $(=1,2)$ can be directly related to the structure amplitudes for the pattern of charges at their surfaces by representing the potential $\varphi(\mathbf{r})$ and the density of fixed charges and condensed counterions $\rho(\mathbf{r})$ through their Fourier transforms [Eq. (26)]. Namely, the interaction energy is given by

$$E(R) = \mathcal{E}(R) - \mathcal{E}(\infty), \tag{41}$$

where R is the distance between molecular axes and

$$\mathcal{E} = \frac{1}{2}\int \varphi(\mathbf{r})\rho(\mathbf{r})d^3\mathbf{r}$$

$$\approx \frac{2\pi e^2}{\varepsilon}\sum_{\nu,\mu=1}^{2}\sum_{i,j} q_i q_j \int \frac{F_i^{T,\nu}(\mathbf{k})F_j^{\mu}(-\mathbf{k})}{k^2+\kappa_D^2}d^3\mathbf{k}. \tag{42}$$

Here $F_i^{T,\nu}(\mathbf{k})$ is the structure amplitude for fixed and image charges and condensed counterions at the surface of molecule ν, while $F_j^{\mu}(-\mathbf{k})$ is the structure amplitude only for fixed charges and condensed counterions. This quantity, in contrast to $F_i^{T,\nu}(\mathbf{k})$, does not include image charges. Both $F_i^{T,\nu}(\mathbf{k})$ and $F_j^{\mu}(-\mathbf{k})$ may depend on the separation between molecules.

Equation (42) assumes the macroscopic ε and utilizes an effective Green's function from the DH theory in the bulk electrolyte solution, but it is not a mean-field approximation. Instead, it explicitly accounts for condensed counterions through their structure amplitudes. The counterions' positions, which determine $F_i^{T,\nu}(\mathbf{k})$ and $F_j^{\mu}(-\mathbf{k})$, may be self-consistently found through the minimization of the total free energy of the counterion system. Utilizing approximations for the counterion atmosphere, one may find forms for these structure amplitudes that recover the results of either the nonlinear PB or the modified PB theories. Similarly Eq. (42) can reproduce the results of theories incorporating counterion fluctuations and correlations at any value of the coupling parameter.

As for image charges, they must be found from the boundary conditions on both dielectric cores, and generally will comprise an infinite series of images. However, the latter may be truncated at the second term in the interaction potential sum [see Eq. (43)] if the interaxial separation between the two cores is larger than the Debye length (Kornyshev and Leikin, 1997).

The idea proposed by Kornyshev and Leikin (1999) is to utilize the symmetry of cylindrical and helical charge patterns, which leads to only a few pertinent peaks in $\langle F_i^{T,\nu}(\mathbf{k})F_j^{\mu}(-\mathbf{k})\rangle$. This symmetry allows one to calculate the integral in Eq. (42) and express the mean force[4] $-\langle dE(R)/dR\rangle$, the mean interaction energy $\langle E(R)\rangle$, and other thermodynamic variables through the cylindrical and/or helical harmonics of the fixed charge and counterion density $n_i(\mathbf{r})$ of each molecule (e.g., θ and ζ_n introduced in Sec. IV.D). These parameters can be reduced to weighted integrals of the azimuthal and axial Fourier transforms of $n_i(\mathbf{r})$ for any distribution of counterions at the molecular surface, including those that extend away from the surface (Kornyshev and Leikin, 1999). This allows one to understand the relationship between the thermodynamic variables and molecular structure and surface charge patterns without any additional approximations.

Sometimes this is all that is needed to understand the physics of an observed phenomenon. We recall that the most important parameters of the structure of a helix (e.g., pitch and axial rise per residue) are extracted from x-ray experiments through the selection rules for the average structure factors (Sec. II). Similarly, some parameters of intermolecular interactions are also determined by the same selection rules for the average charge density. These parameters can be directly deduced from the symmetry of molecular charge patterns without any additional calculations (Kornyshev and Leikin, 1998a).

When necessary, θ and ζ_n introduced in Sec. IV.A (and/or pertinent charge density harmonics due to the discreteness of effective surface charges) can be calcu-

[4]Differentiation of the free energy $\mathcal{F}$ with respect to a thermodynamic variable η [such as the calculation of the force $-d\mathcal{F}(R)/dR$] is performed with $d\mathcal{F}/d\eta=\langle d\mathcal{E}/d\eta\rangle$ (Landau and Lifshitz, 1969).

lated from the theory of choice, for example, nonlinear PB, Wigner crystal models, adsorbed counterion models, and so on, may be obtained from numerical simulations, or even can be extracted from experiments. Finally, although Eq. (42) defines the electrostatic energy rather than the free energy, the calculation of the corresponding partition function is often not needed to specify certain properties of the interaction (see footnote 4).

A. Parallel molecules with arbitrary charge patterns

The simplest, complete derivation of the interaction energy was reported for two parallel molecules (Kornyshev and Leikin, 1997, 1999). In the absence of dielectric boundaries (zwitterionic molecules in a nonpolar environment) the calculation is straightforward. After substitution of the structure factors, Eqs. (4)–(6) of Sec. II, into Eq. (42), the integrals over $\mathbf{K}\equiv(k_x,k_y)$ can be calculated exactly [see Eqs. (43) and (46) below]. For molecules with cylindrical dielectric cores in an electrolyte solution the calculation is a bit more challenging due to the presence of image charges. Nevertheless, this problem still has an exact solution (Kornyshev and Leikin, 1997, 1999). In general, the energy of interaction between two similar molecules (in electrolyte solution, separated by a layer of water larger than $\lambda_D=\kappa_D^{-1}$) is given by

$$\frac{E(R)/L}{k_BT}=\frac{1}{2}\sum_{n,m=-\infty}^{\infty}\sum_{\mu\neq\nu=1}^{2}\int_{-\infty}^{\infty}dk_zS_{n,m}^{\mu,\nu}(k_z)K_{n-m}(\tilde{\kappa}R)\times e^{-in(\Phi_\mu+\pi\delta_{\mu,2})+im(\Phi_\nu+\pi\delta_{\nu,2})+ik_z\delta Z}+\frac{1}{2}\sum_{n,m=-\infty}^{\infty}\sum_{\mu=1}^{2}\int_{-\infty}^{\infty}dk_zS_{n,m}^{\mu,\mu}(k_z)\Omega_{n,m}(\tilde{\kappa}R,\tilde{\kappa}a)\times e^{i(m-n)(\Phi_\mu+\pi\delta_{\mu,2})},\tag{43}$$

where

$$\tilde{\kappa}=\sqrt{\kappa_D^2+k_z^2},\tag{44}$$

$$\Omega_{n,m}(x,y)=-\sum_{j=-\infty}^{\infty}[K_{n-j}(x)K_{j-m}(x)]\frac{I_j'(y)}{K_j'(y)}\tag{45}$$

and $K_n'(x)$ and $I_n'(x)$ are the derivatives of the corresponding modified Bessel functions with respect to their arguments. We should point out here that Eq. (45), for $\Omega_{n,m}(x,y)$, is the limiting expression when the dielectric constant of the core is much smaller than that of the surrounding medium. This is a reasonable approximation for most macromolecules in electrolyte solution. For the case of an isotropic medium with the same dielectric constant as the core, we can simply set $\Omega_{n,m}(x,y)=0$, that is, there are no image charges. In Eq. (43) L is the length of the molecules, a is their dielectric core radius ($L\gg a$), $\delta Z=Z_1-Z_2$, and Z_ν and Φ_ν are the axial and azimuthal coordinates of the molecule ν at its point of origin. The dimensionless coefficients $S_{n,m}^{\nu,\mu}(k_z)$ are independent of R and proportional to molecular structure factors for instantaneous distributions of fixed charges and condensed counterions (Sec. II). Simple examples of $S_{n,m}^{\nu,\mu}(k_z)$, when all charges and counterions are located within a thin layer at the core surface, are given by Eqs. (46)–(48). More general expressions applicable to distributions of fixed charges and condensed counterions within a layer of finite thickness away from the dielectric core are more cumbersome and are presented in the EPAPS Document in the Reference section.

The first term in Eq. (43) accounts for the energy of each molecule in the field created by the other molecule. The second term accounts for image forces, i.e., for the change in the energy of each molecule in its own field due to distortion of the field by the dielectric core of the other molecule. Note that such image forces are often neglected in theories of interaction between rodlike molecules. However, as found in earlier studies of interactions between charged planar surfaces, they become very important in the case of an inhomogeneous distribution of fixed surface charges and/or in the presence of counterion fluctuations and correlations (Kjellander and Marčelja, 1986; Naji *et al.*, 2005).

In the special case of a nonpolar, electrolyte-free medium, there is no Debye screening and image forces are absent, so that $\tilde{\kappa}=k_z$ and $S_{n,m}^{1,1}(k_z)=S_{n,m}^{2,2}(k_z)=0$. The dielectric response of the medium and molecular cores is determined by the same electron polarizability ($\varepsilon\approx2$, provided that all partial charges on polar groups such as amides and carbonyls in proteins are explicitly included into the charge structure factors). Under such conditions the Coulombic Green's function $G(\mathbf{k})=4\pi/\varepsilon k^2$ is valid up to a very small distance scale (large $\mathbf{k}$) and Eq. (43) is *exact* and can be used at all interaxial distances R up to direct molecular contact. In the simplest case, when all fixed charges lie on the same cylindrical surface of the radius a, $S_{n,m}^{1,2}(k_z)$ is given by

$$S_{n,m}^{1,2}(k_z)=\frac{4\pi l_B}{L}\sum_{i,j}q_iq_js_{i,j}^{1,2}(k_z,n,m)I_n(k_za)I_m(k_za),\tag{46}$$

where $s_{i,j}^{1,2}(k_z,n,m)$ are the structure factors defined in Sec. II [cf. Eqs. (5) and (6)].[5]

The formulas for $S_{n,m}^{\nu,\mu}(k_z)$ in an electrolyte solution are more cumbersome due to the effect of image charges. However, in the simplest case when all fixed charges and condensed counterions lie within a thin layer (much smaller than the molecular radius a and λ_D) at the surface of the molecular core, $S_{n,m}^{\nu,\mu}(k_z)$ can be approximated by (Kornyshev and Leikin, 1997, 1999)

[5]Note that the Bessel functions $I_n(k_za)$ originate from integration of $J_n(Ka)$ in Eq. (4) with the Coulombic Green's function. Indeed, this Green's function has a pole at $K=\pm ik_z$ and $I_n(k_za)\equiv J_n(ik_za)$.

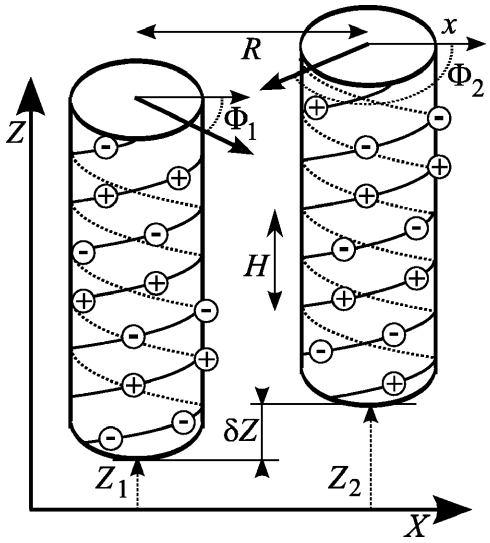

FIG. 5. Schematic drawing of the pattern of fractional ($\sim 0.5e$) charges on amide (+) and carbonyl (−) residues on two interlocked α-helix backbones. The coil of carbonyls is shifted axially from the coil of amides by $\approx H/2$ so that the adjacent, hydrogen-bonded amide and carbonyl are axially aligned. There are about 3.7 carbonyl and amide residues per helical turn in each coil ($H/h \approx 3.7$). Φ_1, Φ_2 and Z_1, Z_2 are the azimuthal orientations and axial coordinates of each helix, correspondingly. They are defined at the point of origin on each helix, which is selected in the middle between the hydrogen-bonded amide and carbonyl. The azimuthal orientation of each helix is the angle between the x axis and the vector pointing from the centerline to the point of origin. The relative azimuthal angle between the two α-helices is defined as $\delta\phi = \Phi_1 - \Phi_2 - 2\pi(Z_1 - Z_2)/H$. The net charge of these zwitterionic helices is zero.

$$S_{n,m}^{\nu,\mu}(k_z) = \frac{4\pi l_B}{L} \sum_{i,j} q_i q_j \frac{s_{i,j}^{\nu,\mu}(k_z,n,m)}{(\tilde{\kappa}a)^2 K_n'(\tilde{\kappa}a) K_m'(\tilde{\kappa}a)}. \tag{47}$$

Here $s_{i,j}^{\nu,\mu}(k_z,n,m)$ are the structure factors only for fixed charges and condensed counterions. The effect of the image charges in Eq. (47) was taken into account by solving the corresponding electrostatic problem (Kornyshev and Leikin, 1997) [cf. Eqs. (46) and (47)]. Complete expressions for $S_{n,m}^{\nu,\mu}(k_z)$ at any thickness of the layer of fixed charges and condensed counterions layer can be found in the EPAPS Document in the Reference section.

B. Parallel zwitterionic helices in a nonpolar environment

Consider the electrostatic interaction between backbones of two α-helices inside a protein (Fig. 5). Since the α-helix backbone does not have a net charge, $S_{n,m}^{\nu,\mu}(k_z) = 0$ at $n = m = 0$. In this simplest case we deal with helical structures considered in Sec. IV.A. Here we have no counterions and only two types of charged groups, which are oppositely charged. Using the equations given in Sec. II, we obtain the following structure factors:

$$s_{k,l}^{1,2}(k_z,n,m) = \frac{N_\alpha^2}{4\pi^2} e^{ik_z(k-l)H/2} \sum_{j,J=-\infty}^{\infty} \delta_{k_z jG-gn} \delta_{m,n+JG/g}, \tag{48}$$

where N_α is the total number for each type of charged group, h is the axial rise per charged group, $G = 2\pi/h$, and all other quantities are defined in Sec. IV.A. The structure factors obey the following relations: $s_{1,1}^{1,2}(k_z,n,m) = s_{2,2}^{1,2}(k_z,n,m)$ and $s_{1,2}^{1,2*}(k_z,n,m) = s_{2,1}^{1,2}(k_z,n,m)$, where the asterisk denotes complex conjugation. Then, after substitution into Eq. (47) and, in turn, Eq. (43), we may obtain the interaction energy. At $gR > 1$, all harmonics except for $n = \pm 1$, $J = 0$, and $j = 0$ may be neglected and

$$\frac{E(R)/L}{k_B T} \approx -\tilde{u}_1 \cos(\delta\phi) K_0(gR). \tag{49}$$

Here we introduced a phase shift between the helices, $\delta\phi = \Phi_1 - \Phi_2 - 2\pi\delta Z/H$ (cf. Fig. 5) and

$$\tilde{u}_1 = 16(l_B/l_c^2)[I_1(ga)]^2 \approx 5.0 \times 10^4 \text{ nm}^{-1}, \tag{50}$$

where l_c is the length per unit charge for each type of charge group since the net charge of the molecule is zero. Provided that their most favorable alignment ($\delta\phi = 0$) is not hindered by collisions between side chains, the two helices will lock into it. This alignment forms an electrostatic zipper (Kornyshev and Leikin, 1999) with a lock-in pair of negative and positive charges on opposing helices repeating every half turn (Fig. 5). The strength of this zipper is $\sim(2-6)k_BT/\text{nm}$ at $R \approx 7-8$ Å (the separation between α-helices without bulky side chains). Since the typical length of an α-helix is $\sim 2-3$ nm, this interaction might be a significant force in protein folding, and it is not even remotely reminiscent of the interaction between two dipoles as described in biochemistry textbooks.

C. Parallel charged cylinders in an electrolyte solution

The more involved case of interactions in solution still challenges theory. Here we give a brief overview of known approximations, in terms of the formalism presented above.

1. Mean-field results

Within the mean-field approximation the counterion density near a homogeneously charged cylinder depends only on the distance from the cylinder axis, so that the charge density structure factors in Eq. (43) are not equal to zero only when $n = m = 0$ and $k_z = 0$, i.e., $S_{n,m}^{\nu,\mu}(k_z) \propto \delta_{n,0}\delta_{m,0}\delta(k_z)$.[6] The energy of interaction between two

[6]This is provided that the molecules are not too close to each other, so the condensed counterion distribution responsible for θ may be assumed to be uniform around the surface of each cylinder.

similar cylinders (Kornyshev and Leikin, 1997, 1999) reduces to

$$\frac{\langle E_{\rm cyl}\rangle/L}{k_BT} \approx 2(1-\theta)^2 \frac{l_B}{l_c^2}\left(\frac{K_0(\kappa_D R)+\Omega_{0,0}(\kappa_D R,\kappa_D a)}{(\kappa_D a)^2[K_1(\kappa_D a)]^2}\right), \tag{51}$$

where θ is determined by the radial distribution of condensed counterions. When condensed counterions are localized within a thin layer δa close to the cylinder surface ($\delta a \ll a,\lambda_D$), θ is approximately the fraction of the molecular charge neutralized by them. An expression for θ can be found in the EPAPS Document in the Reference section.

The classical expression for $E_{\rm cyl}$ derived within the DH approximation (Brenner and Parsegian, 1974) is recovered from Eq. (51) by neglecting the nonlinear effects of screening (i.e., no counterion condensation so that $\theta=0$) and the image forces. Results corresponding to the standard and modified PB theories are recovered by calculating the appropriate θ. When the nonlinear screening layers around the two molecules do not overlap, θ is practically independent of R and its calculation is straightforward (see the EPAPS Document in the Reference section). The theory can be extended to smaller separations as well, where θ becomes dependent on R. However, such cases are important primarily for multimolecular assemblies, where a different approach becomes more accurate and practical (see Sec. VI).

As one would expect, the mean-field force between two cylinders of the same charge is always repulsive, regardless of the surface charge density. However, under certain conditions, counterion density fluctuations and correlations between counterions can lead to attraction (Kirkwood and Schumaker, 1952; Oosawa, 1968; Attard *et al.*, 1988; Marčelja, 1992; Barrat and Joanny, 1996; Kjellander, 1996; Rouzina and Bloomfield, 1996; Grønbech-Jensen *et al.*, 1997; Ha and Liu, 1997, 1998, 1999a; Arenzon *et al.*, 1999, 2000; Golestanian *et al.*, 1999; Levin *et al.*, 1999; Shklovskii, 1999a, 1999b; Solis and de la Cruz, 1999; Lau *et al.*, 2000, 2001; Diehl *et al.*, 2001; Golestanian and Liverpool, 2002; Lau and Pincus, 2002; Levin, 2002; Naji and Netz, 2004; Naji *et al.*, 2004, 2005). The origin of the attractive forces can be understood within the framework of Eq. (43).

2. Wigner crystal model

It is instructive to start the analysis of counterion fluctuation and correlation effects from the strong-coupling limit, when $\Xi \gg 1$ due to multivalent counterions and large surface charge density. It was conjectured that in this limit the energy of electrostatic repulsion between counterions confined at the cylinder surface might become sufficiently large to cause their quasicrystalline ordering (Rouzina and Bloomfield, 1996; Shklovskii, 1999a, 1996b). If this is true, such order will lead to peaks in the molecular structure factors $s^{\nu,\mu}(k_z,n,m)$ at wave numbers n,m and axial wave vectors k_z of the reciprocal lattice in cylindrical coordinates (see the EPAPS Document in the Reference section). Provided that the size of ordered counterion clusters is large enough, the structure factors can be approximated by the corresponding δ functions, and the integral in Eq. (43) can be easily calculated. At sufficiently large surface separations, where image forces may be neglected ($>\lambda_D$), the average energy per unit length between the cylinders is then given by (see the EPAPS Document in the Reference section)

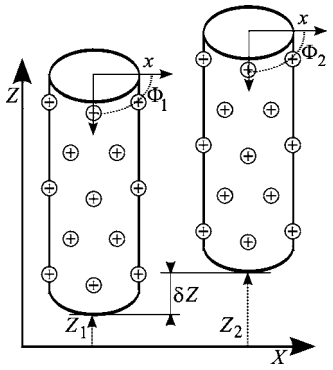

FIG. 6. Wigner crystal of ordered condensed counterions on uniformly negatively charged cylinders. The interaction energy is minimized when correlated counterions on one cylinder oppose correlation holes (negatively charged spaces between adsorbed counterions) on the other. Such a configuration may result in attraction even if there is a net charge on the cylinders.

$$\begin{aligned}\frac{E_{\rm els}(R)/L}{k_BT} &= \tilde{E}_{0,0,0} \\ &\quad - \theta\sum_J \tilde{E}_{J,J,2J}[\cos(2Jn_W\Phi_1) \\ &\quad + \cos(2Jn_W\Phi_2)] \\ &\quad + \theta^2 \sum_{J,J',j} \tilde{E}_{J,J',j}\cos[jn_W(\pi-\Phi_1) \\ &\quad + (2J'+j)n_W\Phi_2 + (2J-j)k_Z\delta Z],\end{aligned} \tag{52}$$

where n_W is the smallest azimuthal wave number and k_Z is the smallest axial wave vector of the Wigner crystal,

$$\tilde{E}_{J,J',j} = \frac{2l_B}{l_c^2}\frac{K_{2J'n_W}(\kappa_{J,j}R)}{(\kappa_{J,j}a)^2 K'_{jn_W}(\kappa_{J,j}a)K'_{(j-2J')n_W}(\kappa_{J,j}a)}, \tag{53}$$

$$\kappa_{J,j} = \sqrt{\kappa_D^2 + (j-2J)^2 k_Z^2}. \tag{54}$$

Equation (52) describes the interaction energy between two parallel uniformly charged cylinders of low dielectric constant for arbitrary azimuthal (Φ_1 and Φ_2) and axial ($\delta Z = z_1 - z_2$) orientations of the Wigner-crystal layers of condensed counterions on their surfaces (Fig. 6). The first term is the contribution from the interaction between "naked" cylinders (without counterions). The second term is the interaction of the counterion crystal on each cylinder with the naked charge of the other cylinder. The third term is the interaction between counter-

ion crystals. The sums in the second and third terms rapidly converge and can be truncated, retaining only the modes $j=0,\pm1,\pm2$ and $J,J'=0,\pm1$.

At $\theta\approx1$, the interaction energy is determined primarily by harmonics with at least one nonzero index (j, J, or J'), which are repulsive or attractive depending on the mutual alignment of the Wigner crystals. The optimum alignment in the ground state is obtained by minimizing the energy given by Eq. (52) with respect to Φ_1, Φ_2, and δZ. At this alignment, counterions on one cylinder interlock with correlation holes (spaces between condensed counterions) on the other cylinder (Fig. 6) and the net interaction becomes attractive [as conjectured by Rouzina and Bloomfield (1996) and Shklovskii (1999a, 1999b)]. However, this ground-state attraction may be significantly weakened by thermal fluctuations. (The energy of a hexagonal array of cylinders with interlocked Wigner crystals calculated at $\theta=1$ is plotted in Fig.22. These results are discussed in the context of DNA condensation in Sec. VII.B.)

The idea of attraction between two similarly charged surfaces in electrolyte solution due to ordering of multivalent counterions was initially studied by Guldbrand *et al.* (1984) and Kjellander and Marčelja (1984). It was later reapplied to the problem of DNA condensation based on a modified calculation of forces between flat surfaces (Rouzina and Bloomfield, 1996) and rough estimates of cohesion energy, but still relying on the known properties of 2D Wigner crystals (Shklovskii, 1999a, 1999b; Grosberg *et al.*, 2002). It was never rigorously analyzed for the cylindrical geometry. However, unlike the 2D geometry where a quasicrystalline (hexatic) long-range order of counterions is possible, no long-range order can exist in one dimension because of diverging thermal fluctuations (Landau and Lifshitz, 1969). Local quasicrystalline ordering of counterions in the quasi-1D cylindrical geometry might exist (this will inevitably depend upon the radius of the cylinder), but so far no rigorous theoretical estimates for the possible range of such order have been reported. Numerical simulations of cylinders with a DNA-like surface charge density found no significant axial correlations beyond nearest neighbors even for trivalent counterions (Deserno *et al.*, 2003), calling into question the application of the Wigner-crystal idea to interaction between two DNA molecules in solution (we return to application of this idea to DNA aggregates in Sec. VII).

3. Standing charge-density waves

Numerical simulations also suggest that a different type of counterion ordering, an azimuthal standing charge-density wave, might form (Deserno *et al.*, 2003). The physics of this phenomenon can be rationalized as follows. The basic set of harmonics for charge-density variation on a cylinder is $\exp(in\phi+ik_z z)$, where n and k_z are the corresponding wave number and wave vector. Equation (43) may thus represent the energy of interaction between two cylinders as a sum of interactions between such charge-density waves (CDWs). The energy of direct interaction between two CDWs with the same k_z at sufficiently large surface separations ($>\lambda_D$) in aqueous solution is given by (Kornyshev and Leikin, 1997, 1999; EPAPS Document)

$$\langle E^{n,m}_{\mathrm{CDW}}/L\rangle \propto (-1)^m\langle\cos(n\phi_1-m\phi_2-k_z\delta Z)\rangle \times K_{n-m}(R\sqrt{\kappa_D^2+k_z^2}), \tag{55}$$

where $\delta Z=z_1-z_2$, and z_ν and ϕ_ν are the axial and azimuthal phases of the CDW on the molecule ν. Provided that the most favorable alignment between CDWs can be established and is not destroyed by thermal fluctuations, $(-1)^m\cos(n\phi_1-m\phi_2-k_z\delta Z)=-1$ and the two CDWs attract each other.

It is worthwhile to emphasize the following property of interaction between CDWs in cylindrical geometry. The attraction between purely azimuthal CDWs ($k_z=0$) decays exponentially with a characteristic length equal to the Debye length [in most cases $\kappa_D R\gg1$ and $K_{n-m}(\kappa_D R)\propto\exp(-\kappa_D R)$]. As follows from Eq. (55), the CDW-correlation attraction decays exponentially with a characteristic length dependent on k_z but not on the azimuthal conjugate n. In contrast, the CDW-mediated force between flat 2D surfaces or between 1D lines always decays exponentially with the characteristic length $(\kappa_D^2+\mathbf{k}^2)^{-1/2}$, where $\mathbf{k}$ is the CDW wave vector. The reason for the qualitatively different interaction between CDWs in the cylindrical geometry and 2D surfaces or 1D lines is that azimuthal correlations cannot exist for these latter geometries. As shown throughout the remainder of this review, azimuthal correlations between rodlike macromolecules appear to be crucial in many phenomena.

Note that the correlation between axial or mixed ($k_z\neq0$) CDWs requires axial order at distance scales much larger than $2\pi/\kappa_D$ (for $k_z>\kappa_D$ the interaction rapidly decreases). As mentioned above, such order appears to be destroyed by thermal fluctuations at physiological temperature. Detailed numerical simulations suggest that the contribution of the axial charge-density waves to the intermolecular force between two homogeneously charged cylinders is very small even for trivalent counterions (Deserno *et al.*, 2003). However, the correlation between azimuthal CDWs does not require axial order and is thus less affected by thermal fluctuations.

Overall, one might expect strongly correlated azimuthal CDWs to form and significantly reduce the interaction energy of the cylinders when (i) the cylinder diameter is comparable to the average distance between counterions, (ii) the interaction between nearest-neighbor counterions is much stronger than k_BT, and (iii) the surface separation between the two cylinders is comparable to the Debye length. All these conditions seem to be satisfied for the interaction between DNA-like cylinders in the presence of trivalent counterions. Indeed, numerical simulations of such cylinders revealed formation of static (standing) azimuthal CDWs, resulting in preferential condensation of counterions between the cylinders and intermolecular attraction (Deserno *et al.*, 2003).

4. Counterion fluctuations

Even in the absence of a static counterion structure, correlated dynamic fluctuations will still create energetically favorable oppositions between correlation holes on one cylinder and adsorbed counterions on the other cylinder. The corresponding correlation attraction was first calculated within the Gaussian approximation in 1D models for the density fluctuations of condensed counterions (Oosawa, 1968; Barrat and Joanny, 1996; Ha and Liu, 1997, 1998, 1999a). However, it was later pointed out that the approximation of unconstrained Gaussian density fluctuations leads to a wrong temperature dependence of the force (Ha and Liu, 1999b; Levin *et al.*, 1999). Such an approximation is valid only in the high-temperature limit, corresponding to an ideal gas description of condensed counterions (Barrat and Joanny, 1996). This limit is incompatible with the counterion condensation requirement (Levin *et al.*, 1999). Models of constrained Gaussian fluctuations recovered the expected temperature dependence, predicting decreasing rather than increasing amplitude of the force with temperature (Arenzon *et al.*, 1999; Ha and Liu, 1999a).

Essentially, the physics of the force is the same as in the Wigner crystal model, which corresponds to the ground state of the system, but the forces are much weaker because of the liquidlike counterion density fluctuations. Note that similar forces were also calculated for charged, flat surfaces (Attard *et al.*, 1988), where it was also pointed out that additional constraints must be imposed on Gaussian fluctuations in order to recover the correct low-temperature limit (Leikin, 1991). In both cases—for 1D charged rods and 2D surfaces—*ad hoc* models of constrained Gaussian fluctuations were used. This reflected the inherent difficulty of describing correlation functions for density fluctuations in a liquid. While useful for understanding the underlying physics, such models might be unreliable for predicting the strength of the force for real systems.

On a cautionary note, it is also useful to keep in mind that quasi-1D theories (Grønbech-Jensen *et al.*, 1997; Ha and Liu, 1997, 1998, 1999a; Arenzon *et al.*, 1999, 2000) and simulations (Stevens, 1995, 1999, 2001) do not allow for the possibility of azimuthal counterion density fluctuations. The latter, as discussed above and indicated by numerical simulations in the cylindrical geometry (Deserno *et al.*, 2003), might play a more important role than the axial fluctuations captured by 1D or quasi-1D models. We are not aware of corresponding theories for counterion fluctuation forces in a true cylindrical geometry.

D. Parallel, rigid, ideal helices in an electrolyte solution

1. Mean-field results

One common lesson from the different models discussed above is that patterning of surface charge and counterions might drastically change the interaction between rods. In molecules with preexisting helical patterns of surface charges such effects become even more rich and nontrivial. At the same time, the symmetry of helical patterns significantly simplifies their theoretical analysis. Here, the mean-field approximation corresponds to the explicit description of the helical pattern of fixed molecular charges and the mean-field assumption that condensed counterions simply follow the helical symmetry of the molecule. The corresponding theory for ideal, rigid helices was developed by Kornyshev and Leikin (1997, 1999).

To illustrate the main results of this theory, consider the interaction between two ideal, identical DNA-like double helices in electrolyte solution (Fig. 7). Now, at surface-to-surface separations larger than λ_D, the coun-

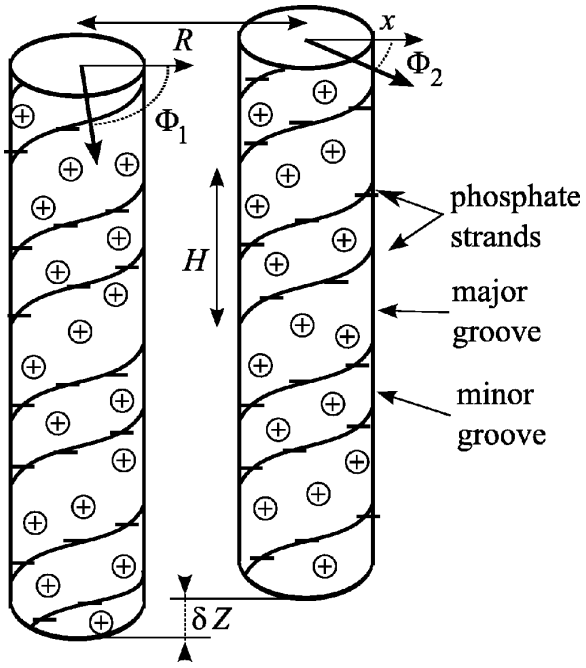

FIG. 7. Schematic diagram for interacting parallel DNA molecules with ideal, negatively charged double helical backbones (phosphate strands) and counterions absorbed in the major and minor grooves. The azimuthal Φ_ν and axial Z_ν coordinates of each molecule are defined with respect to a reference cross section as the azimuthal coordinate of the middle of the minor groove and the height of the cross section, respectively. The reference cross sections for the two molecules are selected consistently so that the backbone of one molecule is completely superimposed onto the backbone of the other molecule upon a lateral shift by **R**, azimuthal rotation by $\Phi_2-\Phi_1$, and axial shift by δZ. The interaction depends only on $\delta\phi=\Phi_1-\Phi_2-2\pi\delta Z/H$. In this diagram, a value of $\delta\phi=0$ is shown, which minimizes the interaction energy at large R by maximizing energetically favorable interactions between negatively charged strands on one molecule and positively charged grooves on the other molecule. The ideal helical structure of the backbones results in the same alignment repeating with the axial periodicity H, creating an electrostatic zipper. Unlike the simpler zipper that locks in opposing negatively and positively charged groups on single-stranded helices at $\delta\phi=0$ regardless of R (cf. Fig. 5), the optimal alignment between the double helices depends on R. The alignment with $\delta\phi\neq 0$ becomes energetically favorable at small R [Eq. (60)].

terion structure factors will not depend on R. Furthermore, the only peaks in $s_{n,m}^{\nu,\mu}(k_z)$ important for calculation of the interaction energy are those with the smallest values of k_z and n. The weighted sum of the structure factors for counterions and phosphates at relevant k_z and n may be written as[7]

$$S_{n,m}^{\mu,\mu}(k_z) = S_{n,m}^{\nu,\mu}(k_z) \approx \frac{2l_B}{l_c^2}\frac{[(1-\theta)^2\delta_{n,0} + \zeta_n^2(1-\delta_{n,0})]\delta_{n,m}\delta(k_z+gn)}{(\tilde{\kappa}a)^2 K_m'(\tilde{\kappa}a)K_n'(\tilde{\kappa}a)}, \tag{56}$$

where ζ_n are the helical moments of the density of fixed charges and condensed counterions on each molecule introduced in Sec. IV.D.

Substitution of this expression into Eq. (43) gives the desired result. If we take into account that at all reasonable distances only the modes with $n=0$, $n=\pm 1$, as well as $n=\pm 2$ are important, but all other ones can be neglected (Kornyshev and Leikin, 1997), it reads

$$\frac{\langle E(R)\rangle}{Lk_BT} \approx u_{\rm cyl}(R) + u_{\rm image}(R) - u_1(R)\cos(\delta\phi) + u_2(R)\cos(2\delta\phi). \tag{57}$$

The first term in this energy $u_{\rm cyl}(R)=\langle E_{\rm cyl}(R)/L\rangle/k_BT$ is given by Eq. (51). It corresponds to approximating DNA by homogeneously charged cylinders. The second term

$$u_{\rm image}(R) \approx \frac{4l_B}{l_c^2}\sum_{n=1}^{2}\zeta_n^2\frac{\Omega_{n,n}(\kappa_n R,\kappa_n a)}{(\kappa_n a)^2[K_n'(\kappa_n a)]^2} \tag{58}$$

is the helical part of the image interaction of one molecule with the core of the other. The corresponding force is always repulsive. The third and fourth components

$$u_n(R) \approx \frac{4l_B}{l_c^2}\zeta_n^2\frac{K_0(\kappa_n R)}{(\kappa_n a)^2[K_n'(\kappa_n a)]^2}, \quad n=1,2, \tag{59}$$

are the first two helical harmonics of the energy of fixed charges and adsorbed counterions on one molecule in the electric field created by the other molecule. The corresponding force and even its sign depend on the mutual azimuthal alignment of the molecules $\delta\phi$ (cf. Fig. 7).

The dependence of the pair interaction potential on the fixed charge and counterion pattern is reduced to just three dimensionless coefficients, the effective charge neutralization fraction (θ) and the first two helical moments of the charge pattern (ζ_1 and ζ_2). For DNA, $l_c \approx 1.7$ Å and we expect $(1-\theta)^2 \leqslant l_c^2/l_B^2 \approx 0.06$ (Sec. IV.B). Multivalent counterions, polycounterions, and chemisorption can further reduce $(1-\theta)^2$, and completely neutralize or even invert the helix charge (Bloomfield, 1996). At the same time, we expect $\zeta_n \sim 1$ regardless of the counterion pattern (unless all of them bind directly onto phosphate strands). For completely delocalized counterions ζ_n are determined only by the fixed charge pattern and $\zeta_1 \approx 0.31$ and $\zeta_2 \approx -0.81$ (Sec. IV.D). Analysis of Eq. (40) or more general expressions for ζ_n (EPAPS Document) shows that ζ_1^2 increases upon preferential condensation and/or adsorption of counterions in the major groove and decreases upon preferential adsorption in the minor groove, while ζ_2^2 increases upon any counterion localization off the phosphate strands.

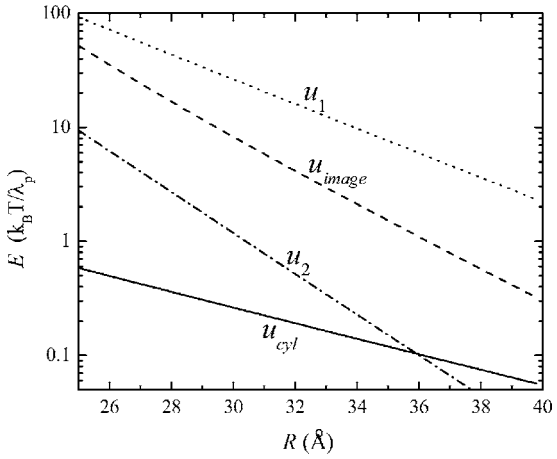

FIG. 8. Electrostatic contributions to the interaction energies given by Eqs. (51), (58), and (59). The interaction energies shown demonstrate the relative importance of including the higher-order helical harmonic contributions in the overall interaction. Here it is assumed that counterions compensate 95% of the DNA phosphate charges, i.e., $\theta=0.95$, and the helical harmonics are set to $\zeta_n=1$. (For this calculation and subsequent calculations, unless noted, the radius of DNA is taken to be $a=9.5$ Å and the Debye screening length is set to $\kappa_D^{-1}=7$ Å.) Note the faster decay for higher-order helical harmonics.

The plots of $u_{\rm cyl}(R)$, $u_{\rm image}(R)$, $u_1(R)$, and $u_2(R)$ show that neither of these interaction components can be neglected *a priori* at relevant distances (Fig. 8). Furthermore, at $\theta > 0.9$ (possible in the presence of divalent, multivalent, or poly-cations), $u_{\rm cyl}(R)$ is the *weakest* of the four components in this distance range. In other words, it appears that DNA might actually behave like the double helix predicted by Watson and Crick rather than the homogeneously charged cylinder of traditional polyelectrolyte theories. Analysis of various experimental observations based on this interaction potential seems to confirm this conclusion (see Secs. VI and VII).

At the optimal azimuthal alignment $\delta\phi=\delta\phi_{\rm min}$ the interaction described by $u_1(R)$ and $u_2(R)$ is attractive. The attraction is caused by "interlocking" of separated positively charged grooves and negatively charged strands

[7]The contribution of the structure factors with $n \neq m$ [Eq. (47)] can be neglected at $H/h \gg 1$ (e.g., $H/h=10$ for DNA) because only the harmonics with the smallest n and m contribute to the interaction. One should not even be concerned about small corrections arising from nondiagonal harmonics in ideal, rigid helices since the corresponding contributions to the energy are completely washed out by thermal fluctuations (see Sec. VI.G). As a result, the molecules behave as if their helical charge patterns were continuous rather than discrete (cf. the continuous helix model in Sec. IV.D).

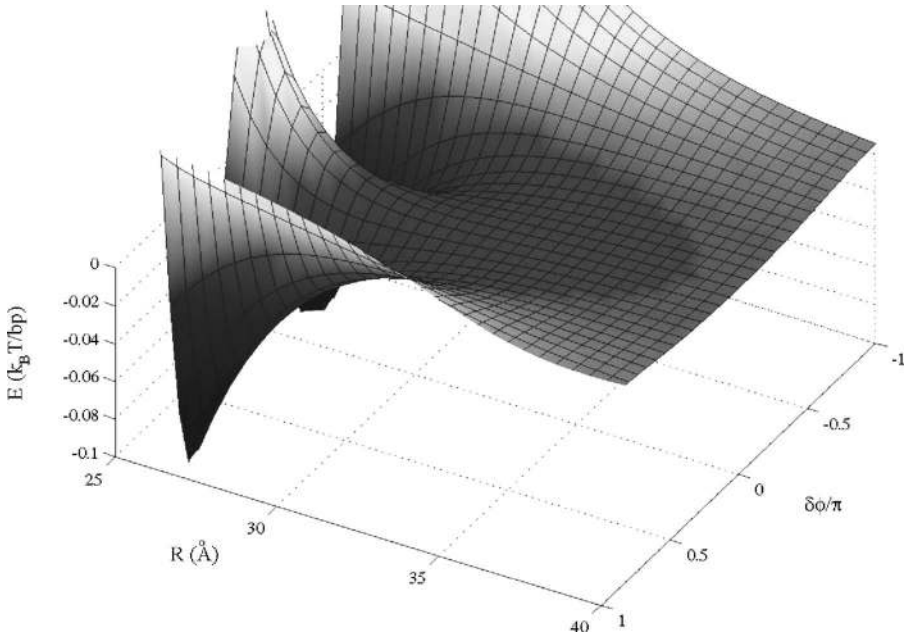

FIG. 9. Interaction energy between two DNA molecules with ideal helical backbones as a function of the interaxial separation R and the relative azimuthal orientation $\delta\phi$ between molecules calculated at $\theta=0.9$ and ζ_n corresponding to 40%:60% minor:major groove distribution [Eq. (40)]. The surface plot shows a bifurcation point at $R\sim 35$ Å, $\delta\phi=0$, resulting from azimuthal frustration in the interaction potential due to the competition between the first and second helical harmonics (u_1 and u_2) in Eq. (57). At larger R, a single $\delta\phi=0$ optimizes the energy. At smaller R, the energy is optimized at two finite $\delta\phi$ given by Eq. (60). At $R<25$ Å (not shown), the interaction becomes repulsive due to the contribution of image forces and possible hard-core clashes between residues on opposing molecules.

on opposing surfaces. The interlocking repeats regularly every half turn of the helix, forming an electrostatic zipper (cf. Fig. 7). The periodicity of the zipper is stabilized by the molecular structure. It is not destroyed by temperature as long as the helix structure remains intact. Counterion-correlation attraction (Sec. V.C) involves interlocking of adsorbed ions and correlation holes. In contrast to the helical electrostatic zipper, it relies exclusively on counterion correlations. Thus it is more easily destroyed by thermal fluctuations. For instance, as shown by numerical simulations, the axial order of interlocked counterion-correlation pairs does not extend much beyond nearest neighbors (Deserno *et al.*, 2003).

The zipper formed by two double-stranded DNA molecules, however, is more complex than the zipper formed by single-stranded α-helices. Its configuration (optimal $\delta\phi$) depends on the interaxial distance. At large separations all helical harmonics, except for $n=1$, are suppressed so that the charge pattern on each molecule effectively blurs into a single helix and $\delta\phi_{\min}=0$. At closer approach, however, the individual strands become distinguishable and the helical harmonic with $n=2$ (for which $\delta\phi_{\min}=\pi/2$) becomes more important. As a result, the optimal alignment approaches $\delta\phi_{\min}\approx\pi/2$ at closest separation. Indeed, from Eq. (57) we find that the optimal azimuthal alignment is given by

$$\delta\phi_{\min}=\begin{cases}\pm\arccos[u_1(R)/4u_2(R)], & R\leqslant R_*\\ 0, & R\geqslant R_*,\end{cases} \tag{60}$$

where R_*, determined by $u_1(R_*)=4u_2(R_*)$, will be referred to as the frustration point [the ratio $u_1(R_*)/4u_2(R_*)$ increases monotonically with increasing R].

The shape of the pair interaction potential is shown by the surface plot in Fig. 9. On this plot, the frustration point shows up as a bifurcation, at which a single potential energy valley (at $R>R_*$) splits into two (at $R<R_*$). The azimuthal correlations and the spontaneous loss of symmetry at $R=R_*$ appear to play an important role in a variety of phenomena observed in DNA aggregates (Sec. VI).

2. Counterion correlations and fluctuations

As suggested by the studies of pointlike counterions condensed onto homogeneously charged cylinders (Sec. V.C), the effects of correlations and fluctuations are expected to become strong when the counterion charge is $|q|\geqslant 3$. In the context of biologically relevant interactions between helices, such counterions are not common (Sec. IV) so that the corresponding effects have not been carefully explored yet. For instance, the only reasonably pointlike $\geqslant 3+$ counterions commonly used in DNA studies are cobalt-amine complexes. The latter are fairly large spheres that bind extremely specifically to certain sites on DNA (Secs. IV.C and VII.A), and they might not be amenable to modeling within the recently advanced counterion correlation and fluctuation theories.

It is worth mentioning that a periodic pattern of fixed surface charges on a flat surface has a significant effect on the pattern of condensed counterions (Moreira and Netz, 2002), including the structure of Wigner crystal, if

the latter is formed. But, to the best of our knowledge, the corresponding effects of helical patterns of fixed charges on a cylinder surface have not been explored. Even more interesting might be a possible coupling between the helical structure and azimuthal and axial standing CDWs. These might enhance counterion fluctuations and result in the appearance of standing CDWs even with more common divalent counterions. It is possible, for example, that the standing axial CDWs of Ba^{2+} observed in aggregates of actin filaments (Angelini *et al.*, 2003, 2005) are a product of such coupling. Development of the theory in this context would be particularly important.

E. Parallel nonideal helices

Motivated by experimental observations, so far the theoretical efforts beyond the mean-field, idealized helix model have been focused on the analysis of interactions between nonideal DNA-like helices with sequence-dependent structure (Kornyshev and Leikin, 2001; Cherstvy *et al.*, 2004; Kornyshev and Wynveen, 2004) and effects of thermal fluctuations in the helix structure (Lee, Wynveen, and Kornyshev, 2004) rather than density of condensed counterions. It was demonstrated, for example, that the sequence-dependent intrinsic twist (Sec. II.E) and its elastic relaxation and thermal fluctuations have dramatic effects on DNA-DNA interactions.[8] In particular, homologous (approximately or exactly identical) sequences interact differently from nonhomologous ones (with uncorrelated base-pair sets).

Interaction between nonhomologous DNA. The nonideality of DNA structure leads to two related effects discussed in Sec. II: (i) it broadens the peaks in the molecular structure factors [Eq. (16)] and (ii) it results in an accumulating deviation of the azimuthal phase of the helix from the ideal one [Eq. (15)]. Indeed, whereas the interaction between ideal helices is described by the same energy density in each cross section, and the total energy is simply proportional to the juxtaposition length, for nonideal helices, the total energy is a functional of local values of $\delta\phi(z)$:

$$E\{\delta\phi(z);R\} = \int_0^L \tilde{E}\{\delta\phi(z),R\}dz, \tag{61}$$

where $\tilde{E}$ is the local energy density. In principle, it is composed of two parts; one is the electrostatic contribution and the other is the torsional elastic energy (Sec. III).

It is instructive to start the analysis of these effects from the limit of infinite torsional rigidity ($C_t \to \infty$), when they are completely determined by the base-pair sequence and not affected by torsional fluctuations.

[8]While intrinsic and thermal bending might also be important at larger separations, their effects are not expected to be as dramatic, at least in aggregates. Therefore these effects have not been carefully studied yet.

The accumulation of twist mismatch for two parallel molecules of length L with uncorrelated base-pair sequences may be written as (Cherstvy *et al.*, 2004)

$$\langle[\delta\phi(z) - \delta\phi^0]^2\rangle = L/2\lambda_c, \tag{62}$$

where $\delta\phi^0 = \langle\delta\phi\rangle$, $\langle\cdots\rangle$ indicates ensemble averaging over possible sequences, and λ_c is the helical coherence length of DNA defined in Sec. II.E. Equation (62) is analogous to accumulation of twist error for single nonideal helices [cf. Eq. (15)]. Estimates made in Sec. II.E suggest that $\lambda_c \gg H$. Provided this is the case, we do not need to use the structure factors calculated for nonideal helices (Secs. II.E and II.F). Instead, we approximate the latter with expressions derived for ideal helices, but take into account that $\delta\phi$ slowly varies with z rather than remaining constant. Using Eq. (57) with the z-dependent $\delta\phi$ to calculate $\tilde{E}\{\delta\phi(z),R\}$, we find (Kornyshev and Leikin, 2001)

$$\frac{E_{\rm el}(R,\{\delta\phi\})}{k_BT} \approx u_{\rm cyl}(R)L + u_{\rm image}(R)L - u_1(R)\int_0^L \cos[\delta\phi(z)]dz + u_2(R)\int_0^L \cos[2\delta\phi(z)]dz. \tag{63}$$

Here the electrostatic energy $E_{\rm el}(R,\{\delta\phi\})$ is still averaged over counterion density fluctuations but not over possible sequences.

For identical sequences and sufficiently long uncorrelated sequences, we can approximate the integrals by

$$\int_0^L \cos[n\,\delta\phi(z)]dz \approx L\cos(\delta\phi^0)\times\left\{1 - s_h\left[1 - \exp\left(-\frac{n^2L}{4\lambda_c}\right)\right]\right\}, \tag{64}$$

where we used the random-walk properties of the intrinsic twist angles (Sec. II.E) and introduced a sequence homology factor s_h. Because the intrinsic twist profile is a *unique* fingerprint of a DNA sequence, $s_h = 0$ only upon juxtaposition of identical sequences; $s_h \approx 0$ for homologous sequences (which are close to being identical) and $s_h = 1$ for uncorrelated sequences. Then,

$$E_{\rm el}(R,\{\delta\phi\}) \approx E_{\rm el}^{\rm id}(R,L) + s_h\Delta E_{\rm el}^{\rm rec}(R,L), \tag{65}$$

where $E_{\rm el}^{\rm id}(R,L)$ is the electrostatic interaction energy between ideal helices [Eqs. (57)–(59)] and

$$\frac{\Delta E_{\rm el}^{\rm rec}(R,L)/L}{k_BT} = u_1(R)\cos(\delta\phi^0)\left[1 - \exp\left(-\frac{L}{4\lambda_c}\right)\right] - u_2(R)\cos(2\delta\phi^0)\left[1 - \exp\left(\frac{L}{\lambda_c}\right)\right] \tag{66}$$

is the recognition energy, i.e., the difference between

the interaction energy for uncorrelated sequences and for identical sequences (the latter equal to $E_{\rm el}^{\rm id}$). A slightly different result for $\Delta E_{\rm el}^{\rm rec}$ was reported by Kornyshev and Leikin (2001) in the approximation when azimuthal orientations were fixed at one of the ends $[\delta\phi(z=0)=0]$.

Two important conclusions follow from this analysis: (i) two DNA fragments can recognize sequence homology through electrostatic interactions and (ii) long, rigid, uncorrelated sequences cannot maintain the alignment of strands and grooves required for the electrostatic zipper attraction over a juxtaposition length larger than $4\lambda_c$. In the latter case we lose both $u_1(R)$ and $u_2(R)$, so that very long rigid molecules behave more like uniformly charged rods.

Whereas the helical symmetry of the molecules affects the recognition law, the qualitive idea of this effect does not depend specifically on helicity. Any pattern of positive and negative charges on a molecular surface interacts more favorably with a complementary pattern on the opposing surface.

Torsional adaptation. However, to regain an energetically favorable attraction, real molecules (with finite torsional rigidity C_t) can adjust the azimuthal phase shift $\delta\phi(z)$ at the cost of the elastic torsional energy

$$\frac{E_{\rm tors}\{\delta\phi\}}{k_BT}=\frac{l_p}{4}\int_0^L\left(\frac{d\,\delta\phi(z)}{dz}-\delta g(z)\right)^2dz, \tag{67}$$

where $l_p=C_t/k_BT$ is the torsional persistence length, $\delta g(z)=g_1(z)-g_2(z)$, and $g_\nu(z)=\Omega_\nu(z)/h$ is the local sequence-dependent intrinsic twist of each DNA (Secs. II.E and III.A). Equations (63) and (67) define the new total interaction energy

$$E(R,\{\delta\phi\})=E_{\rm el}(R,\{\delta\phi\})+E_{\rm tors}\{\delta\phi\} \tag{68}$$

which is affected by both the quenched disorder $\delta g(z)$, as well as thermal fluctuations in $\delta\phi$.

Minimization of this energy in the ground state yields a nonlinear Euler-Lagrange equation (Kornyshev and Leikin, 2001), which is reminiscent of the well-known sine-Gordon equation (Strogatz, 1994)

$$\frac{d^2(\delta\phi)}{dz^2}-\frac{2u_1}{l_p}\sin(\delta\phi)\left\{1-\frac{4u_2}{u_1}\cos(\delta\phi)\right\}=\frac{d}{dz}(\delta g) \tag{69}$$

except with more complex nonlinearity and an "external field" $d(\delta g)/dz$. Without the right-hand side, this equation has a few solutions—the trivial solution with constant $\delta\phi$, kink solitons, as well as "breather" solutions (Bishop, 1978). Breathers can be neglected in first approximation, as the energy associated with them is larger than that of kink solitons. The solitons emerging here may be split into two kinds: (i) large solitons (with a variation of 2π), and (ii) small solitons (with a variation of $\delta\phi$ between the values of $\pm\arccos[u_1(R)/4u_2(R)]$) when the separation between helices is such that $R<R^*$ (Kornyshev and Wynveen, 2004). Both solutions have a higher energy than the trivial one, as long as the right-hand side is zero (identical or homologous sequences). If the right-hand side is nonzero, the balance between these modes of response becomes a complicated mathematical problem (Cherstvy *et al.*, 2004; Kornyshev and Wynveen, 2004). Some simplified approaches to it, however, have revealed the following trends.

In a typical situation, the estimated probability of soliton formation is low, their contribution to the interaction energy is negligible, and one can assume slow accumulation of $\delta\phi$ with z (Kornyshev and Wynveen, 2004). A variational calculation of such $\delta\phi(z)$ in the ground state (Cherstvy *et al.*, 2004) and calculations of thermal fluctuations in $\delta\phi$ combined with Monte Carlo simulations (Lee, Wynveen, and Kornyshev, 2004) have shown that, in the simplest case of infinite juxtaposition between two molecules with uncorrelated sequences, the accumulation of $\delta\phi$ is described by

$$\langle[\delta\phi(z)-\delta\phi^0]^2\rangle\approx\lambda_h\left(\frac{1}{2\lambda_c}+\frac{1}{l_p}\right)\equiv\frac{\lambda_h}{2\lambda_{\rm eff}} \tag{70}$$

rather than by Eq. (62). As a result,

$$\left\langle\int_0^L\cos[n\,\delta\phi(z)]dz\right\rangle\approx L\cos(\delta\phi^0)\exp\left(-\frac{n^2\lambda_h}{4\lambda_{\rm eff}}\right) \tag{71}$$

replaces Eq. (64). Here the averaging $\langle\,\rangle$ is performed over possible realizations of $\delta g(z)$ as well as thermal torsional fluctuations. The values of λ_h and $\delta\phi^0$ are determined self-consistently from minimization of the resulting free energy. For full expressions, we refer the reader to Cherstvy *et al.* (2004); Lee, Wynveen, and Kornyshev (2004); EPAPS Document in the Reference section. However, in the limit of strong intermolecular interaction when $\lambda_h\ll 2\lambda_c$ and $\lambda_h\ll l_p$ (small R away from the frustration point), there is a closed-form result,

$$\lambda_h\approx\sqrt{\frac{l_p}{2[u_1(R)\cos(\delta\phi^0)-4u_2(R)\cos(2\delta\phi^0)]}}, \tag{72}$$

and $\delta\phi^0=\delta\phi_{\rm min}$, where $\delta\phi_{\rm min}$ is the optimal alignment between ideal helices [Eq. (60)].

It is important to realize that for torsionally flexible molecules the $n\neq 0$ helical harmonics are no longer washed out at $L\gg\lambda_c$. Instead, we see that the mean squared deviation $\delta\phi(z)$ is given by Eq. (70), where the torsional adaptation length λ_h is the maximum possible length over which there is a random-walk accumulation of $\delta\phi$. For $L\gg\lambda_h$ this process saturates, so that L in Eq. (62) is replaced by λ_h.

As follows from Eqs. (70) and (71), torsional adaptation limits the accumulation of the mismatch error in $\delta\phi$ due to sequence-dependent nonideality. The electrostatic zipper attraction is regained, provided that the torsional adaptation length is smaller than $4\lambda_c$. But, at the same time, increased torsional flexibility favors thermal fluctuations ($\lambda_h/l_p\propto T/\sqrt{C_t}$), which disrupt the attraction. Calculations based on a value of $C_t=3$–4×10^{-19} erg cm (Sec. III.C) showed that DNA is sufficiently flexible to

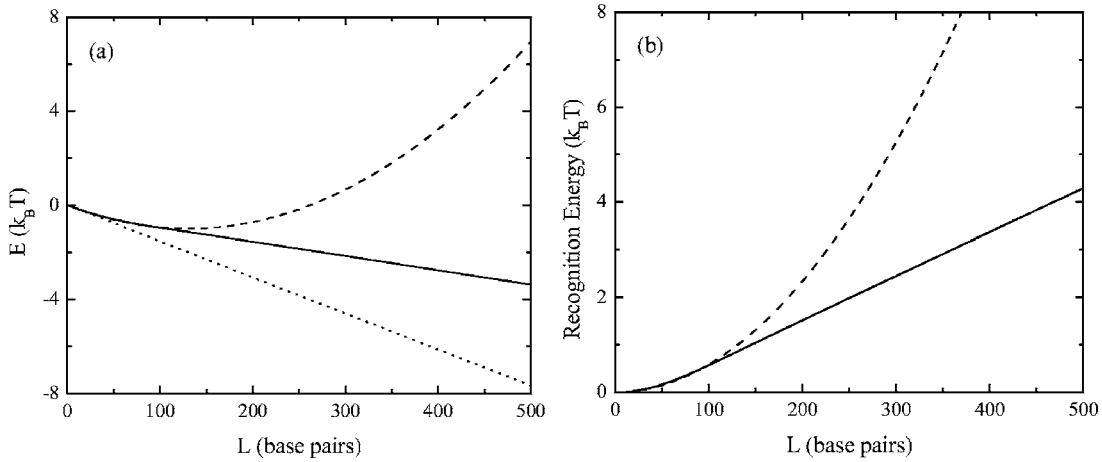

FIG. 10. (a) Pair interaction energy and (b) corresponding recognition energy for nonhomologous torsionally flexible (C_t=3 $\times 10^{-19}$ erg cm, solid line) and rigid ($C_t=\infty$, dashed line) molecules (Cherstvy *et al.*, 2004). The recognition energy [Eq. (66)] is defined as the difference in the pair energy between nonhomologous and homologous (short dashed line) molecular pairs. Results are shown for θ=0.8, ζ_n corresponding to 30%:70% minor:major groove distribution of condensed counterions [Eq. (40)], interaxial separation R=30 Å, and a helical coherence length $\lambda_c \sim 300$ Å. As shown, torsional flexibility reduces the recognition energy but does not totally eliminate it.

allow significant torsional adaptation yet is not too flexible for disruptive thermal fluctuations (Lee, Wynveen, and Kornyshev, 2004). As a result, the net interaction allows the formation of a well correlated, infinitely long electrostatic zipper. It becomes attractive upon strong counterion binding (although at larger θ), like the interaction between ideal helices.

Temperature-induced complementarity. An important consequence of the balance between torsional adaptation and fluctuations is that it leads to a nontrivial temperature dependence of the electrostatic zipper attraction. Indeed, thermal softening reduces C_t and $\lambda_h/2\lambda_c$ ($\propto\sqrt{C_t}$). Therefore this dependence enhances rather than reduces intermolecular attraction, similar to the effect described by Leikin and Parsegian (1994). At the same time, increasing temperature increases fluctuations ($\lambda_h/l_p \propto T/\sqrt{C_t}$). Eventually the latter would win out and the temperature would start reducing the attraction. However, estimates of the corresponding coefficients suggest that at practical conditions DNA interactions might be in the regime of the temperature-enhanced attraction.

Homology recognition. While torsional adaptation significantly reduces the difference, juxtaposition of nonhomologous sequences is still less energetically favorable than juxtaposition of identical or homologous sequences. Double-helical DNA can still recognize the sequence through electrostatic interactions. The dependence of the corresponding recognition energy on the juxtaposition length is shown in Fig. 10 (Cherstvy *et al.*, 2004). It becomes significant compared to k_BT for the juxtaposition length over ~50–200 bp even when two DNA molecules are separated by more than 10 Å of water.

F. Homology recognition in genetic recombination

The theory of electrostatic sequence homology recognition between double-helical DNA molecules prompted a highly speculative yet interesting hypothesis that this mechanism of sequence recognition might be involved in homologous recombination (Kornyshev and Leikin, 2001).

It is generally accepted that understanding recombination of genes is one of the greatest challenges of the postgenomic era (Royal Society Discussion, 2004). Recombination is a process in which fragments are exchanged between two parental copies of DNA. It is crucial for evolution and genetic diversity as well as for repair of damaged DNA. Only identical DNA regions with homologous sequences should be exchanged or used as a template for repair. Recombination mistakes lead to cancer, a variety of genetic diseases, and contributions to aging (Leach, 1996; Lewin, 1997). Fortunately, such mistakes are rare. The recognition of sequence homology occurs with amazing precision. In site-specific recombination, the exchange happens at specific, designated loci recognized by the complex recombination machinery of the cell (involving multiple proteins). In homologous recombination the exchange can occur anywhere. It was established that at least 50–200 bp homology is required for it (Fig. 11) (Singer *et al.*, 1982; Rubnitz and Subramani, 1984; Watt *et al.*, 1985; Shen and Huang, 1986). This ensures that the fragments belong to two alleles of the same gene rather than different genes. However, the mechanism of sequence homology recognition between such long DNA fragments is still unknown.

Textbooks tell us that "we know only one mechanism for nucleic acids to recognize one another on the basis of sequence: complementarity between single strands" (Lewin, 1997). Indeed, the breakage of double-stranded DNA and formation of single strands mediated by specialized proteins (e.g., the RecA family) is known to precede homologous recombination (Lewin, 1997). The single strand recognizes and invades a homologous double helix through hydrogen bond formation with

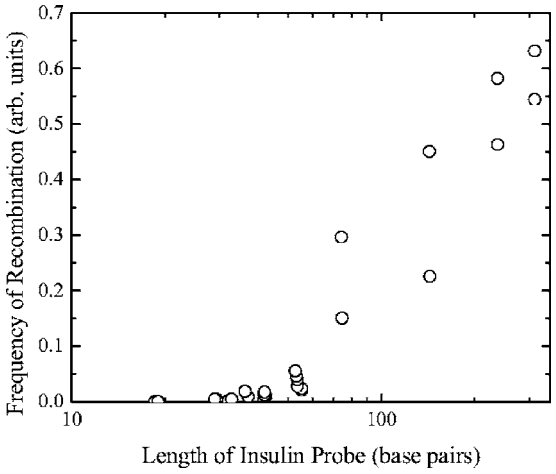

FIG. 11. Frequency of homologous recombination as a function of the base-pair length for homologous DNA molecules. Recombination becomes frequent only for sequences with 50–200 base pairs. Replotted from the data of Watt *et al.*, 1985.

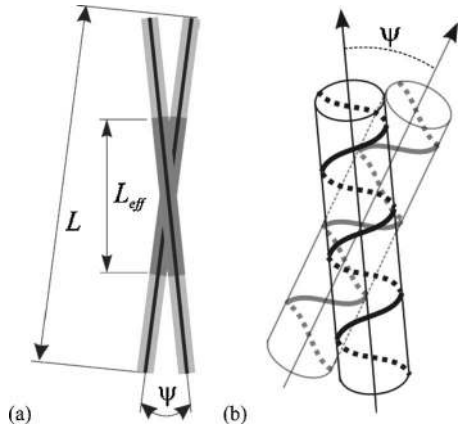

FIG. 12. Schematic illustration of two helices skewed at an angle of ψ. (a) The length of effective juxtaposition (L_{eff}) represents the region of significant overlap between electric fields created by molecules, which determines the electrostatic interaction energy. (b) Relative orientation of strands and grooves within the effective juxtaposition region determines the chiral torque between molecules. The helix with lighter markings lies behind that with darker markings. As shown here, right-handed helices prefer a right-handed twist to prevent crossing of the helical strands (dashed dark lines on the back of the front helix and solid gray lines on the front of the helix in the rear). For cholesteric liquid crystals, such a preferred twist will result in a right-handed cholesteric chirality. In the case of supercoils (or coiled coils), this preferred twist will yield a left-handed supercoil since such a twist will lead to helices wrapping around each other in the chiral sense opposite to their own handedness.

bases, triggering further recombination events. But such recognition achieves high efficiency already for eight to ten base fragments (Hsieh *et al.*, 1992). If it were the only recognition mechanism, frequent recombination mistakes would be inevitable. A clue to another, preceding recognition event was found in recent experiments that showed pairing of homologous, intact, double-stranded DNA, which was observed in the absence of known recombination proteins (Weiner and Kleckner, 1994; Burgess *et al.*, 1999). It was proposed that transient pairing of large, homologous fragments is a first, coarse recognition step. Double-helix breakage, single-strand formation, and fine recognition occur as subsequent steps. The two-step (coarse then fine) recognition process produces a much more efficient search mechanism.

The recognition and pairing of intact double helices was attributed to some unspecified DNA-DNA interaction (Weiner and Kleckner, 1994). Since it is not site specific and involves long stretches of DNA, it clearly cannot be performed by proteins. But what is it? The homologous recombination requirement of 50–200 bp coincides with the requirement for efficient electrostatic recognition between double helices. Thus it was speculated that the electrostatic recognition might be a part of the process (Kornyshev and Leikin, 2001). Of course, DNA molecules in cell nuclei do not interact as they would in a test tube. It is a rather different environment and multiple proteins are likely to be involved. Moreover, this mechanism has not been verified even in a test tube yet. Nevertheless, no other universal mechanisms (not imposing any sequence restrictions, except homology) have been proposed so far.

Having shown that the recognition energy can be a driving force for correct pairing, and that it grows with the increasing length of homology, we should refrain from relating this quantity to the frequency of recombination events. Although pairing is presumably necessary, it may not be the rate determining step. The recombination frequency may be also affected by other factors [see, e.g., the random-walk model of Fujitani *et al.* (1995) and Fujitani and Kobayashi (1995)].

G. Skewed helices: Chiral interactions

The main motivation for developing a theory of interaction between nonparallel, skewed molecules (Fig. 12) is to understand forces responsible for rather nontrivial features of chiral phases formed by them (Harris *et al.*, 1999). For homogeneously charged cylinders, this problem was first addressed by Onsager (1949) within a Derjaguin-like approximation (Derjaguin *et al.*, 1987). A rigorous solution of the same problem, within the DH theory, was obtained about 25 years later (Brenner and Parsegian, 1974). More recently, effects of counterion fluctuations and correlations in the interaction between rodlike molecules were investigated by utilizing chain models consisting of points or spherical monomers (Lee, Borukhov *et al.*, 2004).

However, cylinders and 1D chains of points are not chiral. Calculation of chiral interactions requires one to account for molecular structure even in "zero approximation." Some analytical results for forces between helices freely rotating around their long axes have been published [see, e.g., Van der Meer *et al.* (1976), Kats (1978), and Issaenko *et al.* (1999)]. Such approximation, however, cannot be used for central-force electrostatic potentials, which require biaxial correlations in order to

remain chiral (Harris *et al.*, 1997). It was argued that the approximation of freely rotating molecules does not work so well even for dispersion (van der Waals) forces (Issaenko and Harris, 2000).

Complete, analytical solutions for electrostatic interaction between skewed helices at arbitrary, fixed azimuthal orientations were obtained based on calculation of the integrals in Eq. (42) (Kornyshev and Leikin, 2000; Kornyshev, Leikin *et al.*, 2002). The results revealed a number of conceptually important features on chiral interactions, which can be understood based on simplified asymptotic expansions.

Consider the interaction between two ideal, long ($L \gg \lambda_D, H$), charged helices in electrolyte solution in the simplest geometry shown in Fig. 12. When the skew angle ψ between the axes of the two molecules exceeds $\sqrt{2\pi\lambda_D R}/L$, the effective juxtaposition length along which their electric fields overlap becomes independent of L and the interaction energy can be calculated in the limit of infinite L. The resulting expression derived by Kornyshev and Leikin (2000) can be simplified at $\sqrt{2\pi\lambda_D R}/L < |\psi| \ll 1$ and $R\kappa_D \gg 1$,

$$E \approx \frac{\sqrt{2\pi\lambda_D R}}{|\sin\psi|}\left(\mathcal{U}_0' + \psi\mathcal{T}_\psi' + \frac{\psi^2}{2}\mathcal{M}_{\psi\psi}' + \cdots\right), \tag{73}$$

where $\sqrt{2\pi\lambda_D R}/|\sin\psi|$ is the effective juxtaposition length,

$$\mathcal{U}_0'/k_BT = u_{\mathrm{cyl}}(R) - \sqrt{\kappa_D/\kappa_1}u_1(R)\cos(\delta\phi), \tag{74}$$

$$\mathcal{T}_\psi'/k_BT = -[g(\kappa_D)^{1/2}/(\kappa_1)^{3/2}]u_1(R)\cos(\delta\phi), \tag{75}$$

$$\mathcal{M}_{\psi\psi}'/k_BT = [(\kappa_1 R - 3)(\kappa_D)^{1/2}g^2/4(\kappa_1)^{5/2}] \times u_1(R)\cos(\delta\phi), \tag{76}$$

and $u_{\mathrm{cyl}}(R)$ and $u_1(R)$ are defined by Eq. (51) (excluding the image charge term) and Eq. (59), respectively.

One intuitive conclusion from these equations is that intermolecular attraction ($\mathcal{U}_0' < 0$) favors parallel orientation of helices, while repulsion tends to twist them out of energetically unfavorable parallel alignment. The requirement for the attraction between skewed helices at $\sqrt{2\pi\lambda_D R}/L < |\psi| \ll 1$ is more stringent than for parallel ones [cf. Eq. (57)]. A slightly higher charge neutralization by condensed counterions is needed here.

It is a little less obvious that the chiral torque ($\propto \mathcal{T}_\psi'/|\psi|$) favors a right-handed skew angle ($\psi > 0$) between right-handed helices ($g > 0$) and a left-handed twist between left-handed helices at optimal azimuthal alignment ($\delta\phi = 0$), the same-handedness rule. This can be rationalized by the simple cartoon of single-stranded helices shown in Fig. 12(b). Such direction of the twist favors juxtaposition of strands and grooves while the opposite direction favors strand crossing. However, for double-stranded DNA helices, Eqs. (73)–(76) can be used only at sufficiently large R, beyond the frustration point. At smaller R, azimuthal frustration leads to $\delta\phi \neq 0$. In this case, the simple same-handedness rule may be violated and an inversion of the twist may occur (Kornyshev and Leikin, 2000).

Finally, as predicted by Harris *et al.* (1997), Eqs. (73)–(76) show that uncorrelated rotations of molecules around their long axes ($\langle\cos\delta\phi\rangle = 0$) would wipe out the chiral interaction and would make the helices behave like homogeneously charged cylinders. But these equations (as well as the full equations at all ψ) were derived by neglecting the image interaction of one helix with the core of the other one. From Eqs. (57) and (58) we know that the image interaction is not dependent on $\delta\phi$. It cannot be wiped out by the rotation because an image rotates together with its source. Based on cartoons and analogy with the derivation reported by Kornyshev and Leikin (1997), one might expect image forces to contribute to the chiral torque. If correct, this assumption suggests a rather nontrivial chiral electrostatic torque between freely rotating molecules. To determine whether this is indeed the case, the problem of image interactions between skewed helices has to be solved. Work in this direction is currently in progress.

For nearly parallel helices at much smaller angles ($|\psi| \ll \sqrt{2\pi\lambda_D R/L}$), the interaction changes qualitatively because the effective juxtaposition length becomes equal to the length of the molecules. In the same asymptotic limit of $R\kappa_D \gg 1$ (Kornyshev, Leikin, *et al.*, 2002),

$$E \approx L(\mathcal{U}_0 + \psi\mathcal{T}_\psi + \psi^2\mathcal{M}_{\psi\psi}/2 + \cdots), \tag{77}$$

where

$$\mathcal{U}_0/k_BT = u_{\mathrm{cyl}}(R) - u_1(R)\cos(\delta\phi), \tag{78}$$

$$\mathcal{T}_\psi/k_BT = (g/\kappa_1^2)[\partial u_1(R)/\partial R]\cos(\delta\phi), \tag{79}$$

and

$$\frac{\mathcal{M}_{\psi\psi}}{k_BT} = \frac{L^2}{12R}\left(\frac{\partial u_{\mathrm{cyl}}(R)}{\partial R} - \frac{\partial u_1(R)}{\partial R}\cos(\delta\phi)\right). \tag{80}$$

Here the tendency of molecules to twist is determined not by the sign of $\mathcal{U}_0$ but by the nonzero value of the chiral torque $L\mathcal{T}_\psi$ and by the sign of the second moment $L\mathcal{M}_{\psi\psi}$. Again, repulsive interactions will twist the molecules out of this nearly parallel alignment. Attractive interactions will tend to keep the molecules nearly parallel ($\mathcal{M}_{\psi\psi} > 0$) to maximize the energetically favorable large juxtaposition length ($\mathcal{M}_{\psi\psi} \propto L^2$). But the chiral torque will always skew them out of completely parallel alignment. Since $[\partial u_1(R)/\partial R]\cos(\delta\phi) < 0$ at optimal $\delta\phi$, a right-handed twist is still favored for right-handed helices.

Provided that the net interaction is attractive ($\mathcal{M}_{\psi\psi} > 0$) and that the equilibrium twist angle ψ_* is small enough to be within the range of the current approximation,

$$\psi_* = -\frac{12Rg}{L^2\kappa_1^2}\frac{[\partial u_1(R)/\partial R]\cos(\delta\phi)}{(\partial u_{\rm cyl}(R)/\partial R - [\partial u_1(R)/\partial R]\cos(\delta\phi))}. \tag{81}$$

In theory, the approximation of small ψ should always work for sufficiently long, rigid molecules that attract each other (because of the L^{-2} dependence on the equilibrium angle). In practice, however, molecules are rarely long enough and almost never rigid enough for this to be the case.

H. Supercoiling

The electrostatics of supercoiling has not been rigorously analyzed, although structure factors for coiled coils were derived by Crick (1953a, 1953b) more than 50 years ago (see Sec. II.G). We will report detailed results of the corresponding study elsewhere, but this review would not be complete without at least a brief, heuristic analysis of the interaction between two helices coiled around each other.

Consider the simplest example of two right-handed, zwitterionic helices discussed in Sec. V.C (Fig. 5), which form a straight coiled coil with unconstrained ends (Fig. 4). The two helices attract each other at all R and their interaction can be described with one helical harmonic ($n=\pm 1$). The conflict between the chiral torque forcing them out of parallel alignment and the attraction forcing them back is resolved most efficiently when they form a coiled coil. The same-handedness rule discussed in Sec. V.G applies to them at all R. Thus we would expect a right-handed twist between their axes to result in formation of a left-handed coiled coil [Figs. 4 and 12(b)].

Assume that these helices have infinite torsional rigidity (to keep their twist constant) and large bending rigidity B. Then, they would form a coiled coil with a large pitch $P\equiv 2\pi/Q$. After substitution of the structure factors for such a coiled coil (Crick, 1953a; EPAPS Document)[9] into Eq. (42), calculation of the integrals, and minimization with respect to the alignment of the two helices, we find that at small Q the energy of the electrostatic interaction in the coiled coil is given by

$$\frac{E_{\rm int}(R)/L}{k_BT} \approx -\tilde{u}_1\left(K_0(Rg) - RQ\frac{g}{|g|}K_1(Rg)\right) + O(Q^2). \tag{82}$$

Here $\tilde{u}_1$ is defined by Eq. (50) and $g=2\pi/H=$const ($g,Q>0$ correspond to right-handed coiling, as above). R is now not only the distance between the axes of the two helices but the supercoiling diameter as well. For derivation of Eq. (82) see the EPAPS Document in the Reference section.

When $QR\ll 1$, the bending energy of the two helices in the coiled coil may be approximated by

$$\frac{E_B(R)/L}{k_BT} \approx \frac{Q^4R^2\lambda_p}{4}, \tag{83}$$

where λ_p is the persistence length of each helix. Assuming that the pitch of the coiled coil is set by the balance of these two energies, we find

$$P = -2\pi\frac{g}{|g|}\left(\frac{R\lambda_p}{\tilde{u}_1K_1(Rg)}\right)^{1/3}. \tag{84}$$

As expected, Eq. (84) predicts a left-handed coiled coil ($P<0$) formed by two right-handed helices.[10]

In real life, α-helices do tend to form left-handed coiled coils. But we caution the reader against rushing to compare this model with the corresponding data. In its current form, this model was designed only to demonstrate the nontrivial and interesting physics of electrostatic forces that cause supercoiling rather than to be seriously compared with experiments. In addition to the simplifying assumptions discussed above (see footnote 10), it neglects crucial steric restrictions on fitting ridges of atoms on one helix into grooves of the other helix. The latter, hard-core interactions clearly affect the geometry of α-helix packing in proteins (Chothia *et al.*, 1981). Nevertheless, the electrostatics of α-helix backbones can contribute as well. By neglecting the electrostatic contribution one could also "throw the baby out with the bath water."

I. Nonelectrostatic forces

We have focused this review primarily on electrostatics since there has been less work done concerning the relation of other types of forces to the helical structure of molecules. Nevertheless, some reported results are worth mentioning in the context of our discussion.

Hard-core forces are clearly important, and in many cases their contribution might be dominant, as mentioned above. They are present in virtually all computer simulations of helix-helix interactions. Even when not described explicitly, they are generally incorporated into analytical theories, including the theories discussed above (distance of closest approach, self-avoidance, water-impermeable cores, etc.). However, few models looked explicitly at the physics of the relationship between helical hard-core structure (ridges and grooves) and intermolecular forces (Straley, 1976).

The dispersion (van der Waals) forces are more amenable to traditional theoretical analysis (Mahanty and Ninham, 1976; Parsegian, 2005). The conceptual physics of their relationship to the structure of helices is therefore somewhat better understood. Several models of the

[9]For this calculation, one must include higher-order terms in Q that were omitted from Eq. (21).

[10]We presently do not know how realistic are the simplifying assumptions which allowed us to expand the electrostatic energy in powers of Q and retain only the first-order term. To describe any real coiled coil, it may be necessary to include higher-order terms as well as allowing molecules to change their intrinsic twist. Complete results will be reported elsewhere.

corresponding pair interaction potentials between helices have been published (Van der Meer *et al.*, 1976; Kats, 1978; Issaenko *et al.*, 1999; Issaenko and Harris, 2000). However, estimates suggest that the contribution arising from their dependence on the helical structure (e.g., into chiral torque) might be small (Harris *et al.*, 1999; Issaenko *et al.*, 1999).

Potentially more important are the hydration (structural or solvation) forces often invoked to explain interactions observed in the last 10–20 Å of molecular separation between biological helices (Rau and Parsegian, 1990, 1992a, 1992b; Leikin *et al.*, 1993, 1995, 1997; Mariani and Saturni, 1996). Because water is structured by biological macromolecules, it would be natural to expect formation of a layer where the hydrogen bond (HB) network structure relaxes from the one imposed by the surface to the one characteristic of bulk solvent. Overlap of such layers should have energetic consequences, just like the overlap of electrostatic screening layers. Opponents suggest that forces in excess of expectations from simplified, macroscopic electrostatic theories might be corrections (although not always small), e.g., due to the nonmacroscopic dielectric response of water, lower effective dielectric constant (see footnote 3), etc. But such corrections are also likely to be one of the consequences of the HB network in water. These two (seemingly different) points of view are not necessarily mutually exclusive. For instance, hydrogen bonding is an electrostatic interaction, but it does have a quantum flavor (proton delocalization) and a structural flavor (geometry of the water molecule and the HB network). Is the energy expended to deform a HB network a consequence of structural or electrostatic forces? While most agree on the substance, different people choose different words to talk about such forces. A phenomenological approach (Kornyshev and Leikin, 1989, 1997) based on an order-parameter model (Marčelja and Radic, 1976) allows one to describe such forces without specifying their nature. However, further pursuit of this speculative approach and development of detailed theories based on it might be premature.

J. Summary and comments

A consensus is now emerging that patterning and density fluctuations of counterions condensed on highly charged surfaces is important for intermolecular interactions. The molecular geometry and structure are even more important because they define the patterning of the fixed molecular charges and thus influence the patterning of condensed counterions as well. The last decade has brought significant advances in understanding how to account for the molecular structure and for static and dynamic surface charge patterns. The corresponding theories discussed above do require more involved algebra, but the effort is worthwhile. Just as the algebra of molecular structure factors has led to the discovery of DNA structure, understanding the relationship between these structure factors and the charge patterns of molecules is necessary for characterizing intermolecular interactions. The challenge of fully understanding many experiments (which are still far ahead of the theory) discussed here and in subsequent sections makes this subject particularly exciting and ripe for new developments.

VI. COLUMNAR, NEMATIC, AND CHOLESTERIC ASSEMBLIES

Multimolecular assemblies of parallel (columnar) and nearly parallel (nematic and cholesteric) helices are not only model systems for studies *in vitro*, they also occur in vivo. For instance, collagen helices self-assemble into fibers. Tendons are essentially just bundles of such fibers. A balance of repulsive and attractive pair interactions between collagen helices determines formation and swelling of fibers (Leikin *et al.*, 1995), which plays a crucial role in tendon mechanics [see, e.g., Misof *et al.* (1997), and refrences therein].

Short-range interactions between zwitterionic macromolecules, e.g., between collagen helices (Leikin *et al.*, 1994) or between backbones of α-helices (Sec. V.D), involve only nearest neighbors and are generally pairwise additive. The energy of a multimolecular, columnar aggregate of such helices at given positions and azimuthal orientations of the molecules, if they are rigid enough, is simply a sum of all pair interactions.

In contrast, interactions between highly charged macromolecules, e.g., DNA, might not be additive. Aggregates of such molecules trap free counterions to neutralize the charge. Trapped counterions attract water and build up osmotic pressure, which extends throughout the aggregate. Furthermore, the local concentration of counterions depends exponentially on the electrostatic potential resulting in cumulative rather than additive contributions of molecules into the energy. We show below that the ideas and results developed for pair interactions between charged helices can be successfully applied to multimolecular assemblies, but the effect of the trapped counterions will require special consideration. Thus before going into a more complicated description of assemblies of helical molecules, it is essential to focus first on the theory of assemblies of homogeneously charged cylinders.

A. Donnan equilibrium

The simplest estimate of the average electrostatic potential inside an aggregate can be done utilizing the model of Donnan equilibrium between a polyelectrolyte "gel" and bulk electrolyte solution (Donnan, 1924; Overbeek, 1956). This model assumes a uniform density of fixed charges ρ, so that the densities of all mobile ions are also uniform. The Boltzmann distribution relates the concentration of each ion i inside the gel,

$$n_i = n_i^0 \exp(-q_i e\bar{\varphi}/k_B T), \tag{85}$$

to its concentration n_i^0 in the bulk electrolyte and to the average electrostatic potential $\bar{\varphi}$ in the gel (often re-

ferred to as the Donnan potential). The electroneutrality condition

$$\sum_i q_i e n_i + \rho = 0 \tag{86}$$

then yields the following equation for the average potential:

$$\sum_i q_i e n_i^0 \exp(-q_i e\bar{\varphi}/k_B T) + \rho = 0. \tag{87}$$

In the simplest case of a 1:1 electrolyte ($n_0 = n_-^0 = n_+^0$) we have

$$\sinh(e\bar{\varphi}/k_B T) = \rho/2en_0. \tag{88}$$

Once the concentration of polyelectrolyte charges in the gel (ρ/e) exceeds the concentration of ions in the bulk, the electrostatic potential ($e\bar{\varphi}/k_B T \geqslant 1$) becomes a nonlinear function of the charge density, i.e., the contributions of molecules to the potential become nonadditive. For instance, at interaxial distances of 25–40 Å between DNA molecules, where the most interesting (and biologically relevant) interactions are observed, the aqueous concentration of phosphates is ~0.9–3M (excluding the volume of DNA cores). Even if 75% of phosphates are neutralized by bound counterions, the concentration of the unbalanced charges (0.3–1M) is still higher than typical ion concentrations used in experiments (e.g., at physiological ion concentrations, $n_0 = 0.15M$, we find $\rho/2en_0 \sim 0.7$–3).

B. Cell model for charged, cylindrical rods

Nonlinear PB. The Donnan model provides a simple illustration of how to calculate the electrostatic potential within a dilute polyelectrolyte assembly and an estimate of when to expect a nonlinear potential. But it cannot be used for calculating the energy of an aggregate of parallel charged rods because it oversimplifies the charge distribution. Instead, a combination of the nonlinear PB theory with a cylindrical cell model is commonly used as a better approximation (Alfrey *et al.*, 1951; Fuoss *et al.*, 1951; Lifson and Katchalsky, 1953; Katchalsky, 1971; Wennerström *et al.*, 1982; Zimm and LeBret, 1983; Alexander *et al.*, 1984; LeBret and Zimm, 1984b; Mandel, 1992). The simplest form of this model describes rigid, infinitely long, homogeneously charged rods packed parallel to each other in a hexagonal array (Fig. 13). The hexagonal Wigner-Seitz cell around each rod is approximated by a cylindrical cell of the same volume. The radius of the latter is

$$R_s = R\sqrt{\sqrt{3}/2\pi}, \tag{89}$$

where R is the interaxial distance between the rods. The potential $\varphi(r)$ is calculated from the PB equation [Eq. (29)] with the following boundary conditions:

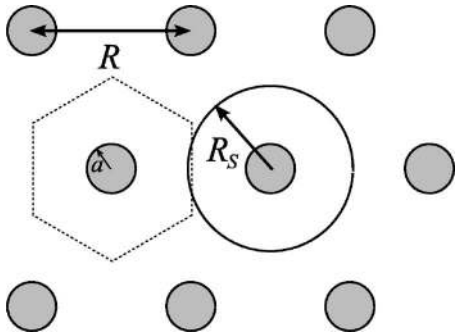

FIG. 13. Cross-sectional diagram of a hexagonal columnar assembly of cylinders. The hexagonal Wigner-Seitz cell (dotted line) about each molecule can be approximated as a cylinder with radius $R_s = R\sqrt{\sqrt{3}/2\pi}$, where R is the lattice spacing between nearest-neighbor cylinders.

$$\left.\frac{\partial\varphi}{\partial r}\right|_{r=a} = \frac{4\pi\sigma}{\varepsilon} \quad \text{and} \quad \left.\frac{\partial\varphi}{\partial r}\right|_{r=R_s} = 0, \tag{90}$$

where a is the radius of the rod and σ is its surface charge density. In a salt-free case, the PB equation [Eq. (29)] has a compact, exact analytical solution within this model (Alfrey *et al.*, 1951; Fuoss *et al.*, 1951, Zimm and LeBret, 1983; LeBret and Zimm, 1984b). In the presence of salt, it is usually solved numerically (Wennerström *et al.*, 1982; Alexander *et al.*, 1984; LeBret and Zimm, 1984a), although some analytical results have been reported as well (Tracy and Widom, 1997).

Once the potential at the cell boundary $\varphi(R_s)$ is known (e.g., from a numerical solution), the osmotic pressure of trapped counterions and excess electrolyte at the cell boundary can be calculated as

$$\Pi_{\text{cyl}}(R_s) = k_B T \sum_i n_i^0 \left[\exp\left(-\frac{q_i e\varphi(R_s)}{k_B T}\right) - 1\right]. \tag{91}$$

Because the electric field at the cell boundary is assumed to be zero, the work of compressing a cell of length L is

$$dW = -\Pi_{\text{cyl}}(R_s) 2\pi L R_s dR_s. \tag{92}$$

The electrostatic energy of bringing N molecules from infinite separation to interaxial distance R is calculated by simple integration of this work,

$$E_{\text{el}}^{\text{cyl}}(R) = N\int dW = -\sqrt{3}NL\int_\infty^R \Pi_{\text{cyl}}(R')R'dR', \tag{93}$$

where Eq. (89) is used to express $E_{\text{el}}^{\text{cyl}}(R)$ through R rather than R_s.

Note that the thermodynamic "trick" of calculating electrostatic interactions between uniformly charged molecules through the osmotic pressure of counterions (Langmuir, 1938) is quite general and is often used in colloid science. For more detailed discussion of such procedures and their rigorous thermodynamic justification, see, e.g., Verwey and Overbeek (1948) and Derjaguin *et al.* (1987).

Linearized PB with renormalized charge. An alternative approach to calculating the electrostatic energy

builds on the idea of counterion condensation. It assumes that a fraction θ of the charge of the rod is neutralized by condensed and adsorbed counterions so that the surface charge density of the rod becomes $(1-\theta)\sigma$. The variation of the potential outside the layer of condensed or adsorbed counterions is considered to be small and the PB equation is linearized. However, unlike the DH theory, where the linearization is made when the absolute value of φ is small, here the PB equation is linearized with respect to $\varphi-\varphi_s$ [$\varphi_s \equiv \varphi(R_s)$],

$$\nabla^2(\varphi-\varphi_s) = \kappa^2(\varphi-\varphi_s) + \frac{4\pi e}{\varepsilon}\sum_i n_i^0 q_i e^{-q_i e\varphi_s/k_BT}, \quad (94)$$

where

$$\kappa = \sqrt{4\pi l_B\left(\sum_i n_i^0 q_i^2 e^{-q_i e\varphi_s/k_BT}\right)} \quad (95)$$

is the renormalized inverse screening length. The solution of this equation is given by

$$\frac{e\varphi(r)}{k_BT} = \frac{e\varphi_s}{k_BT} + \left(\sum_i n_i^0 q_i e^{-q_i e\varphi_s/k_BT} \Big/ \sum_i n_i^0 q_i^2 e^{-q_i e\varphi_s/k_BT}\right) + \frac{2l_B(1-\theta)}{l_c\kappa a}\frac{I_0(\kappa r)K_1(\kappa R_s)+K_0(\kappa r)I_1(\kappa R_s)}{I_1(\kappa a)K_1(\kappa R_s)-K_1(\kappa a)I_1(\kappa R_s)}. \quad (96)$$

The value of φ_s is calculated by setting $r=R_s$ in Eq. (96), with $\kappa(\varphi_s)$ given by Eq. (95), and solving the resulting transcendental equation. Having calculated φ_s one obtains the effective screening length. In the end, the electrostatic energy is determined as a function of R and θ from Eqs. (91)–(93).

The benefit of this model as compared to the nonlinear PB description is in its flexibility in handling the degree of counterion condensation. The value of θ can be calculated, e.g., from the nonlinear PB as well as other theories that are more appropriate when $\Xi \gg 1$ where the PB theory is expected to fail (divalent counterions already lead to $\Xi \approx 24$ for DNA; Sec. IV.B). This model can also be combined with theoretical or empirical adsorption isotherms to calculate θ self-consistently in cases of significant counterion chemisorption (Cherstvy *et al.*, 2002). This is particularly important for DNA since evidence of site-specific chemisorption was found for virtually all biologically important DNA counterions (Sec. IV.C). In some cases purely empirical models for θ might be also productive, as well as fitting θ to experimental data.

The main limitation is that this model requires the thickness of the layer of condensed and adsorbed counterions to be small compared to the rod radius. While there might be exceptions, such an approximation is quite reasonable for DNA at physiological or higher salt concentrations (Sec. IV.B).

Flexible rods. Once the electrostatic energy per bending persistence length (λ_p) becomes smaller than k_BT at large R, it becomes important to account for bending and thermal undulations of the rods (Podgornik and Parsegian, 1990; Selinger and Bruinsma, 1991; Odijk, 1993; Strey *et al.*, 1997, 1999). It was demonstrated, for example, that undulations significantly extend the range of electrostatic interactions by allowing molecules to approach each other much more closely than the average R (Podgornik and Parsegian, 1990; Selinger and Bruinsma, 1991; Strey *et al.*, 1997, 1999). Additional corrections, for example, for bending of molecules trapped in randomly folded rather than straight conformations have also been discussed (Odijk, 1993).

C. Helices: Azimuthally dependent interactions and correlations

The PB theory corrected for undulations as well as fluctuations has proven to be quite successful in describing the measured osmotic pressure of DNA aggregates at large distances (Podgornik *et al.*, 1994; Strey *et al.*, 1997, 1999). But measurements in the last 2 nm of surface separation revealed significant deviations from the PB theory which could not be explained by simple corrections (Rau *et al.*, 1984; Rau and Parsegian, 1992a, 1992b). Similar behavior was also observed in columnar assemblies of charged helical polysaccharides (Rau and Parsegian, 1990). These deviations were attributed to hydration forces (Rau *et al.*, 1984; Rau and Parsegian, 1992a, 1992b; Leikin *et al.*, 1993). However, later calculations of pair interaction potentials in models with inhomogeneous surface charge indicated that the observed deviations are at least partially related to the helical symmetry of DNA surface charge patterns (Kornyshev and Leikin, 1997, 1998a).

Interaction energy. A generalization of the linearized PB model that accounts for helical charge patterns was suggested by Cherstvy *et al.* (2002). Within this approach the electrostatic interaction energy in an aggregate of N parallel helices is calculated as

$$E_{\rm el} = E_{\rm el}^{\rm cyl}(\theta,R) + \frac{1}{2}\sum_{\mu,\nu=1}^{N} E_{\mu,\nu}^{\rm hel}(\kappa,R,\Phi_\mu-\Phi_\nu). \quad (97)$$

Here $E_{\rm el}^{\rm cyl}(\theta,R)$ is the energy due to the net charge $e(1-\theta)L/l_c$ of the molecules, which is calculated within the cylindrical-cell model as described in Sec. VI.B. The second term is associated with helical harmonics of the charge density on each helix, Φ_μ is the azimuthal phase of the helix μ. The latter contributions are pairwise additive, and only interactions between nearest neighbors need to be included into the sum since the helical harmonics of the pair potential decay quickly with R due to the screening by the electrolyte.

Each pair interaction energy (Sec. V.E)

$$\frac{E_{\mu,\nu}^{\rm hel}/L}{k_BT} = u_{\rm image}(\kappa,R) - u_1(\kappa,R)e^{-\Delta_\phi^2}\cos(\Phi_\mu-\Phi_\nu) + u_2(\kappa,R)e^{-4\Delta_\phi^2}\cos[2(\Phi_\mu-\Phi_\nu)], \quad (98)$$

is a sum of the helical harmonics of image ($u_{\rm image}$) and

direct (u_1 and u_2) forces [Eqs. (58) and (59)], in which the effective κ from Eq. (95) should be used instead of κ_D. Finally,

$$\Delta_\phi^2 = \lambda_h/4\lambda_{\text{eff}} \tag{99}$$

is the mean square "nonideality" of each helix associated with sequence-related torsional deformations and torsional fluctuations (described by the effective helical persistence length λ_{eff}) discussed in Sec. V.E. Similar to pair interactions, the torsional adaptation length λ_h characterizes the effect of intermolecular forces on helix nonideality. But the value of λ_h is different since each molecule interacts with six rather than one nearest neighbor. The value of λ_h at each R can be calculated in the mean-field approximation (Cherstvy *et al.*, 2004; see also EPAPS Document). Here we focus on the most important predictions of this model.

Azimuthal correlations. Equations (97) and (98) describe the energy, which is dependent on azimuthal orientations of the molecules. The azimuthal dependence qualitatively distinguishes helices from homogeneously charged rods. Simple estimates show that the resulting azimuthal correlations could be quite strong (see the electrostatic zipper in Fig. 7 in Sec. V). One may define the degree of fluctuations in the azimuthal orientation of a molecule, averaged along its length, as $\Delta_\Phi^2 = \langle \delta\Phi_\mu^2 \rangle$, where $\delta\Phi_\mu$ is a fluctuation in the azimuthal orientation of a helix μ with respect to its nearest neighbors. Ground-state (Kornyshev, Leikin *et al.*, 2002) and statistical (Sec. VI.I) calculations suggest, for example, that in columnar and even more hydrated cholesteric aggregates of 150 bp DNA fragments $\Delta_\Phi \sim 0.1-0.5$ rad.

The value of Δ_Φ^2 is expected to decrease with increasing length of the helix, but only up to a certain point. For the case of very long DNA molecules, it is important to take into account that azimuthal rotations of the double helix are likely to be decoupled on two sides of various defects, e.g., (i) open and unstacked base pairs due to thermal fluctuations, (ii) nonlinear, solitonlike torsional deformations described by Eq. (69), (iii) kinks, (iv) cuts in the sugar-phosphate backbone, etc. As a result, a very long DNA molecule behaves roughly as if it were a collection of separate helical fragments. Although the average length L of such fragments is difficult to predict accurately, estimates based on the known probability of base-pair opening (Saenger, 1984) and calculated energy of torsional solitons (Kornyshev and Wynveen, 2004) suggest $L \sim 200-500$ base pairs.

D. A new look at old pictures: X-ray evidence of strong azimuthal correlations

The prediction of strong azimuthal correlations (Kornyshev and Leikin, 1997; Kornyshev, Leikin *et al.*, 2002) prompted the reevaluation of classical fiber x-ray-diffraction patterns in the search of corresponding experimental evidence (Kornyshev *et al.*, 2005). As discussed in Sec. II, x-ray-diffraction peaks from a highly ordered DNA fiber lie at layer lines with $k_z = -n(2\pi/H) + j(2\pi/h)$. The scattering intensity at a layer line n ($j=0$) given by Eq. (1) can be rewritten as

$$I_{n,0}(\mathbf{K}) \approx N I_n^M(K) + I_n^M(K) \sum_{\mu \neq \nu} \langle e^{-in(\phi_\mu - \phi_\nu)} e^{i\mathbf{K}\cdot(\mathbf{R}_\mu - \mathbf{R}_\nu)} \rangle, \tag{100}$$

where $\phi_\mu = \phi_\mu(z)$ is the azimuthal orientation of each helix at the axial position z, $\mathbf{R}_\mu = \mathbf{R}_\mu(z)$ is the lateral coordinate of the helix centerline, and

$$I_n^M(K) \propto \cos^2(n\tilde{\phi}_s) J_n^2(Ka) \tag{101}$$

is the scattering intensity from a single molecule. The first term on the right-hand side of Eq. (100) describes the contribution of intramolecular scattering from N helices. The second term describes the contribution of intermolecular scattering. It is dependent on the azimuthal orientations and therefore it should be sensitive to azimuthal correlations.

In the simplest case of Gaussian fluctuations in ϕ_μ,

$$\langle e^{-in(\phi_\mu - \phi_\nu)} \rangle = e^{-n^2(\Delta_\phi^2 + \Delta_\Phi^2)} e^{-in(\bar{\Phi}_\mu - \bar{\Phi}_\nu)}, \tag{102}$$

where $\bar{\Phi}_\mu$ is the average azimuthal orientation of each helix, and $\exp[-n^2(\Delta_\phi^2 + \Delta_\Phi^2)]$ is a Debye-Waller-like factor due to torsional disorder and fluctuations [Δ_ϕ^2, Eq. (99)] and azimuthal fluctuations (Δ_Φ^2) of the entire molecule. For uncorrelated molecules, $\exp[-n^2(\Delta_\phi^2 + \Delta_\Phi^2)] = \delta_{n,0}$ and intermolecular scattering should be observed only at $n=0$. This simplifying assumption, formulated by Franklin and Gosling (1953), became the dogma of DNA fiber x-ray diffraction. According to it, all nonequatorial diffraction spots in hydrated, noncrystalline DNA fibers originate from intramolecular scattering (Vainshtein, 1966). So strong was the power of the dogma that experimental indications of intermolecular scattering off the equator were overlooked until recently. But the evidence was, in fact, there for many years.

Indeed, at strong azimuthal correlations [$(\Delta_\phi^2 + \Delta_\Phi^2) \leqslant 1$], intermolecular scattering should contribute to the diffraction spots at $n \neq 0$ as well. As a result, the positions of nonequatorial diffraction spots at layer lines with small $|n|$ should become dependent on the aggregate density (since the intermolecular scattering is determined by the distance between molecules). This dependence should disappear on layer lines with larger $|n|$ due to the rapidly decreasing $\exp[-n^2(\Delta_\phi^2 + \Delta_\Phi^2)]$ factor.

This is exactly what was found upon reevaluation (Kornyshev *et al.*, 2005) of the x-ray data published by Zimmerman and Pheiffer (1979) almost 30 years ago [Fig. 14(a)]. Upon variation in fiber density, the positions of the diffraction spots at $|n|=1$ and even at $|n|=2$ tend to track with the reciprocal spacings between molecules rather than remain constant as predicted for uncorrelated molecules [Fig. 14(b)]. Only at $|n|=3$ do the positions of the maxima become independent of the aggregate density. If the dependence of the signal on the aggregate density had been caused by change in the

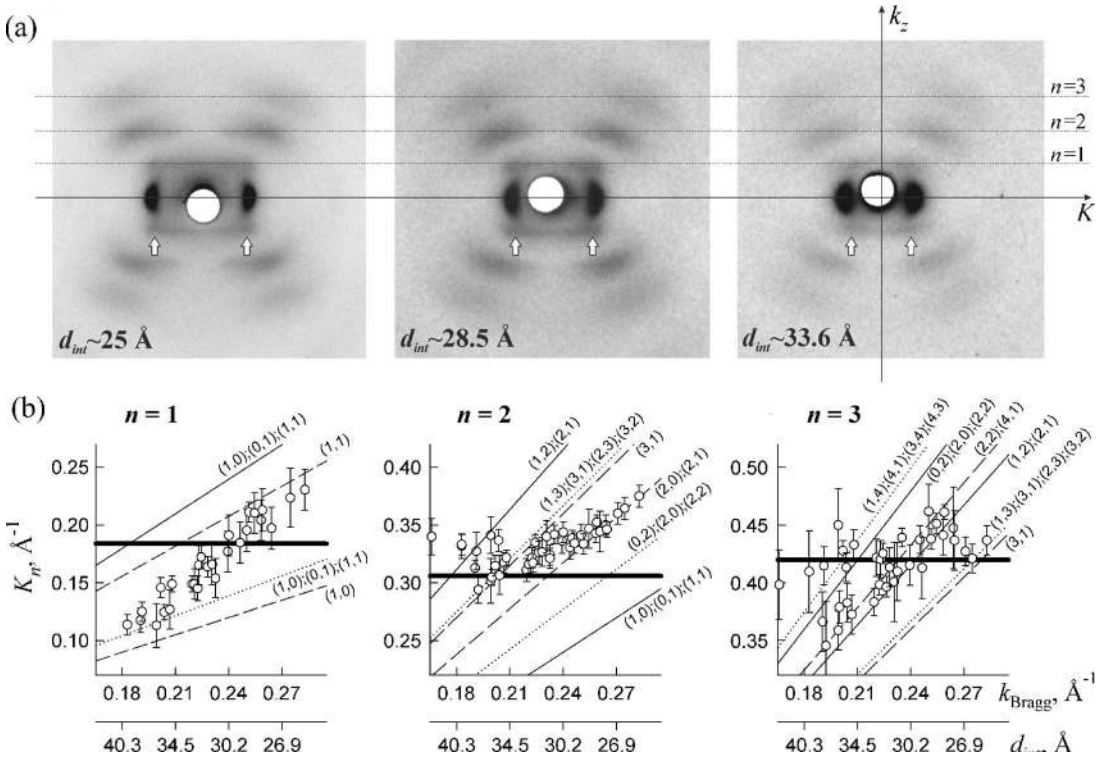

FIG. 14. X-ray studies of columnar DNA assemblies at different densities. (a) Diffraction patterns of hydrated DNA fibers (cf. Fig. 2) at three different interaxial spacings d_{int} between adjacent double helices. The interaxial spacings are calculated from the positions of the Bragg peaks (the two dark spots on the equator), $K=k_{\text{Bragg}}$. The locations of the diffraction maxima on the first layer line are marked by white arrows, highlighting their change with d_{int}. These maxima follow the Bragg peaks, suggesting a large intermolecular contribution to the scattering. (b) Variation in the locations $\mathbf{K}_n$ of the diffraction maxima on the first ($n=1$), second ($n=2$), and third ($n=3$) layer lines with separation (d_{int}) between DNA. The bold lines show expected locations of the intramolecular maxima [Eq. (101)]. Thin solid lines show the locations of the diffraction peaks in hexagonal crystals with the same azimuthal orientation of all molecules; dashed lines, in crystals with alternating orientations of molecules in consecutive rows; dotted lines, in crystals with different azimuthal orientations of all three molecules in the unit cell (see Fig. 20). The corresponding Miller indices are shown near each line. Intermolecular scattering appears to determine $\mathbf{K}_1$ at all separations. $\mathbf{K}_2$ are dominated by intramolecular scattering at $d_{\text{int}}>35$ Å resulting in flattening of the observed dependence. $\mathbf{K}_3$ are consistent with intramolecular scattering at all d_{int}. Reproduced from Kornyshev *et al.*, 2005.

structure of each individual molecule in the assembly, then one would expect the same effect for all layer lines, but this is not what was observed.

E. Cholesteric aggregates

One of the most interesting, common and biologically important examples of chiral assemblies is the cholesteric phase. Cholesteric phases of α-helices (Robinson, 1961; Dupre and Duke, 1975), collagen (Giraud-Guille, 1996), DNA (Evdokimov *et al.*, 1988; Strzelecka *et al.*, 1988; Van Winkle *et al.*, 1990; Livolant, 1991; Leforestier and Livolant, 1993), viral particles (Dogic and Fraden, 2006 and references therein), and other biological helices have been described. Cholesteric assemblies of DNA have been observed *in vivo* (Livolant, 1984 and references therein). Cholestericlike packing of collagen and α-chitin has been suggested to play an important role in formation of bone in vertebrates (Giraud-Guille *et al.*, 2003) and exoskeletons in arthropods (e.g., crabs) (Belamie *et al.*, 2004). It is, of course, the chiral nature of these molecules that is responsible for the existence of these phases.

Forces arising from the direct electrostatic interaction between helical distributions of charges (or hydration-force equivalents) can be chiral only in the presence of azimuthal correlations (Harris *et al.*, 1997) (Sec. V). Thus, to understand the physics of cholesteric phases, it is particularly important to establish a relationship between the azimuthal interactions or correlations and the structural parameters of the phase, e.g., the cholesteric pitch (Ferrarini *et al.*, 1995, 1996a, 1996b; Harris *et al.*, 1999).

The traditional approximation of weak azimuthal order (Straley, 1976) may not always work. At least in DNA assemblies, the azimuthal correlations might be strong in the whole range of interaxial distances where the cholesteric phase is observed (Kornyshev *et al.*, 2005). The data used to arrive at this conclusion were obtained for very long, stretched DNA in fibers rather than 150 bp DNA fragments typically used in the studies of the cholesteric phase (Livolant, 1991). But long DNA fibers form the cholesteric phase at about the same hy-

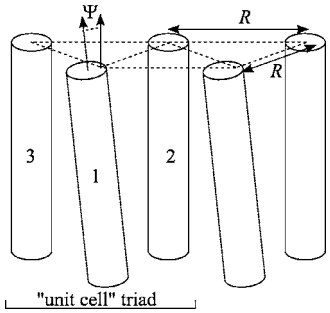

FIG. 15. Simplified side view of an elementary building block (unit cell) that has the characteristic symmetry of a cholesteric liquid crystal. The cholesteric liquid crystal can be viewed as a stack of molecular layers where local packing of molecules is hexagonal and the molecules in each layer are twisted by an angle Ψ with respect to another layer. The unit cell consists of a molecular triad with two parallel molecules (labeled 2 and 3) and a third molecule (labeled 1) twisted in the direction parallel to the plane formed by the first two molecules. The liquid crystal is an assembly of such triads where molecules may have random shifts (not shown) along their axes.

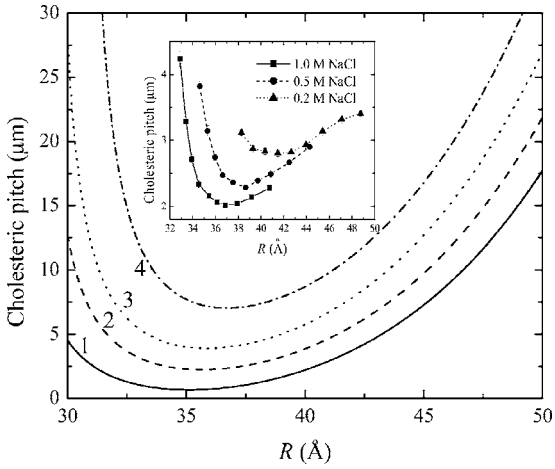

FIG. 16. Cholesteric pitch shown as a function of the interaxial distance between 146 base-pair DNA molecules with radii $a=9$ Å, as found from Eq. (103) at $\theta=0.7$. The different curves were calculated at ζ_n corresponding to different distributions of condensed counterions [Eq. (40)]: (1) $f_1=0.3$, $f_2=0.6$, $f_3=0$; (2) $f_1=0.35$, $f_2=0.6$, $f_3=0$; (3) $f_1=0.35$, $f_2=0.55$, $f_3=0$; (4) $f_1=0.4$, $f_2=0.55$, $f_3=0$ (Kornyshev, Leikin, *et al.*, 2002). Inset: The pitch measured experimentally for DNA molecules of the same size in solutions with different salt concentrations (reproduced from Stanley *et al.*, 2005). The estimated and measured pitch vs distance curves share the same qualitative behavior, i.e., a minimum at intermediate separations, a sharp rise at shorter separations (higher densities), and a gradual rise at larger separations (lower densities).

dration (Podgornik *et al.*, 1996; Strey *et al.*, 2000). Furthermore, the extent of azimuthal correlations between 150 bp fragments is not expected to be dramatically different from that in long DNA (Sec. VI.C).

A formalism that allows one to calculate the parameters of a chiral phase from the pair potential between molecules without assuming weak azimuthal correlation has been developed (Emelyanenko *et al.*, 2000; Emelyanenko, 2003). Based on a mean-field theory, this involved formalism operates with two order parameters: one for the nematic orientation, the other one describing the biaxial order. The capabilities of this formalism have been demonstrated for a model of steric interactions combined with van der Waals interactions, but its validity criteria were not defined, and it was not tested on electrostatic interactions of chiral charge distributions.

Some insight into nontrivial and potentially important physics stemming from strong azimuthal dependence of electrostatic interactions between nearest-neighbor molecules can be gained from ground-state estimates for the simplest unit cell (Fig. 15), which has the characteristic symmetry of a cholesteric liquid crystal (Kornyshev, Leiken *et al.*, 2002). This unit-cell triad is composed of two parallel molecules and a third molecule whose long axis is twisted by a small angle Ψ in the parallel plane. The dependence of the ground-state energy of such triad on Ψ at $\Psi \ll \lambda_D/L$ is similar to Eqs. (77)–(80), but the dependence of the corresponding chiral torque and the second moment on the interaxial distances and relative azimuthal orientations of the molecules in the triad is qualitatively different. The interaction energy of the triad is $E=\tilde{U}_0+\tilde{U}_1\Psi+(1/2)\tilde{U}_2\Psi^2$, for small Ψ. The expressions for the $\tilde{U}_n$ coefficients may be found in Kornyshev, Leikin, *et al.* (2002) or the EPAPS Document in the Reference section. In the triad, a nearly parallel configuration is more stable for a net repulsive interaction between molecules, i.e., $\tilde{U}_2>0$. It is also essential to account for the contributions from both the first and second helical harmonics in $\tilde{U}_1$, which have opposite signs and result in nontrivial effects.

Minimization of the triad energy with respect to Ψ gives the cholesteric pitch as

$$P=-\sqrt{3}\pi R\tilde{U}_2/\tilde{U}_1. \tag{103}$$

This expression predicts a nonmonotonic dependence on the interaxial distance R between molecules in the triad (Fig. 16), which was observed in certain experiments (Leonard *et al.*, 2001; Stanley *et al.*, 2005). Such dependence is caused by the azimuthal frustration in the pair interaction potential, Eqs. (57)–(60) (see also Sec. VI.I). Competing first and second helical harmonics favor different azimuthal orientations and, as a result, different directions of the cholesteric twist. At large R, the contribution from the first helical harmonic dominates. The expected pitch decreases with decreasing R simply because of the strengthening chiral interaction (an increase in the ratio of $\tilde{U}_1$ to $\tilde{U}_2$). At smaller R, the second helical harmonic becomes more important. It produces a chiral torque of opposite handedness (Kornyshev and Leikin, 2000), which reduces $\tilde{U}_1$ and causes a minimum followed by an increase in P upon further decrease in R (Kornyshev, Leikin, *et al.*, 2002).

Both the value of P (~0.5–30 μm) and its nonmonotonic dependence on R predicted by ground-state esti-

mates are in good agreement with experiments (Van Winkle *et al.*, 1990; Livolant, 1991; Livolant and Leforestier, 1996; Pelta, Durand *et al.*, 1996; Stanley *et al.*, 2005); cf. Fig. 16. Furthermore, the puzzling transition from the cholesteric to hexagonal, columnar (Durand *et al.*, 1992), or line-hexatic (Strey *et al.*, 2000) phase of DNA observed at $R \leqslant 32-35$ Å might also be related to the azimuthal frustration in the interaction potential. It has been proposed that azimuthal disorder caused by the frustration (cf. Sec. VI.I) might effectively destroy the cholesteric phase (Kornyshev and Leikin, 2000; Strey *et al.*, 2000; Kornyshev, Leiken *et al.*, 2002). Provided that the agreement with the experiments is not a coincidence, the short-range azimuthal interactions and/or correlations are closer to the low-temperature (ground-state) limit than the high-temperature approximations usually employed in molecular models. But a statistical theory that would properly account for such strong azimuthal order has not yet been developed.

F. Predicted and measured forces: DNA, guanosine, and collagen

Osmotic stress force measurements. A large body of data on interactions between helices in columnar aggregates at the last few nanometers of separation was collected over the past 30 years (Rau *et al.*, 1984; Parsegian *et al.*, 1986, 1987; Podgornik *et al.*, 1989, 1994; Rau and Parsegian, 1992a, 1992b; Leikin *et al.*, 1994, 1995; Mariani and Saturni, 1996; Strey *et al.*, 1997, 1999). In most cases, the osmotic pressure of an aggregate is determined by equilibration in a solution of a polymer which cannot penetrate inside the aggregate (Rau and Parsegian, 1992a). In a hexagonal aggregate, the osmotic pressure is related to the interaction energy as

$$\Pi = -\left\langle \frac{\partial E_{\mathrm{aggr}}}{\partial V_w} \right\rangle = -\frac{1}{NL\sqrt{3}R}\left\langle \frac{\partial E_{\mathrm{aggr}}}{\partial R} \right\rangle, \tag{104}$$

where V_w is the volume of water in the aggregate. The interaxial distance between molecules R is measured by x-ray diffraction. The results are often interpreted in terms of an effective pair interaction force f_{pair} between the molecules (per unit length),

$$\frac{f_{\mathrm{pair}}}{L} = -\frac{1}{3NL}\left\langle \frac{\partial E_{\mathrm{aggr}}}{\partial R} \right\rangle = \frac{\Pi R}{\sqrt{3}}, \tag{105}$$

where the factor of $1/3$ takes into account that there are three $(6/2)$ pair interactions per molecule in a hexagonal aggregate. This interpretation facilitates the intuitive perception of the results, but it is important to keep in mind that it yields a true pair interaction force only when such forces are pairwise additive.

DNA. Interactions between DNA molecules have been studied at different ionic strength, composition of bulk electrolyte, temperature, and so on (Rau *et al.*, 1984; Parsegian *et al.*, 1986; Podgornik *et al.*, 1989, 1994; Rau and Parsegian, 1992a, 1992b; Strey *et al.*, 1997, 1999). In many cases DNA forms cholesteric and line-hexatic rather than columnar assemblies (Sec. VI.E). However, for our present discussion, only the local (several nearest neighbors), approximately columnar structure is important and we can temporarily ignore the difference.

Several examples of measured force curves, illustrating commonly observed features, are shown in Fig. 17(a).

(i) At large distances ($R \geqslant 35-40$ Å) the forces decay with the characteristic length determined by salt concentration (Podgornik *et al.*, 1989, 1994; Strey *et al.*, 1997, 1999). The forces measured in NaCl are in good agreement with the predictions of the PB theory (Odijk, 1993; Podgornik *et al.*, 1994; Strey *et al.*, 1999), but the force amplitude strongly depends on (even monovalent) cations (Podgornik *et al.*, 1994). The agreement with theory can still be achieved if one accounts for cation adsorption (including chemisorption) by renormalizing the surface charge within either the nonlinear or linearized PB model (Podgornik *et al.*, 1994).

(ii) At $27-30 \leqslant R \leqslant 35-40$ Å (depending on counterions), a strong attractive component of the force can be detected in the presence of some counterions. In 50 mM $MnCl_2$, this attraction causes the jumps (dashed lines) at 5 and 35 °C [Fig. 17(a)] (Rau and Parsegian, 1992b). At 50 °C, the force becomes purely attractive in this distance range. Similar behavior was observed with other counterions as well (Rau and Parsegian, 1992b). This midrange attraction appears to be in good qualitative and quantitative agreement with forces predicted by Eqs. (97)–(99) and (104), Fig. 17(b). Within such an interpretation, the electrostatic zipper attraction (Sec. V.D, Fig. 7) is determined by the balance between the helical components $u_1(\kappa, R)$ and $u_2(\kappa, R)$ of the interaction. Its counterion specificity is reasonably well explained by the preferences of different counterions to bind at different locations (considered in Sec. VII). Its strengthening with temperature might be caused by increased torsional adaptation (smaller λ_h, Sec. V.E), repartitioning of bound Mn^{2+} with temperature (Cherstvy *et al.*, 2002), or both. The specificity of the nature of counterion absorption (not just its valence) and temperature-induced strengthening of attraction do not appear to be consistent with the theories of counterion-correlation forces proposed to date (Sec. V.C). Within the idea of attractive hydration forces, these properties can be explained by possible effects of bound counterions on the structure of surface water (Rau and Parsegian, 1992a) and by the entropically favorable release of such structured water, respectively (Rau and Parsegian, 1992b).

(iii) At smaller separations ($R \leqslant 27-30$ Å) the force curves, measured at different temperatures and Mn^{2+} concentrations (Rau and Parsegian, 1992a, 1992b), seem to follow a common short-range repulsion. Within the PB theory, the independence of salt concentration would not be surprising because the concentration of the mobile ions inside the aggregate at such separations is also expected to become almost salt independent. More surprising is that the repulsion remains strong when the charge of DNA is almost completely neutralized by

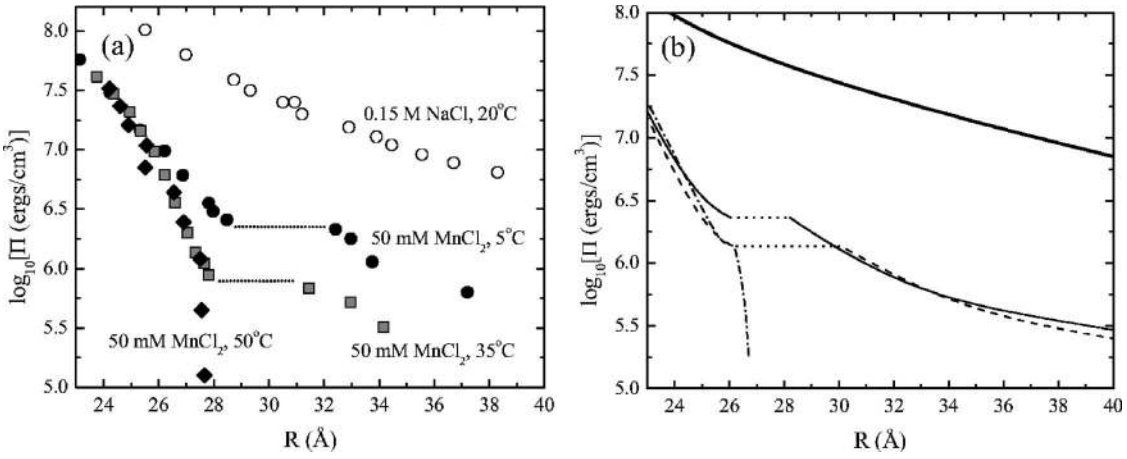

FIG. 17. Experimental and theoretical plots of osmotic stress in columnar DNA assemblies. (a) Measured osmotic stress vs interaxial separation in DNA solutions with different salts at different concentrations and temperatures (Rau and Parsegian, 1992b, data kindly provided by D. Rau). For monovalent NaCl, repulsion is always seen and can be fitted by the PB theory. However, for $MnCl_2$, at intermediate separations the system is metastable or unstable (collapses) at constant pressure (dotted lines). At higher temperatures, the range of the attraction increases, which may occur due to redistribution of Mn^{2+} between binding sites in minor and major grooves (Cherstvy *et al.*, 2002). (b) Calculated osmotic pressure vs separation in aggregates of torsionally flexible, nonideal DNA (Sec. V.D, V.E, VI.B, and VI.C). The top curve (thick solid line) shows the pressure calculated at 0.15*M* monovalent salt concentration assuming $\theta=0.1$. The lower plots show the pressure at 50 m*M* concentration of 2:1 electrolyte, $\theta=0.8$, $\lambda_c=300$ Å, and different torsional rigidities C_t and partitioning of condensed counterions between minor and major grooves [Eq. (40)]: $C_t=3\times10^{-19}$ erg cm and 40%:60% minor:major groove distribution (thin solid curve); $C_t=0.5\times10^{-19}$ erg cm and the same counterion distribution (dashed curve); and $C_t=0.5\times10^{-19}$ erg cm and 20%:80% minor:major groove distribution (dash-dotted curve). The dotted tie lines represent first-order transitions, resulting in part from the azimuthal frustration of the pair interaction potential (Secs. V.D and VI.I).

strongly bound multivalent or polycounterions (Rau and Parsegian, 1992a, 1992b). The exponential dependence of this force on R with a very short decay length $\lambda\sim2$ Å is not expected from the PB theory for homogeneously charged cylinders. However, this force appears to be in good agreement with the helical harmonics of image repulsion $[u_{\text{image}}(\kappa,R)]$ predicted by Eqs. (97)–(99) and (104), as illustrated in Fig. 17(b) (Kornyshev and Leikin, 1997).

Recently short-range repulsive and midrange attractive forces between DNA in the presence of several polyamines and cobalt hexaamine have been carefully mapped by combination of osmotic stress and magnetic tweezer measurements (Todd *et al.*, 2007). An exponential repulsion with ~2.4 Å decay length has been observed in the presence of putrescine. In addition to the same repulsion, a roughly exponential attractive contribution with ~4.8 Å decay length and smaller preexponential factor has been observed with spermine, spermidine, and cobalt hexaamine. The amplitude of the attraction was dependent on the counterion. The authors interpreted the attraction and the short-range repulsion as hydration forces. Alternatively, these forces can be interpreted as a sum of electrostatic zipper attraction and image repulsion (the net charge of DNA under conditions of these experiments was small, $\theta\approx0.9$–1, as indicated by the absence of longer-range electrostatic repulsion). For polyamines and cobalt hexaamine, which exhibit a preference for binding in the major groove of *B*-DNA (Sec. IV.C), the attraction is mostly determined by $u_1(\kappa,R)\propto K_0(R/\lambda_{\text{attr}})\propto\exp(-R/\lambda_{\text{attr}})$, where

$$\lambda_{\text{attr}}=\frac{H/2\pi}{\sqrt{1+(\kappa H/2\pi)^2}} \tag{106}$$

(Kornyshev and Leikin, 1999). At $\kappa^{-1}\geqslant10$ Å (as was the case in the experiments of Todd *et al.*, 2007), Eq. (106) predicts $\lambda_{\text{attr}}\approx H/2\pi\approx5$ Å, independent of the ionic strength, exactly as observed. The expected decay length of the first helical harmonic of the image repulsion is $\lambda_{\text{rep}}=\lambda_{\text{attr}}/2\approx2.5$ Å, also as observed. The factor of 1/2 is due to the interaction of each charge with its image, which effectively doubles the distance (Landau and Lifshitz, 1982) or halves the decay length (Kornyshev and Leikin, 1997). Full fitting of the osmotic pressures measured by Todd *et al.* (2007) yields good quantitative agreement with Eq. (98) (to be reported elsewhere), clearly indicating the important contribution of electrostatic interactions (although a contribution from hydration forces cannot be excluded either).

Guanosine. Another interesting and instructive example is the interaction between four-stranded guanosine helices. These helices self-assemble from deoxyguanosine monophosphates. The monomers associate into tetramers that stack on top of each other, forming helices with four equally spaced strands. Such molecules present a special case of helical symmetry in which the only nonzero harmonics of the charge pattern are $n=jN_s$, where N_s is the number of strands and $j=\pm1,\pm2\ldots$ (Kornyshev and Leikin, 1997). The corre-

sponding interaction energy is determined by the lowest harmonic with $n=\pm N_s$,

$$\frac{E^{\mathrm{hel}}_{\mu,\nu}/L}{k_BT} \approx u_{\mathrm{image}}(\kappa,R) + u_{N_s}(\kappa,R)e^{-N_s^2\Delta_\phi^2}\cos[N_s(\Phi_\mu-\Phi_\nu+\pi)], \tag{107}$$

where

$$u_{\mathrm{image}}(\kappa,R) \approx \frac{4l_B}{l_c^2}\zeta_{N_s}^2\frac{\Omega_{N_s,N_s}(\kappa_{N_s}R,\kappa_{N_s}a)}{(\kappa_{N_s}a)^2[K'_{N_s}(\kappa_{N_s}a)]^2} \propto \exp(-2\kappa_{N_s}R), \tag{108}$$

$$u_{N_s}(\kappa,R) \approx \frac{4l_B}{l_c^2}\zeta_{N_s}^2\frac{K_0(\kappa_{N_s}R)}{(\kappa_{N_s}a)^2[K'_{N_s}(\kappa_{N_s}a)]^2} \propto \exp(-\kappa_{N_s}R), \tag{109}$$

and

$$\kappa_{N_s}=\sqrt{\kappa^2+N_s^2 4\pi^2/H^2}. \tag{110}$$

The first contribution to this energy originates from image repulsion. For $N_s=4$ it should decay exponentially with a very short characteristic length, $H/16\pi\approx 0.7$ Å ($H\approx 40.8$ Å) (Mariani and Saturni, 1996; Kornyshev and Leikin, 1997, 1998a). The attraction, given by the second term in Eq. (107), is likely to be weak due to its strong dependence on torsional fluctuations [$\propto\exp(-16\Delta_\phi^2)$] and inherent torsional flexibility of the unlinked stacks of deoxyguanosine tetramers, which is actually poorly known.

In other words, no helix-specific interactions are expected beyond 5–10 Å surface separation, and none are observed (Mariani and Saturni, 1996). In contrast to the case of DNA, the forces measured in this distance range agree with the PB theory for homogeneously charged cylinders. Only in the last few angstroms do the forces at different salt concentrations appear to merge into a common exponential repulsion with the decay length ~0.7 Å (Fig. 18). While a macroscopic dielectric response is unlikely to be a good approximation when the surfaces are separated by one to two monolayers of water, the coincidence of the decay lengths might not be accidental. The predicted decay length of the image repulsion is determined entirely by the pitch of the helix ($H/16\pi$). It relies and depends only on the symmetry of the helix and not on details of the dielectric response of water. But, more than that, a macroscopic electrostatic calculation (Rudd *et al.*, 2006) reproduces fairly well even the absolute values of the measured forces (Mariani *et al.*, 1998). However, the observed short-range repulsion could also be caused, for example, by hard-core collisions of guanosine monomers protruding from the helix due to thermal motions or by hard-core interactions involving one monolayer of water adsorbed on each surface.

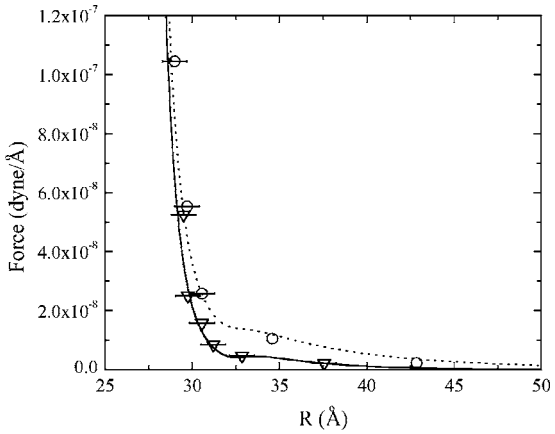

FIG. 18. Mean repulsive force per unit length between guanosine molecules from experiment (symbols) (Mariani and Saturni, 1996, data kindly provided by P. Mariani) and from theoretical fits (lines) using ground-state calculations, Eqs. (107)–(110) (Rudd *et al.*, 2006). Data are shown for solutions with 0.1 (open circles, dashed lines) and 0.5*M* (open triangles, solid lines) NaCl salt concentrations. Theoretical fits were made assuming an effective radius of each guanosine stack of 13.2 Å where ~84% of the guanosine charge was compensated by condensed counterions.

Interestingly, the apparent decay length of an attraction measured between guanosine helices at very high concentrations of buffer electrolyte, 3–4*M* KCl, also coincides with the one predicted by the second term in Eq. (107) (Mariani *et al.*, 1998). But interpretation of a force at such high salt concentrations as the electrostatic zipper attraction would be even more speculative.

Collagen. An exponential repulsion with ~0.7 Å decay length was measured from ~1 to ~8 Å surface separation between collagen triple helices (Fig. 19) (Leikin *et al.*, 1994, 1995). The balance of this repulsion with a longer-range attractive force is responsible for keeping collagen fibers in tendons and ligaments properly hydrated and flexible. As for guanosine helices, one cannot expect electrostatic calculations with the macroscopic water dielectric constant to be quantitatively accurate here, but qualitative analysis of collagen electrostatics is also very instructive.

Approximately ~15% of collagen amino acids have charged side chains; about half of them are negative and the other half positive. These charges do not follow the helical symmetry of the molecule. The positive and negative charges are clustered together along the helix, many forming "salt bridges" with each other. It has been suggested that interactions between charged amino acids are important for proper staggered alignment of triple helices in fibers (Hulmes *et al.*, 1973), but it was also argued that they do not contribute significantly to the net measured force (Leikin *et al.*, 1995). For instance, forces measured between collagenlike triple helical peptides without charged side chains were the same as between full-length collagen fibers (Leikin, 1999).

In contrast, a pair of one positive and one negative partial (~0.5*e*) charges is present on the backbone of

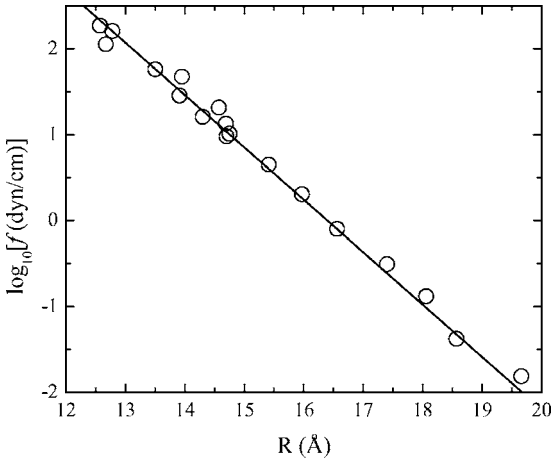

FIG. 19. Measured (open circles) and predicted (thin solid line) repulsive forces between collagen triple helices at *p*H 6.0 and low ionic strength (reproduced from Kornyshev and Leikin, 1997). The prediction was based on the mean-field theory of hydration forces (Kornyshev and Leikin, 1997). The corresponding expression for the repulsive hydration force can be obtained from Eqs. (105), (108), and (110) using the correlation length in water (≈4 Å) instead of κ^{-1} and replacing the factor $4l_B\zeta_{N_s}^2/l_c^2$ with a phenomenological constant (determined by fitting the data). However, electrostatic image repulsion of partial charges on the collagen backbone from dielectric cores of surrounding collagen molecules fits the data as well (assuming $\kappa=0$ and $5\leqslant\varepsilon\leqslant 80$ so that $7\leqslant l_B\leqslant 100$ Å).

every amino acid regardless of its side chain (similar to α-helices, Sec. IV.A). These charges do follow the helical symmetry of the molecule and, because of their large number, can produce a significant, although rapidly decaying, electric field. Their contribution to the interaction energy can be estimated from Eqs. (107)–(110) with $N_s=1$ (while collagen is a triple helix, its three strands are essentially fused into one; Fraser *et al.*, 1979, 1983), $H=9.6$ Å, $\kappa=0$, $l_c\sim 3$ Å, and $\zeta_1\sim 1$. As in the case of guanosine helices, the measured decay length closely matches the prediction $H/4\pi\approx 0.75$ Å for the image repulsion. The observed amplitude also lies within the possible range of the predictions (defined by the uncertainty in the effective value of the dielectric constant, $5\leqslant\varepsilon\leqslant 80$). Thus the measured force could be the image repulsion. However, it could also originate from the energetic cost of deforming the hydrogen bond network in water (hydration forces), as suggested by measurements in polar, nonaqueous solvents (Kuznetsova *et al.*, 1997) and by Raman spectroscopy (Leikin *et al.*, 1997). The mean-field model for hydration forces (Marčelja and Radic, 1976) is closely related to the formalism of the DH theory (Kornyshev and Leikin, 1989). It yields equations similar to Eqs. (107)–(110) with $4l_B\zeta_{N_s}^2/l_c^2$ and κ replaced by phenomenological constants (Kornyshev and Leikin, 1997), and it gives essentially the same prediction $\approx H/4\pi$ for the decay length of the repulsion (Fig. 19). Regardless, it appears that the interaction between collagen molecules is also intimately related to the structure of their helices.

G. Integral screw puzzle

Since intermolecular interactions appear to be significantly affected by the structure of the helix, the structure must be affected by interactions as well. Several examples of such effects in DNA aggregates have been known experimentally for 25–50 years, but this had not been addressed theoretically because the DNA structure was simply not accounted for in the theory of intermolecular interactions. In particular, since the early crystallographic studies, *B*-DNA was known to have an approximately ideal helical structure with ten base pairs per turn in fibers (Saenger, 1984) (Secs. II.D–II.F). A crystallographic model attempted to explain this in terms of repeated hard-core interactions, in a densely packed nonhexagonal lattice of the molecules (Dover, 1977). However, hydrated DNA in a columnar, hexagonal lattice was found to retain the ideal helix structure with 10 bp/turn with up to at least 10–15 Å surface separation (Zimmerman and Pheiffer, 1979; Rhodes and Klug, 1980). At the same time the structure of DNA in solution was found to be nonideal with an average of ~10.5 bp/turn (Griffith, 1978; Levitt, 1978; Wang, 1979). It was therefore concluded by Rhodes and Klug (1980) that "in …fibres of DNA, the molecules still interact, however weakly, through several layers of water and influence each other to produce an integral screw." This appeared to be the property only of fibers from long, natural DNA. The structure of synthetic DNA oligomers in crystals was determined to be closer to the nonideal helical structure in solution than to the ideal structure in fibers (Dickerson, 1983).

The first theoretical attempts to address this long-standing puzzle were made by Kornyshev and Leikin (1998a, 2001). It was pointed out that sequence-dependent variations in the twist angles between adjacent base pairs would prevent proper azimuthal alignment in juxtaposition of long molecules with uncorrelated sequences. Without torsional adaptation, the misalignment would accumulate with the juxtaposition length L as $2\Delta_\phi^2=L/2\lambda_c$ [Sec. V.E, Eq. (62)], where $\Delta_\phi^2=\langle(\phi_\nu-2\pi z/\langle H\rangle)^2\rangle$ is the mean-square nonideality of each helix. This would completely disrupt the energetically favorable contribution from helical harmonics of charge-charge interactions [second and third terms in Eq. (98)]. The gain in the electrostatic interaction energy from reestablishing the alignment is higher than the energetic cost of the corresponding torsional deformation resulting in torsional adaptation of molecules to each other (Sec. V.E).

In pairs, only relative alignment of molecules is important and they can adapt to each other without becoming ideal helices (Sec. V.E). In fibers, each molecule interacts with six neighbors. This increases the energy gain and enhances torsional adaptation. Furthermore, energetically favorable alignment between all neighbor pairs in a columnar aggregate is possible only for molecules with identical sequences (oligomers in crystals) or for ideal helices with limited rather than accumulating Δ_ϕ^2. Based on calculations of the corresponding energies, it was

concluded that helical harmonics of electrostatic interactions induce torsional deformation and idealize each helix (Cherstvy *et al.*, 2004).

While the origin of the ideal average helical conformation of long, natural DNA in fibers now appears to be reasonably clear, the physics of overwinding from 10.5 bp/turn in solution to 10 bp/turn in fibers is still a mystery.

The following hypothesis has been suggested (Kornyshev and Leikin, 1998a). The structure factors of an ideal helix,

$$s_{p,p}^{\nu,\mu}(k_z,n,m) \propto \sum_{j,J=-\infty}^{\infty} \delta(k_z + gn - Gj)\delta_{m,n+JG/g}, \qquad (111)$$

have additional maxima at integral $G/g \equiv H/h$ (e.g., at $k_z=0$, $n=m=jG/g$; $k_z=0$, $n=0$, $m=JG/g$; $k_z=0$, $m=0$, $n=-JG/g$; at $j\neq 0$ and $J\neq 0$). These peaks in the structure factors result in corresponding contributions to the intermolecular interactions. The corresponding interaction modes disappear in helices with a nonintegral screw. An estimate comparing the interaction energies at $G/g=H/h=10$ and $H/h\approx 10.5$, both in ideal helical conformations, suggested that the energy gain upon establishing the integral screw might be sufficient to induce the overwinding (Kornyshev and Leikin, 1998a).

However, this was a ground-state estimate. It did not take into account torsional and azimuthal fluctuations. Consider, for example, integral screw interaction modes with $k_z=0$, $n=0$, $m=\pm 10$ and $k_z=0$, $m=0$, $n=-\pm 10$. For the tenth-order term [analogous to the lower orders of Eqs. (57), (59), and (98)], we find that their maximal contribution to the pair interaction energy at the optimal alignment of a given pair within the aggregate is

$$\frac{\delta E(R)/L}{k_B T} \sim -\frac{8l_B}{l_c^2}\frac{(1-\theta)[K_{10}(\kappa R)+\Omega_{0,10}(\kappa R,\kappa a)]}{(\kappa a)^2 K_1(\kappa a)K_{10}'(\kappa a)} \times e^{-50(\Delta_\phi^2+\Delta_\Phi^2)}. \qquad (112)$$

The integral screw interactions depend on the torsional (Δ_ϕ^2) and azimuthal (Δ_Φ^2) displacements as $\exp[-50(\Delta_\phi^2+\Delta_\Phi^2)]$. From the same x-ray data that established the integral screw we know that the torsional and azimuthal fluctuations (while small) are still sufficient to suppress the intermolecular scattering at $n=3$ due to the fluctuation factor of $\exp[-n^2(\Delta_\phi^2+\Delta_\Phi^2)]$ (Sec. VI.D). Thus $\exp[-9(\Delta_\phi^2+\Delta_\Phi^2)]\ll 1$, consistent with theoretical estimates (Lee and Wynveen, 2006). Because of their incredibly strong dependence on Δ_ϕ^2 and Δ_Φ^2, the integral screw interaction modes considered above, which at first glance explained the effect, should be completely washed out by fluctuations. The same conclusion could be made if the interactions arise from hydration, steric, or any other forces. The idea of intermolecular interactions being directly responsible for setting the integral screw through the corresponding interaction modes simply does not work.

Presently, we are aware of only two possible explanations of the integral screw. (i) It was suggested that the intrinsic pitch of the DNA double helix changes continuously with the interaxial distance in columnar aggregates, and therefore the apparent integral screw is not an exact but rather an approximate value at typical aggregate densities. However, this idea, proposed by Durand *et al.* (1992), was based on rather low-quality x-ray data, which required corrections for imperfect orientations of molecules. Therefore the separation dependence of the pitch might be an artifact of the corrections. Indeed, the integral screw of 10 bp/turn independent of the aggregate density was based on much higher-quality x-ray data, which did not require such corrections (Zimmerman and Pheiffer, 1979; Rhodes and Klug, 1980). (ii) Alternatively, 10 bp/turn could be an intrinsic property of the ideal double helix, e.g., the average structure of synthetic DNA with the *ATATAT*… sequence is an ideal helix with 10 bp/turn, both in solution and in aggregates (Saenger, 1984). The role of intermolecular interactions might be in enforcing the ideal average structure of DNA with random base-pair sequences while the overwinding from 10.5 to 10bp/turn might be an intrinsic property of such a structure (which is still not understood). Regardless, the puzzle of the integral screw has not yet been solved.

H. Electrostatics of the *B*-*A* transition in DNA

Other polymorphic transitions may also be attributed to the helical interactions between molecules. One such transition is that from the *B* to the *A* form of DNA (Langridge *et al.*, 1960; Ivanov *et al.*, 1974; Ivanov and Krylov, 1992), observed for a single DNA molecule in mixed solvent solutions (Ivanov *et al.*, 1974) and for DNA aggregates upon removal of water (Langridge *et al.*, 1960). A number of studies of this transition for an isolated DNA molecule in solution (see, e.g., Yang and Pettit, 1995; Cheatham and Kollman, 1996; Jayaram *et al.*, 1998; Banavali and Roux, 2005; Elsawy *et al.*, 2005; and references therein) considered potential roles of hydration and counterions. However, the role of intermolecular interactions in this transition was not explored until recently, despite clear experimental evidence of their importance in aggregates (Lavalle *et al.*, 1990; Rupprecht *et al.*, 1994).

The interaction-driven *B* to *A* transition occurs in dense aggregates containing little water. Although hard-core interactions between DNA might be very important in such aggregates, electrostatics is also likely to play a large role. To learn the qualitative physics of the latter, the following model was proposed (Kornyshev and Leikin, 1998b). To avoid limitations of the PB theory and the poorly known dielectric response of water at small distances, all ions and partial charges on water molecules were treated explicitly, on the same footing as DNA phosphates. The Coulombic Green's function (Sec. IV.A) with $\varepsilon\approx 2$ of a sterically confined, frozen, interstitial solution was used to describe interactions between all these charges. In the first approximation, the osmotic pressure of trapped counterions in such a dense aggregate is determined simply by their total

TABLE I. Structural parameters of *A* and *B* forms of DNA.

Structure type	b (Å)	H (Å)	$\tilde{\phi}_s$ (rad)	l_c (Å)
A	9	28.2	0.66π	1.3
B	9	33.8	0.40π	1.7

concentration. Therefore it does not contribute to the transition energy at constant hydration. As above, the energy associated with helical harmonics of the molecular charge pattern was calculated as a sum of all pair interaction energies E_{pair} between nearest-neighbor molecules. It was argued that at constant hydration the main contribution into E_{pair} can be approximated by

$$\frac{E_{\text{pair}}/bp}{k_BT} \approx \frac{8l_B}{l_c}\sum_{n=1}^{\infty}(-1)^n\tilde{\zeta}_n^2K_0(ngR)I_n^2(nga)\cos(n\delta\phi), \tag{113}$$

where the dimensionless parameter $\tilde{\zeta}_n$ [cf. Eqs. (39) and (40)] is determined by the patterns of fixed DNA charges, counterions, and fractional water charges (analogous to ζ_n at larger distances, Secs. IV.D and V.D), $g=2\pi/H$ is the intrinsic twist (reciprocal pitch) in each helical form, and $\delta\phi$ is the difference in the azimuthal phases of molecules.

The difference of the interaction energies between DNA of the *B* and *A* forms primarily results from their distinct structural parameters (see Table I), with the chief difference originating from the disparity in the azimuthal width $\tilde{\phi}_s$ of their minor grooves and in the charge density (l_c). It has been suggested that some insight into the electrostatics of the transition at constant hydration can be gained even without detailed knowledge of the pattern of counterion and water charges (Kornyshev and Leikin, 1998b). For instance, one would expect the main contribution into the electrostatics of the transition to originate from phosphate-phosphate interactions. Their contribution into the interaction energy is given by Eq. (113) with $\tilde{\zeta}_1^2=\cos^2(\tilde{\phi}_s)$, yielding $\tilde{\zeta}_1^2 \approx 0.23$ for *A*-DNA and $\tilde{\zeta}_1^2 \approx 0.1$ for *B*-DNA. Substitution of these values into Eq. (113) revealed that the *B* to *A* transition reduces the corresponding energy of pair interactions between DNA by $\sim 2k_BT$ per base pair at an interaxial separation of $R \approx 23$ Å (Kornyshev and Leikin, 1998b). The phosphate pattern of the *A* form, more favorable for electrostatic interactions between DNA molecules, outweighs the unfavorable increase in their surface density. It is indeed more favorable for interactions, as it allows for a stronger separation of positive and negative charge motifs within each molecule. Moreover, at higher aggregate densities, the optimal alignment of phosphates on the opposing molecules is achieved at $\delta\phi=0$ in the *A* form and at $\delta\phi \neq 0$ in the *B* form. As discussed in the next section, $\delta\phi=0$ is the only alignment that prevents the energetically unfavorable azimuthal frustration on a densely packed lattice, resulting in an additional energetic advantage of the *A* form. Note that the corresponding different alignment for the two forms in natural DNA fibers was observed by x-ray diffraction (Langridge *et al.*, 1960; Dover, 1977).

A subsequent study explored additional electrostatic contributions arising from the effects of different condensed counterion distributions and from many-body correlations at $\delta\phi \neq 0$ (Rudd *et al.*, 2007). Analysis of various approximations with fixed fractions of counterions at different locations suggest that counterion absorption in grooves results in the increased importance of intramolecular electrostatic interactions near the *B* to *A* transition. However, for the weak localization expected for monovalent counterions, the electrostatics of the transition appears to be driven by the phosphate-phosphate interactions discussed above. A predominant adsorption of counterions in the wider groove provides a particularly strong intermolecular impetus towards the *B* to *A* transition (Kornyshev and Leikin, 1998b).

I. *XY* models of mesomorphic transitions in DNA aggregates

Crystallographic studies of aggregates revealed not only the cholesteric-hexagonal transition and DNA polymorphism discussed above but also various mesomorphic changes in the symmetry of lateral packing of both *B*- and *A*-DNA (Langridge *et al.*, 1960). While quantitative modeling of such mesomorphic transitions is hindered by the lack of exact knowledge of the full interaction potentials at short distances, much can still be learned from the general form of the dependence of the interaction energy on azimuthal orientations of individual molecules (Kornyshev and Leikin, 1997).

We start from the simplest case of ideal, rigid double helices, where the energy of interaction between parallel molecules of a columnar assembly can be written in a form of a new kind of frustrated *XY* model. Both in highly hydrated and in dense aggregates, the interaction energy can be rewritten as [see Eq. (98)]

$$\frac{E}{k_BT} = \frac{L}{2}\sum_{\nu,\mu}\{u_0(R_{\mu,\nu}) - u_2(R_{\mu,\nu}) - u_1(R_{\mu,\nu})(\mathbf{s}_\nu\cdot\mathbf{s}_\mu) + 2u_2(R_{\mu,\nu})(\mathbf{s}_\nu\cdot\mathbf{s}_\mu)^2\}. \tag{114}$$

Here the summation is performed only over nearest neighbors, as the coupling constants exponentially decrease with the distance between sites (molecules). The spins

$$\mathbf{s}_\nu = \cos(\Phi_\nu/2)\hat{\mathbf{x}} + \sin(\Phi_\nu/2)\hat{\mathbf{y}} \tag{115}$$

represent azimuthal orientations Φ_μ of the double helices. The positive coefficients $u_0(R_{\mu,\nu})$, $u_1(R_{\mu,\nu})$, and $u_2(R_{\mu,\nu})$ are determined by the interaction potentials [e.g., Eq. (59)]. Unlike Eqs. (97) and (98), here the interaxial distance $R_{\mu,\nu}$ between nearest-neighbor helices μ and ν is not assumed to be the same throughout the

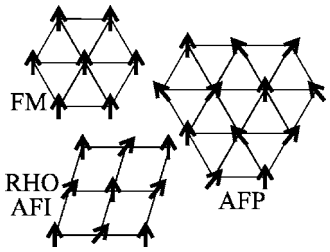

FIG. 20. Different spin configurations and lattice types for columnar assemblies of DNA in the ground state (Harreis *et al.*, 2002). The FM (ferromagnetic) state corresponds to when the spins (azimuthal orientations of the molecules) are all aligned. The RHO AFI state corresponds to an antiferromagnetic, rhombic lattice where spins on one sublattice have one value and those on the other sublattice have another. The rhombic packing of this lattice reduces less favorable interactions between like spins. The AFP is a hexagonal antiferromagnetic Potts state that has three sublattices with different spin orientations. In both the AFI and AFP lattices, the relative spin angles tend to increase with increasing molecular density.

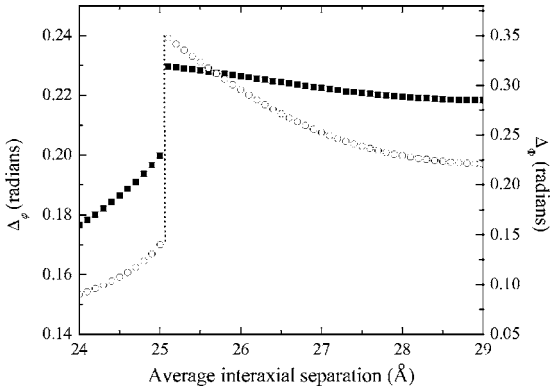

FIG. 21. Estimated torsional Δ_ϕ (solid squares) and rigid-body Δ_Φ (open circles) fluctuations in an assembly of 500-Å-long DNA fragments at $C_t=3.0\times10^{-19}$ erg cm, a DNA charge compensation $\theta=0.7$, and ζ_n corresponding to 30%:70% minor:major groove distribution [Eq. (40)] (Lee and Wynveen, 2006). The break at ~25 Å corresponds to the transition from the ferromagnetic state to the rhombic antiferromagnetic state (at smaller molecular separations).

assembly. This generalized formulation allows one to describe lattice distortions as well as liquidlike phases and it also provides useful analogies with magnetic systems (Izyumov and Skryabin, 1988). The peculiar feature of Eq. (114) is that the first ferromagnetic term tends to align the spins parallel to each other while the second term favors a perpendicular orientation, resulting in azimuthal frustration (Sec. V). This second term provides for much of the interesting many-body physics of the problem.

Ground state. The competition between these two terms leads to ground states with different lattice symmetry and spin configurations (Fig. 20), depending on distribution of counterions and density of the molecules (Harreis *et al.*, 2002, 2003). At low DNA density, the ferromagnetic term dominates and a hexagonal, ferromagnetic phase with parallel spin is expected (Fig. 20, FM). At higher density, azimuthal frustration leads to hexagonal packing with three alternating spin orientations (Fig. 20, AFP), when the dominating contribution into the energy comes from $u_0(R_{\mu,\nu})$ and $u_2(R_{\mu,\nu})$. A rhombic lattice with two alternating spin orientations forms when the contribution from the first and second helical harmonics [$u_1(R_{\mu,\nu})$ and $u_2(R_{\mu,\nu})$] becomes more important. Similar mesophases were also predicted using a phenomenological Landau theory (Lorman *et al.*, 2001).

Statistical mechanics. Calculation of the partition function of spins on a 2D hexagonal lattice with the interaction Hamiltonian given by Eq. (114) formally predicts two additional mesophases where the spins are topologically disordered (Wynveen *et al.*, 2005). One of these phases is a Berezinskii-Kosterlitz-Thouless vortex state (Kosterlitz and Thouless, 1973). The other is a more exotic state formed by domain walls between two possible lattice configurations with three alternating spin orientations[11] (Wynveen *et al.*, 2005). Self-consistent approximations and simulations that treat the positional and spin degrees of freedom on the same footing revealed evidence for a first-order transition between the ferromagnetic state and the rhombic antiferromagnetic state, instead of the second-order transition predicted in the ground state (Wynveen *et al.*, 2005). Furthermore, frustration of the molecular orientations leads to a counterintuitive reduction in the crystalline ordering of the system at large densities so that the system becomes more liquidlike with increasing density.

Another putative state of liquid crystal order is hexatic (Toulouse, 1977), which is defined as having long-ranged bond-orientation ordering but short-ranged liquidlike positional order. This state has been reported in experiments with long densely packed DNA (Podgornik *et al.*, 1996; Strey *et al.* 2000) and has been rationalized in terms of frustrated azimuthal interactions (Strey *et al.*, 2000). Such a state cannot be described by existing XY models with fixed molecular positions.[12]

Finally, a model incorporating nonideality of molecules in the manner similar to Sec. V.E. (Lee, 2006; Lee and Wynveen, 2006) allows one to estimate torsional and azimuthal fluctuations of molecules (Fig. 21). The root-mean-square amplitudes of these fluctuations (Δ_ϕ,Δ_Φ ~0.1–0.4 rad) are consistent with the values based on x-ray-diffraction patterns of hydrated DNA fibers

[11]States akin to this have been seen in other frustrated magnetic systems (Lee *et al.*, 1986).

[12]It is known experimentally that shorter DNA duplexes form hexagonal columnar rather than hexatic phases. It is thus not excluded that the apparent line-hexatic phase may be a consequence of entanglement of long DNA. However, similar order was found for shorter molecules in simulations in which the positions of the molecules were not fixed for assemblies of intermediate density (Wynveen *et al.*, 2005).

(Kornyshev *et al.*, 2005; Sec. VI.D). They are also sufficiently small and consistent with the values estimated for Gaussian fluctuations near the ground state (Kornyshev, Leikin, *et al.*, 2002), further supporting the low-temperature behavior of azimuthal correlations. As expected based on the latter Gaussian estimates, azimuthal correlations weaken upon approach to the transition from the ferromagnetic to the frustrated (rhombic antiferromagnetic) state. However, helix nonideality drastically reduces this effect so that the correlations remain strong at all relevant interaxial spacings.

Although intriguing and qualitatively consistent with some experimental observations [cf., e.g., the observed structural transitions in assemblies of guanosine columns (Rudd *et al.*, 2006)], these results are still based on a crude quasi-2D approximation, as well as popular approximations of the many-body theory (such as the Hartee approximation, etc.). Furthermore, their most interesting predictions refer to fairly dense aggregates (e.g., $R<25$ Å for DNA) where the basic expression for the pair potential may not be justified. Thus, although XY models might provide some insight into the qualitative physics of mesophases associated with frustrated azimuthal interactions and can be helpful in rationalizing the cholesteric-to-columnar transition, one should take their predictions with a grain of salt. A significant, but challenging, step would be to develop true 3D calculations which allow for staggered alignments of adjacent helices.

J. Summary and comments

Aggregates or liquid crystalline phases formed by biological helices pose challenges for both theory and experiments. Progress has been made in modeling interaction potentials that account not only for the structure of individual molecules but also for at least some of the many-body effects of assemblies. But the statistical physics of such assemblies is still in its infancy. Some of the experimental observations can be rationalized in terms of the existing models, providing some confidence of theories being on the right track. However, few ideas have been rigorously proven and many experimental observations still seek explanation.

VII. COUNTERION-INDUCED DNA CONDENSATION

When added to DNA solution, some counterions induce aggregation of DNA double helices. On addition of these condensing agents, a single (or many) long DNA molecules will condense primarily into dense toroidal structures and, to a lesser extent, rodlike particles (Lang, 1973; Eickbush and Moudrianakis, 1976; Lang *et al.*, 1976; Chattoraj *et al.*, 1978; Marx and Ruben, 1983; Arscott *et al.*, 1990; Hud *et al.*, 1993; Hud and Vilfan, 2005). Condensation into these structures has been found to occur for only molecules longer than 400 base pairs (Widom and Baldwin, 1980). However, at high DNA concentrations or under osmotic stress, short DNA fragments, of the order of a persistence length, can be condensed into liquid crystalline phases (Robinson, 1961; Rill *et al.*, 1983; Rill, 1986; Sikorav *et al.*, 1994; Livolant and Leforestier, 1996; Pelta, Livolant, and Sikorav, 1996; Podgornik *et al.*, 1996; Strey *et al.*, 2000, Raspaud *et al.*, 2005), as discussed in the previous section. While the outside morphology (toroids, spheroids, rods, fibers, etc.) depends on a variety of factors, for example, length and concentration of DNA, inside the aggregates DNA molecules are generally packed into similar, ordered (usually columnar) arrays. This counterion-induced condensation of DNA is readily reproduced in a test tube and yet it is one of the most fundamental processes crucial for our very existence. Protamine, a basic polypeptide acting as a DNA counterion, binds and condenses DNA into compact toroidal subunits in the sperm of most vertebrates, inactivating and packaging centimeters of DNA in a micron-size sperm head until it is reactivated after fertilization.

It does not come as a surprise that counterion-induced DNA condensation is one of the most extensively studied, most frequently discussed, and best reviewed topics in the interaction between biological helices (Robinson, 1961; Lang, 1973; Laemmli, 1975; Eickbush and Moudrianakis, 1976; Gosule and Schellman, 1976; Lang *et al.*, 1976; Chattoraj *et al.*, 1978; Wilson and Bloomfield, 1979; Widom and Baldwin, 1980, 1983; Marx and Ruben, 1983; Rill *et al.*, 1983; Rill, 1986; Knoll *et al.*, 1988; Arscott *et al.*, 1990; Strzelecka and Rill, 1990; Bloomfield, 1991, 1996, 1997; Hud *et al.*, 1993, 1995; Ma and Bloomfield, 1994; Ubbink and Odijk, 1995; Pelta, Livolant, and Sikorav, 1996; Kassapidou *et al.*, 1998; Raspaud *et al.*, 1998, 2005; Deng and Bloomfield, 1999; Stevens, 2001; Burak *et al.*, 2003; Hud and Vilfan, 2005). Not only is it relevant for the understanding of how DNA is compacted in sperm heads, viral capsids, and in the cell, but there is also speculation that the nature of the condensed phases of DNA may play an important role in the function of nucleic acids in biological systems (Krasnow and Cozzarelli, 1982; Sikorav and Church, 1991; Sikorav *et al.*, 1994). Nevertheless, it is only in the last few years that theories and experiments have reached sufficient sophistication and detail to reveal which of the many proposed concepts and models actually fit the condensation data.

A. Experimental observations

Cations that condense DNA. By commonly referring to "DNA condensation by multivalent cations" (Bloomfield, 1997), the biochemical and biophysical literature on this subject implicitly creates an image of DNA being condensed by small, pointlike ions with $\geqslant$3+ charge. Many interpretations have been built on this image, including most recently proposed physical theories. But none of the commonly used DNA-condensing cations with $\geqslant$3+ charge fit this picture.

Spermine (Sp), spermidine (Spd), protamine, polylysine, and other *polycations* that condense DNA *in vivo* and *in vitro* are not pointlike charges and cannot be even roughly approximated as such. The distance be-

tween ionic groups in these polymers is at least comparable to and often larger than all pertinent lengths in the problem, that is l_B, λ_D, l_σ, l_c, and even the radius of DNA. It would be better to model them as 1+ charges connected by flexible chains.

Cobalt hexamine (Co-hex, $Co[NH_3]_6^{3+}$) is the only commonly used multivalent cation that is not a polymer, but it is also fairly large. Its diameter (~6 Å; Deng and Bloomfield, 1999) is bigger than l_σ and l_c and comparable to l_B and λ_D. Its approximation as a pointlike charge is marginal, at best.

The only reasonable pointlike cations that condense *B*-DNA without significantly affecting its structure (as confirmed by x-ray diffraction) are divalent Mn^{2+} and Cd^{2+} (Knoll *et al.*, 1988; Rau and Parsegian, 1992b). Interestingly, unlike Sp, Spd, and Co-hex, Mn^{2+} condenses DNA much more efficiently at elevated temperatures, e.g., $MnCl_2$ condenses DNA only above 40–45 °C [Fig. 17(a)] (Rau and Parsegian, 1992b). In 150 mM $Mn(ClO_4)_2$, DNA is condensed already at 5 °C (Rau and Parsegian, 1992b), but the strength of the attraction between DNA molecules still increases with increasing temperature, as indicated by decreasing interaxial spacing (Rau and Parsegian, 1992b) and measured intermolecular forces (Leikin *et al.*, 1994). Notably, the alkaline-earth ions Ca^{2+} and Mg^{2+} do not cause DNA condensation at the same conditions (Knoll *et al.*, 1988; Rau and Parsegian, 1992b; Bloomfield, 1996).

Such remarkable cation specificity is not an exception but rather a common feature of all counterions used to condense DNA. For instance, (i) for several polymeric diamines with different spacers between their two charged amine groups, few were able to condense DNA and few were not (Zinchenko *et al.*, 2004). (ii) The potency of spermine homologues, as condensing agents, with different spacers between two central amines was found to depend on the spacer length in a nonmonotonic fashion (Vijayanathan *et al.*, 2001). (iii) DNA condensation by Co-hex, tris(ethylenediamine) cobalt (Co-en), and cobalt sepulchrate (Co-sep) was studied by Deng and Bloomfield (1999). All three cations are cobalt-amines and all of them have 3+ charge, but a much lower concentration of $Co\text{-}sep^{3+}$ was needed to condense DNA. Furthermore, one of the two stereoisomers of $Co\text{-}en^{3+}$ was selectively bound in DNA aggregates, suggesting that it is a stronger condensing agent than the other isomer.

Physics or chemistry? At the same time, a similar extent of DNA charge neutralization was found at the onset of condensation (~80–90%) (Wilson and Bloomfield, 1979; Widom and Baldwin, 1983; Matulis *et al.*, 2000; Burak *et al.*, 2003; Baigl and Yoshikawa, 2005). At the scale of several nearest neighbors, similar hexagonal packing of condensed *B*-DNA was observed in toroids and other forms of aggregates induced by different counterions (Schellman and Parthasarathy, 1984; Hud, 1995; Livolant and Leforestier, 1996). Molecules were found to be packed at the same spacing of about $R \sim 30 \pm 3$ Å (Hud and Downing, 2001; Raspaud *et al.*, 2005) and similar forces were measured upon osmotic compression of aggregates induced by different counterions (Rau and Parsegian, 1992b).

These similarities suggest that it should be possible to think about DNA condensation in terms of the common physical forces organizing molecules. Partly motivated by this problem, significant progress has been made in recent years in theories of counterion-induced electrostatic attraction between like charged rods. A variety of different models, all predicting such attraction, have been developed (Sec. V.C). The challenge now is to reconcile the predictions of these models with the data, for example, to understand why some counterions condense DNA better than others. The pertinent chemistry of counterions is likely to be simple, for example, counterions having different binding constants and/or sites on DNA. But it cannot be ignored. Both the physics and chemistry of the system appear to be important.

The problem of resolubilization of DNA aggregates (Pelta, Durand, *et al.*, 1996; Pelta, Livolant, and Sikorav, 1996; Raspaud *et al.*, 1998, 1999; Saminathan *et al.*, 1999) is an excellent illustration of the latter point. Reversal of DNA charge from negative to positive may be invoked to explain the resolubilization of DNA aggregates observed at high concentrations of Sp and Spd (Shklovskii, 1999b; Nguyen *et al.*, 2000a, 2000b, 2000c). One might expect sufficiently strong binding to cause adsorption of more multiply charged counterions than what is needed to neutralize the charge of DNA, thereby resulting in effective charge reversal. Certain theories have suggested that for highly charged surfaces and multivalent point charges (strong coupling, $\Xi \gg 1$) such charge reversal would not even require chemical adsorption (Shklovskii, 1999b; Nguyen *et al.*, 2000b, 2000c). However, there may be important chemical aspects missing in such descriptions when applied to real systems that, in turn, could have important consequences for the physics of these systems. Also, Sp and Spd cannot be considered as single point charges. Furthermore, at the concentrations ($\geqslant$100 m*M*) required for DNA resolubilization they might not even be fully dissociated. This means that $SpdCl_3$ solution might contain not only Spd^{3+} and Cl^- ions, but also $SpdCl^{2+}$ and potentially even $SpdCl_2^+$. Spd that may not be completely dissociated would then compete for binding to DNA and displace the fully dissociated Spd, potentially reducing the extent of charge neutralization at high Spd concentration. This hypothesis was tested by detailed measurements of the structure of DNA aggregates condensed with different Spd salts (with different dissociation constants) and by competitive binding studies (Yang and Rau, 2005). The results seem to suggest that incomplete dissociation of Spd salts does occur at these concentrations. A possible interpretation would be that it is underneutralization (due to preferential binding of the partially dissociated species) rather than charge reversal that underlies the weakened attraction between DNA molecules at high Spd concentration (Yang and Rau, 2005).

B. Counterion-correlation models

Most models describe DNA condensation in terms of electrostatic forces in the context of pair interactions, which were discussed in Sec. V. Before proceeding with comparisons of these models with experimental data, however, we note two other hypotheses. Attractive hydration forces due to water structuring by phosphates and counterions have been discussed by Leikin *et al.* (1991, 1993) and Rau and Parsegian (1992a). But, for highly charged DNA, they are difficult to distinguish (both conceptually and quantitatively), for example, from corrections associated with the nonmacroscopic dielectric response of water (Sec. V.A). Bridging of DNA, for example, by spermine or spermidine molecules spanning across the water gap between DNA molecules has been proposed (Allison *et al.*, 1981; Schellman and Parthasarathy, 1984; Raspaud, *et al.*, 1998, 1999; Bloomfield *et al.*, 2000). Such bridging might contribute to DNA condensation by long polyamines, but it cannot explain, for example the Mn^{2+} and Cd^{2+} data. Thus it is not likely to be a universal mechanism for DNA condensation (Rau and Parsegian, 1992a).

In all electrostatic models, the attraction responsible for DNA condensation is between negatively charged phosphates on one molecule and positively charged counterions condensed onto the other molecule. Counterion-correlation models approximate DNA as a homogeneously charged rod and condensed counterions as pointlike charges. Juxtaposition of positive and negative charges occurs due to alignment of cations on one rod opposite to "correlation holes" (spaces between cations) on the opposing rod (Oosawa, 1971, Marquet and Houssier, 1991). The correlations between positions of condensed counterions are generally liquidlike (Arenzon *et al.*, 1999; Ha and Liu, 1999a, 1999b; Levin *et al.*, 1999; Sec. V.C). It has been argued, however, that $\geqslant$3+ charges might begin organizing themselves into a quasicrystalline lattice (Rouzina and Bloomfield, 1996), akin to the Wigner crystal (Shklovskii, 1999a, 1999b; Grosberg *et al.*, 2002). Computer simulations of rods with DNA surface charge density in a continuum dielectric with $\varepsilon=80$ found no evidence of crystallinelike organization of trivalent point charges on rods (Deserno and Holm, 2002). But the effective ε within the layer of condensed counterions might be much smaller than 80, increasing the effective coupling parameter $\Xi \propto \varepsilon^{-2}$ by up to two orders of magnitude. If that were the case, the coupling might become strong enough for formation of large quasicrystalline domains by 3+ point charges. Because of the quasi-1D nature of the DNA cylindrical geometry, this may not be guaranteed due to thermal fluctuations (Sec. V.C).

Regardless of whether such crystalline domains form or not, the Wigner-crystal model provides the best way to obtain an accurate upper estimate for the attractive interaction energy due to counterion-correlation forces. Indeed, this model corresponds to the formal low-temperature limit for counterion-correlation forces, which become stronger with decreasing temperature due to the increasing strength of counterion correlations (Levin *et al.*, 1999). In the Wigner-crystal model the attractive interaction energy between rods can be calculated exactly at any interaxial distance as described in Sec. V.C. The results of such a calculation (Fig. 22) show that the attraction becomes strong enough to contribute to the observed DNA condensation only when the charge of the pointlike cations is 3+ or larger (Rouzina and Bloomfield, 1996).

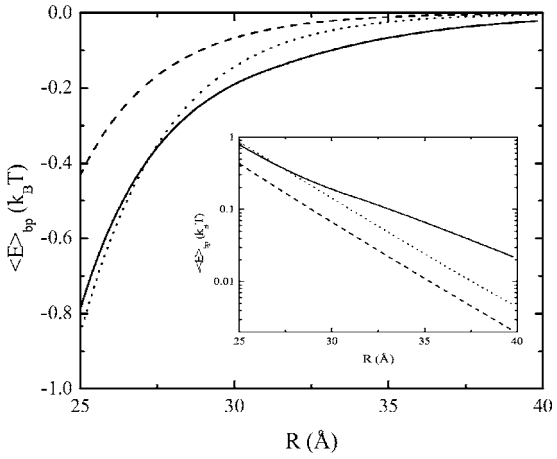

FIG. 22. Comparison of attractive interaction energies per base pair in a hexagonal aggregate calculated within different models at complete charge compensation (θ=1, no image charge repulsion). (1) (Long dashed) Wigner crystal model [Eqs. (52)–(54)] with 2+ counterions (calculated as described in Sec. V.C.2, but with the complete set of harmonics). (2) (Short dashed) Wigner-crystal model with 3+ counterions. (3) (Solid line) Electrostatic zipper model [calculated from Eqs. (57) and (59)] at 30:70 minor:major groove ratio of condensed:bound counterions; $\zeta_1^2=0.5$ and $\zeta_2^2=3.3$, Eq. (40). Inset: The same results on a logarithmic scale, demonstrating the slower decay of the energy within the electrostatic zipper model.

Thus counterion-correlation forces, on their own, are likely not strong enough to explain DNA condensation by Mn^{2+} and Cd^{2+}. Furthermore, selectivity (condensation by Mn^{2+} and Cd^{2+} but not by Mg^{2+} or Ca^{2+}) and temperature-favored DNA condensation by these divalent ions are inconsistent with the counterion-correlation model as well. For spermine, spermidine, and other cationic polymers, these forces should be even weaker. With regard to counterion-correlation forces, such molecules, which are essentially flexible chains of monovalent ions, are expected to behave more like monovalent rather than multivalent ions, since they are longer than the surface separation and the average distance between fixed charges.

In other words, counterion-correlation forces are likely to be a factor only in DNA condensation by cobalt amines. But, even in this case, they are not likely to be the only or the dominant condensation mechanism. For homogeneously charged rods the larger and more hydrophobic Co-sep^{3+} ion would be expected to have a lower binding constant, in comparison to Co-hex^{3+}. Therefore one would predict a higher concentration nec-

essary for the onset of DNA condensation. The experimental observations are exactly opposite. The preferential condensation by one of the Co-en^{3+} stereoisomers is equally difficult to explain within this mechanism. It comes into conflict with the basic idea of ion correlations based on the ability of condensed counterions to move freely along the DNA surface. Instead, such stereoisomer specificity suggests the importance of preferential binding at some specific sites, which can be described only if one incorporates the DNA structure into the theory.

C. Electrostatic zipper model

Because they are based on the homogeneously charged rod approximation, counterion-correlation models inherently account only for positional correlations of condensed counterions with each other. The theory of interactions between inhomogeneously charged rods (Kornyshev and Leikin, 1997, 1999) accounts for all correlations: counterion-counterion, phosphate-phosphate, and phosphate-counterion (Sec. V). The latter manifests itself in excess positive charge in DNA grooves and excess negative charge on phosphate strands, allowing for an attractive zipperlike juxtaposition of the strands and grooves (Sec. V.D, Fig. 7) (Kornyshev and Leikin, 1999). The strength of this attraction is determined by the extent of DNA charge neutralization θ and by the two dimensionless, weighted helical moments ζ_1 and ζ_2 of the distribution of fixed charges and condensed counterions. Complete expressions relating ζ_1 and ζ_2 to the density profiles of fixed charges and condensed counterions are given in the EPAPS Document in the Reference Section.

This electrostatic zipper model predicts the onset of DNA condensation at $\theta=\theta_c\sim 0.8–0.9$ (Fig. 23), similar to most other models. Unlike other models, it predicts a significant dependence of the condensation onset on the charge asymmetry of the major and minor grooves (Fig. 7). A simple heuristic model of counterion adsorption relating the values of ζ_1 and ζ_2 used in Figs. 22 and 23 to fractions of counterions adsorbed at different locations on DNA surface is described in Sec. IV.D, Eq. (40). In general, larger partitioning of counterions into the major grove increases ζ_1^2 and so favors the condensation (Sec. V.D).

Rigorous quantitative analysis of the zipper model would require a self-consistent calculation of θ, ζ_1, and ζ_2 at all values of R. However, to first approximation one can assume θ, ζ_1, and ζ_2 to be independent of R at surface separations larger than λ_D (Kornyshev and Leikin, 1997), which covers the observed range of equilibrium R in DNA condensates. Detailed comparison of the predictions of the zipper model within this approximation with other models and experimental observations (Kornyshev and Leikin, 1999; Cherstvy *et al.*, 2002, 2004) reveals the following.

Condensation energy. At $R=30\pm3$ Å (the observed spacing in DNA condensates), the electrostatic zipper attraction is much stronger than that for counterion-correlation forces for 1+ and 2+ point charges and somewhat stronger or comparable to the correlation forces for 3+ point charges (Fig. 22). Note that the real energy of counterion-correlation interactions should be much smaller than its upper estimate at $T=0$ shown in Fig. 22 (particularly for 1+ and 2+ charges). In other words, the electrostatic zipper attraction is likely to be the dominant or at least a major condensation force even for 3+ point charges. The corresponding condensation energy predicted for the electrostatic zipper mechanism is in agreement with measured values, $\sim(0.1–0.2)k_BT$/bp (Rau and Parsegian, 1992a, 1992b; Raspaud *et al.*, 2005) (Fig. 23).

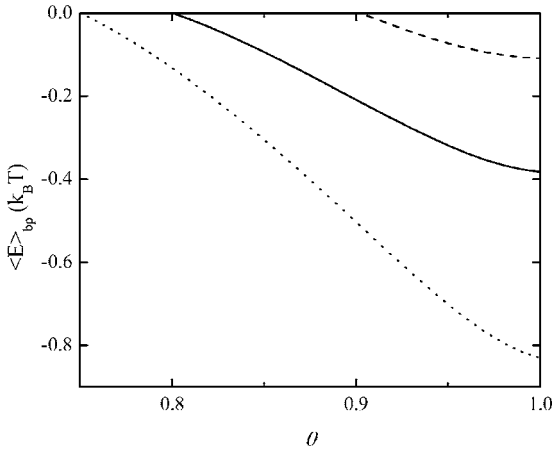

FIG. 23. Aggregation energy (per base pair) for a hexagonal aggregate of long flexible DNA as a function of charge compensation fraction θ, calculated for the electrostatic zipper mechanism from Eqs. (58) and (59) (parallel nonideal helical pairs from Sec. V.E) and Eqs. (97)–(99) (aggregates of parallel molecules from Sec. VI) at $\lambda_c=300$ Å, $C_t=3\times10^{-19}$ erg cm. The values of ζ_1 and ζ_2 were selected to match the counterion adsorption model [Eq. (40)] with 50:50 (long dashed), 30:70 (solid curve), and 20:80 (dotted curve) minor:major groove ratios of condensed counterions.

Counterion specificity. The electrostatic zipper mechanism of DNA condensation requires only the following. (i) A sufficient fraction of the DNA charge should be neutralized. Hence the condensation is not induced by monovalent metal ions. (ii) A sufficient fraction of condensed counterions should be located in the major groove. Hence the condensation is not induced by Mg^{2+} and Ca^{2+} which have very high affinity for phosphates and preferentially adsorb onto phosphate strands and/or the minor groove (Grzeskowiak *et al.*, 1998; Minasov *et al.*, 1999; Tereshko *et al.*, 1999; Egli, 2002).

This mechanism does not require a high valence of component charges on polyions. It suggests that the condensation of DNA by Mn^{2+}, Cd^{2+}, Co-amines, Sp, Spd, and some polymeric diamines might be the result of their strong binding to DNA and their known preference for binding in the major groove (Sec. IV.C; Deng and Bloomfield, 1999). The higher potency of Co-sep^{3+} vs Co-en^{3+} and Co-hex^{3+}, the difference between stere-

oisomers of Co-en^{3+}, and the differences between polyamines with spacers of different length could be caused by differences in their binding constants to DNA overall and/or to specific sites in the DNA major groove. Presently, we do not know whether this is really the case, but this hypothesis can certainly be experimentally tested.

Temperature dependence. As DNA condensing agents, Mn^{2+} and Cd^{2+} have two peculiar properties that distinguish them from other divalent counterions. First, they decrease the thermal stability of DNA, while the other ions increase it (Daune, 1974; Duguid *et al.*, 1995). Closer to the melting point one would expect stronger relative changes in the torsional rigidity of DNA with temperature. Rapid softening of the helix might result in temperature-induced condensation by allowing better torsional adaptation and stronger attraction (Sec. V.E). Second, both of these ions can bind in the minor and major grooves (Clement *et al.*, 1973; van Steenwinkel *et al.*, 1981; Granot and Kearns, 1982; Saenger, 1984; Duguid *et al.*, 1993; Froystein *et al.*, 1993; Moldrheim *et al.*, 1998; Davey and Richmond, 2002). A shift from the minor into the major groove upon DNA condensation (expected from the electrostatic zipper mechanism) could also contribute to the observed temperature effect (Cherstvy *et al.*, 2002). Both of these effects are hypothetical. But, they are consistent with what we know and, again, they are experimentally verifiable.

DNA structure and sequence.[13] Finally, the higher content of GC base pairs does promote DNA condensation by Mn^{2+} and Co-hex, potentially because it provides the N7 atoms of guanine needed for more efficient binding of these ions in the major groove. It was also reported that Ni^{2+} converts poly(dG-dC) from the *B* into the *Z* form followed by condensation, but it does not efficiently condense poly(dA-dT) (Sitko *et al.*, 2003). Analysis of the structural differences in these two forms of DNA within the electrostatic zipper model revealed a much higher propensity of *Z*-DNA for aggregation (Sitko *et al.*, 2003). Interestingly, of all the common forms of DNA (*A*, *B*, *C*, and *Z*), the ratio of the groove widths for the *B* form makes it the most resistant to nonspecific aggregation by counterions. Does its higher solubility play a part in nature's design?

[13]An interesting study of single-molecule DNA condensation was recently reported by Besteman *et al.* (2007). They observed a variation in the condensation force upon winding 8 kbp DNA by magnetic tweezers from −20 to +40 turns, but no further change in the force from −20 up to ∼−1000 turns. It would be worthwhile, however, to exercise caution in interpreting the latter observation without knowing the condensed DNA structure. DNA unwinding may disrupt the double helix and cause hairpins and other alternative structures, which will form even more readily under tension and may occur already at −20 turns. The further increase in the number of negative turns may simply change the fraction of alternate DNA structures coexisting with the double helix. The constant condensation force within such a "two-phase" region would be niether surprising nor revealing.

D. Summary and comments

DNA condensation is, in many ways, a paradigm for interactions between biological helices and a testing ground for the corresponding theories. To fully understand this phenomenon, it is essential to account for all relevant details and observations. As we argued, biological DNA counterions are not and cannot be modeled as multivalent pointlike charges. They are polyions, which usually bind to DNA in a stretched conformation by fitting into one of the grooves. Even the charge of these ions cannot be strictly defined, because under certain conditions their amine groups may not retain the extra proton which provides the expected charge. We also cannot discard the fact that two stereoisomers of the same ion have entirely different effects on DNA condensation. Only by paying attention to these details of the underlying structure and chemistry can we hope to arrive at a real understanding of biological macromolecules and their interactions.

VIII. CONCLUSIONS AND OUTLOOK

The study of interactions between biological macromolecules is a fascinating subject at the crossroads of physics, chemistry, and biology. In this review we focused on one aspect of this problem—the physics relating microscopic structure of helical macromolecules to macroscopic properties of various objects they compose. We argued that the foundation for understanding this physics was laid by a simple theory of structure factors for helical chains of atoms, derived by Cochran, Crick, and Vand (1952). In less than a year these structure factors were used by Watson and Crick for their remarkable discovery of the structure of the DNA double helix. However, more than half a century later, we are just beginning to understand that the same structure factors determine not only the diffraction pattern from the double helix but also important features of interactions between DNA molecules. For instance, as discussed in Sec. VI.D, the same classical x-ray-diffraction patterns that were used to solve the DNA structure appear to contain information about azimuthal correlations and interaction-induced torsional deformation of the double helix in liquid crystalline aggregates.

In fairness, not everyone shares the view that the helical structure is important for intermolecular forces and that it determines at least some macroscopic properties of various assemblies of biological helices. Many alternative models of various phenomena have been proposed. Our goal here was to analyze these models on the same footing and compare them with all available experimental data rather than a few selected measurements that fit the best. To be sure, there are still more questions than answers, but we believe that this rapidly developing field is ripe for new major advances. It is difficult to predict where such advances might come. Nevertheless, in our opinion, some of the most important and interesting unresolved problems are as follows.

The nature of measured forces. Very similar, short-

range, exponential forces have been measured between DNA, polysaccharides, collagen, and guanosine helices within the last 1–2 nm of surface-to-surface separation. These forces do not appear to conform to the traditional theory of interaction between uniformly charged cylinders in electrolyte solution. The deviations have been attributed, for example, to (i) hydration (Sec. V.I), (ii) correlations and fluctuations in the density of counterions condensed or adsorbed on molecular surfaces (Sec. V.C), and (iii) corrections to electrostatic interaction associated with helical patterns of fixed charges and condensed counterions (Sec. V.D). The corresponding models are not mutually exclusive, that is, all of these effects can contribute. Our analysis of the experiments (Sec. VI.F) suggests that the effects of the helical structure on electrostatic interactions provide the most consistent explanation for many nontrivial observations. There is still no direct proof of such an interpretation. Accurate quantitative comparisons of the corresponding theoretical predictions with measurements are hindered by inherent problems of mesoscopic electrostatics, i.e., insufficient knowledge of the dielectric response of water and counterion distribution in thin water layers at molecular surfaces. Potentially, all-atom computer simulations could help to resolve these issues, but they also suffer from model uncertainties. Furthermore, such simulations of multimolecular, liquid crystalline assemblies of helices are far beyond the capabilities of present computer systems. The best hope therefore lies in formulation of targeted experiments, which could test qualitative differences in the predictions of different models.

Mechanism of counterion-induced DNA condensation. A distinct set of predictions for structure-dependent electrostatic interactions between DNA has been formulated within the electrostatic zipper model. In particular, this model predicts that counterion adsorption in the major groove of DNA will promote a zipperlike alignment between the negatively charged strands and positively charged grooves on opposing helices (Fig. 7), resulting in intermolecular attraction and aggregation. In the aggregate, intermolecular separation is determined by the balance between the attraction and a shorter-range image repulsion of fixed and adsorbed charges from the dielectric cores of neighboring molecules. Compaction (condensation) of DNA into densely packed aggregates by counterions is a very important biological phenomenon, and it has been extensively studied experimentally *in vivo* and *in vitro*. In Sec. VII we argued that nontrivial qualitative features of DNA condensation observed *in vitro* are more consistent with the zipper model than with counterion-correlation effects. These features include, for example, counterion specificity (which correlates with the known preferential counterion adsorption in the major groove), dependence on the base-pair composition of DNA (modulating the major groove adsorption), and the dependence on DNA structure (the higher solubility of *B*-DNA compared to other forms of DNA). Moreover, the decay lengths of the longer-range attraction and the shorter-range repulsion predicted within the electrostatic zipper model were found to be the same as those measured in counterion-condensed DNA aggregates with less than a 5–10 % difference (Sec. VI.F). Such evidence suggesting the importance of DNA structure in counterion-induced aggregation speaks for itself. But it does not exclude hydration forces (Sec. V.I), as an addition rather than an alternative to electrostatic interactions. It is difficult to discriminate between the two contributions, as qualitatively they must give similar effects. Distinguishing electrostatics from hydration is still an open challenge.

Physics of chiral interactions and chiral assemblies. The role of the helical structure in chiral interactions is unquestionable. A uniformly charged cylinder is not chiral. Significant progress has been made recently in theoretical modeling of chiral pair interaction potentials between helical macromolecules (Secs. V.G and VI.E). Our understanding of such interactions in supercoiled structures and in multimolecular aggregates is still far from being complete (Secs. V.H and VI.E). These interactions depend strongly on azimuthal correlations between neighboring molecules. Estimates and experimental evidence suggest, for example, that the azimuthal correlations between DNA molecules in the chiral, cholesteric phase may be strong enough that various high-temperature approximations developed over the years may not be appropriate. To the best of our knowledge, no low-temperature statistical theory that would properly account for such correlations in a liquid crystalline cholesteric array has been proposed yet. A variety of experimental observations, such as the dependence of the cholesteric pitch on the aggregate density, the transition between the cholesteric and hexagonal (line hexatic) phase, and so on, have only hypothetical explanations.

Biology inspired by physics. The simple theory of Cochran, Crick, and Vand (1952) triggered a true revolution in biology and medicine. The potential impact of its new applications to understanding helix-helix interactions is difficult to predict today. We do not know yet whether the predicted sequence homology recognition through electrostatic interactions between double helices plays any role in pairing of homologous DNA fragments preceding genetic recombination (Sec. V.F), but the speculation is intriguing and well worth pursuing. The importance of electrostatic interactions between α-helix backbones are in the formation of α-helix coiled coils and protein folding, in general is not clear. Are there any other potentially important applications of these ideas to biology? Rapid advances in this field suggest that this question may well be answered soon.

ACKNOWLEDGMENTS

We are grateful to Adrian Parsegian, Rudolf Podgornik, Don Rau, and Brian Todd for stimulating discussions and providing valuable comments during the preparation of this article. In writing this paper we were influenced by joint work and/or useful discussions with Andrey Cherstvy, Serge Lemay, Christos Likos, Harmut Löwen, Sergey Malinin, Wilma Olson, Gleb Oshanin,

Mickey Schurr, Boris Shklovskii, and Godehard Sutmann. The work has been supported by the Royal Society (A.A.K., A.W.), the EPSRC (A.A.K., D.J.L.), and the NIH. Part of this work was performed during participation of one of us (A.A.K.) in the 2006 program New Approaches to Biological and Molecular Machines at the Kavli Institute of Theoretical Physics, University of California at Santa Barbara.

REFERENCES

Akiyama, T., and M. E. Hogan, 1997, Biochemistry **36**, 2307.
Alexander, S., P. M. Chaikin, P. Grant, G. L. Morales, P. Pincus, and D. Hone, 1984, J. Chem. Phys. **80**, 5776.
Alfrey, T., P. W. Berg, and H. J. Morawetz, 1951, J. Polym. Sci. **7**, 543.
Allahyarov, E., and H. Löwen, 2000, Phys. Rev. E **62**, 5542.
Allemand, J. F., D. Benimon, R. Lavery, and V. Croquette, 1998, Proc. Natl. Acad. Sci. U.S.A. **95**, 14152.
Allison, S. A., J. C. Herr, and J. M. Schurr, 1981, Biopolymers **20**, 469.
Allison, S. A., and J. M. Schurr, 1979, Chem. Phys. **41**, 35.
Angelini, T. E., H. Liang, W. Wriggers, and G. C. L. Wong, 2003, Proc. Natl. Acad. Sci. U.S.A. **100**, 8634.
Angelini, T. E., H. Liang, W. Wriggers, and G. C. L. Wong, 2005, Eur. Phys. J. E **16**, 389.
Antman, S. S., 2005, *Nonlinear Problems of Elasticity*, 2nd ed. (Springer, New York).
Arenzon, J. J., Y. Levin, and J. F. Stilck, 2000, Physica A **283**, 1.
Arenzon, J. J., J. F. Stilck, and Y. Levin, 1999, Eur. Phys. J. B **12**, 79.
Arscott, P. G., A. Z. Li, and V. A. Bloomfield, 1990, Biopolymers **30**, 619.
Attard, P., R. Kjellander, D. J. Mitchell, and B. Jonsson, 1988, J. Chem. Phys. **89**, 1664.
Baigl, D., and K. Yoshikawa, 2005, Biophys. J. **88**, 3486.
Balaeff, A., L. Mahadevan, and K. Schulten, 2006, Phys. Rev. E **73**, 031919.
Banavali, N. K., and B. Roux, 2005, J. Am. Chem. Soc. **127**, 6866.
Barakat, R., 1987, Acta Crystallogr., Sect. A: Found. Crystallogr. **43**, 45.
Barkley, M. D., and B. Zimm, 1979, J. Chem. Phys. **70**, 2991.
Barrat, J. L., and J. F. Joanny, 1993, Europhys. Lett. **24**, 333.
Barrat, J. L., and J. F. Joanny, 1996, Adv. Chem. Phys. **94**, 1.
Bednar, J., P. Furrer, V. Katritch, A. Z. Stasiak, J. Dubochet, and A. Stasiak, 1995, J. Mol. Biol. **254**, 579.
Belamie, E., P. Davidson, and M. M. Giraud-Guille, 2004, J. Phys. Chem. B **108**, 14991.
Benham, C. J., 1983, Macromolecules **22**, 2477.
Benham, C. J., and S. P. Mielke, 2005, Annu. Rev. Biomed. Eng. **7**, 21.
Besteman, K., S. Hage, N. H. Dekker, and S. G. Lemay, 2007, Phys. Rev. Lett. **98**, 058103.
Beveridge, D. L., and K. J. McConnell, 2000, Curr. Opin. Struct. Biol. **10**, 182.
Bishop, A. R., 1978, in *Springer Series in Solid State Sciences*, edited by A. R. Bishop and T. Schneider (Springer, Berlin), Vol. 8, p. 85.
Bleam, M. L., C. F. Anderson, and M. T. Record, 1980, Proc. Natl. Acad. Sci. U.S.A. **77**, 3085.
Bloomfield, V. A., 1991, Biopolymers **31**, 1471.
Bloomfield, V. A., 1996, Curr. Opin. Struct. Biol. **6**, 334.
Bloomfield, V. A., 1997, Biopolymers **44**, 269.
Bloomfield, V. A., D. M. Crothers, and I. Tinoco, Jr., 2000, *Nucleic Acids: Structures, Properties, and Functions* (University Science Books, Sausalito, CA).
Bockris, J. O'M., and A. K. N. Reddy, 1970, *Modern Electrochemistry* (Plenum, New York), Vol. I.
Bolshoy, A., P. McNamara, R. E. Harrington, and E. N. Trifonov, 1991, Proc. Natl. Acad. Sci. U.S.A. **88**, 2312.
Bopp, Ph., A. A. Kornyshev, and G. Sutmann, 1996, Phys. Rev. Lett. **76**, 1280.
Bopp, Ph., A. A. Kornyshev, and G. Sutmann, 1998, J. Chem. Phys. **109**, 1939.
Borukhov, I., D. Andelman, and H. Orland, 2000a, Electrochim. Acta **46**, 221.
Borukhov, I., D. Andelman, and H. Orland, 2000b, Phys. Rev. Lett. **79**, 435.
Bouchiat, C., and M. Mézard, 1997, Phys. Rev. Lett. **80**, 1556.
Bouchiat, C., and M. Mézard, 2000, Eur. Phys. J. E **2**, 377.
Brenner, S. L., and V. A. Parsegian, 1974, Biophys. J. **14**, 327.
Bryant, Z., M. D. Stone, J. Gore, S. B. Smith, N. R. Cozzarelli, and C. Bustamante, 2003, Nature (London) **424**, 338.
Bryson, K., and R. J. Greenall, 2000, J. Biomol. Struct. Dyn. **18**, 393.
Burak, Y., G. Ariel, and D. Andelman, 2003, Biophys. J. **85**, 2100.
Burgess, S. M., N. Kleckner, and B. M. Weiner, 1999, Genes Dev. **13**, 1627.
Bustamante, C., J. F. Marko, E. D. Siggia, and S. B. Smith, 1994, Science **265**, 5178.
Calladine, C. R., and H. R. Drew, 1986, J. Mol. Biol. **192**, 907.
Chattoraj, D. K., L. C. Gosule, and J. A. Schellman, 1978, J. Mol. Biol. **121**, 327.
Cheatham, T. E., and P. A. Kollman, 1996, J. Mol. Biol. **259**, 434.
Cherstvy, A. G., A. A. Kornyshev, and S. Leikin, 2002, J. Phys. Chem. B **106**, 13362.
Cherstvy, A. G., A. A. Kornyshev, and S. Leikin, 2004, J. Phys. Chem. B **108**, 6508.
Chiu, T. K., and R. E. Dickerson, 2000, J. Mol. Biol. **301**, 915.
Chothia, C., M. Levitt, and D. Richardson, 1981, J. Mol. Biol. **145**, 215.
Chung, D. S., G. B. Benedek, F. M. Konikoff, and J. M. Donovan, 1993, Proc. Natl. Acad. Sci. U.S.A. **90**, 11341.
Clement, R. M., J. Sturm, and M. P. Daune, 1973, Biopolymers **12**, 405.
Cloutier, T. E., and J. Widom, 2004, Mol. Cell **14**, 355.
Cluzel, P., A. Lebrun, C. Heller, R. Lavery, J. L. Viovy, D. Chatenay, and F. Caron, 1996, Science **271**, 792.
Cochran, W., F. H. C. Crick, and V. Vand, 1952, Acta Crystallogr. **5**, 581.
Coleman, B. D., W. K. Olson, and D. Swigon, 2003, J. Chem. Phys. **118**, 7127.
Coleman, B. D., and D. Swigon, 2004, Philos. Trans. R. Soc. London, Ser. A **362**, 1281.
Crick, F. H. C., 1953a, Acta Crystallogr. **6**, 685.
Crick, F. H. C., 1953b, Acta Crystallogr. **6**, 689.
Crothers, D. M., J. Drak, J. D. Kahn, and S. D. Levene, 1992, Methods Enzymol. **212**, 3.
Das, R., T. T. Mills, L. W. Kwok, G. S. Maskel, I. S. Millett, S. Doniach, K. D. Finkelstein, D. Herschlag, and L. Pollack, 2003, Phys. Rev. Lett. **90**, 188103.
Das, T., D. Bratko, L. B. Bhuiyan, and C. W. Outhwaite, 1997,

J. Chem. Phys. **107**, 9197.
Daune, M., 1974, in *Metal Ions in Biological Systems*, edited by H. Sigel (Dekker, New York), Vol. 3, p. 1.
Davey, C. A., and T. J. Richmond, 2002, Proc. Natl. Acad. Sci. U.S.A. **99**, 11169.
Deng, H., and V. A. Bloomfield, 1999, Biophys. J. **77**, 1556.
Denisov, V. P., and B. Halle, 2000, Proc. Natl. Acad. Sci. U.S.A. **97**, 629.
Denton, A. R., 1999, J. Phys.: Condens. Matter **11**, 10061.
Derjaguin, B. V., N. V. Churaev, and V. M. Muller, 1987, *Surface Forces* (Consultant Bureau, New York).
Deserno, M., A. Arnold, and C. Holm, 2003, Macromolecules **36**, 249.
Deserno, M., and C. Holm, 2002, Mol. Phys. **100**, 2941.
Deserno, M., C. Holm, and S. May, 2000, Macromolecules **33**, 199.
Dickerson, R. E., 1983, J. Mol. Biol. **166**, 419.
Dickerson, R. E., 1992, Methods Enzymol. **211**, 67.
Dickerson, R. E., and H. R. Drew, 1981, J. Mol. Biol. **149**, 761.
Diehl, A., H. A. Carmona, and Y. Levin, 2001, Phys. Rev. E **64**, 011804.
Dogic, Z., and S. Fraden, 2006, Curr. Opin. Colloid Interface Sci. **11**, 47.
Dolgov, O. V., D. A. Kirzhnitz, and E. G. Maximov, 1981, Rev. Mod. Phys. **53**, 81.
Donnan, F. G., 1924, Chem. Rev. (Washington, D.C.) **1**, 73.
Dover, S. D., 1977, J. Mol. Biol. **110**, 699.
Drew, H. R., and R. E. Dickerson, 1981, J. Mol. Biol. **151**, 535.
Du, Q., C. Smith, N. Shiffeldrim, M. Vologodskaia, and A. Vologodskii, 2005, Proc. Natl. Acad. Sci. U.S.A. **102**, 5397.
Duguid, J., V. A. Bloomfield, J. Benevides, and G. J. Thomas, 1993, Biophys. J. **65**, 1916.
Duguid, J. G., V. A. Bloomfield, J. M. Benevides, and G. J. Thomas, 1995, Biophys. J. **69**, 2623.
Dupre, D. B., and R. W. Duke, 1975, J. Chem. Phys. **63**, 143.
Durand, D., J. Doucet, and F. Livolant, 1992, J. Phys. II **2**, 1769.
Egelman, E. H., and D. J. DeRosier, 1982, Acta Crystallogr., Sect. A: Cryst. Phys., Diffr., Theor. Gen. Crystallogr. **38**, 796.
Egelman, E. H., N. Francis, and D. J. DeRosier, 1982, Nature (London) **298**, 131.
Egli, M., 2002, Chem. Biol. **9**, 277.
Eickbush, T. H., and E. N. Moudrianakis, 1976, Cell **13**, 295.
Elsawy, K. M., M. K. Hodgson, and L. S. D. Caves, 2005, Nucleic Acids Res. **33**, 5749.
Emelyanenko, A. V., 2003, Phys. Rev. E **67**, 031704.
Emelyanenko, A. V., M. A. Osipov, and D. A. Dunmur, 2000, Phys. Rev. E **62**, 2340.
Evdokimov, Yu. M., S. G. Skurdin, and V. I. Salyanov, 1988, Liq. Cryst. **3**, 1443.
Fedorov, M. V., and A. A. Kornyshev, 2007, Mol. Phys. **105**, 1.
Ferrarini, A., G. L. Moro, and P. L. Nordio, 1995, Liq. Cryst. **19**, 397.
Ferrarini, A., G. L. Moro, and P. L. Nordio, 1996a, Phys. Rev. E **53**, 681.
Ferrarini, A., G. L. Moro, and P. L. Nordio, 1996b, Mol. Phys. **87**, 485.
Feuerstein, B. G., N. Pattabiraman, and L. J. Marton, 1986, Proc. Natl. Acad. Sci. U.S.A. **83**, 5948.
Feuerstein, B. G., N. Pattabiraman, and L. J. Marton, 1990, Nucleic Acids Res. **18**, 1271.
Fisher, M. E., 1994, J. Stat. Phys. **75**, 1.
Fixman, M., and J. Kovac, 1973, J. Chem. Phys. **58**, 1564.
Frank-Kamenetskii, M. D., V. V. Anshelevich, and A. V. Lukashin, 1987, Sov. Phys. Usp. **151**, 595.
Franklin, R. E., and R. G. Gosling, 1953, Nature (London) **171**, 740.
Fraser, R. D. B., T. P. MacRae, A. Miller, and E. Suzuki, 1983, J. Mol. Biol. **167**, 497.
Fraser, R. D. B., T. P. MacRae, and E. Suzuki, 1979, J. Mol. Biol. **129**, 463.
Froystein, N. A., J. T. Davis, B. R. Reid, and E. Sletten, 1993, Acta Chem. Scand. **47**, 649.
Fujitani, Y., and I. Kobayashi, 1995, Phys. Rev. E **52**, 6607.
Fujitani, Y., K. Yamamoto, and I. Kobayashi, 1995, Genetics **140**, 797.
Fuoss, R. M., A. Katchalsky, and S. Lifson, 1951, Proc. Natl. Acad. Sci. U.S.A. **37**, 579.
Gallagher, K., and K. Sharp, 1998, Biophys. J. **75**, 769.
Giraud-Guille, M. M., 1996, Int. Rev. Cytol. **166**, 59.
Giraud-Guille, M. M., L. Besseau, and R. Martin, 2003, J. Biomech. **36**, 1571.
Goldstein, R. E., A. Goriely, G. Huber, and C. W. Wolgemuth, 2000, Phys. Rev. Lett. **84**, 1631.
Golestanian, R., M. Kardar, and T. B. Liverpool, 1999, Phys. Rev. Lett. **82**, 4456.
Golestanian, R., and T. B. Liverpool, 2002, Phys. Rev. E **66**, 051802.
Gorin, A. A., V. B. Zhurkin, and W. K. Olson, 1995, J. Mol. Biol. **247**, 34.
Gosule, L. C., and J. A. Schellman, 1976, Nature (London) **259**, 333.
Granot, J., and D. R. Kearns, 1982, Biopolymers **21**, 873.
Griffith, J. D., 1978, Science **201**, 525.
Grønbech-Jensen, N., R. J. Mashl, R. F. Bruinsma, and W. M. Gelbart, 1997, Phys. Rev. Lett. **78**, 2477.
Grosberg, A. Yu., T. T. Nguyen, and B. I. Shklovskii, 2002, Rev. Mod. Phys. **74**, 329.
Grzeskowiak, K., K. Yanaga, G. G. Prive, and R. E. Dickerson, 1998, J. Biol. Chem. **266**, 8341.
Guldbrand, L., B. Jönsson, H. Wennerström, and P. Linse, 1984, J. Chem. Phys. **80**, 2221.
Ha, B.-Y., and A. J. Liu, 1997, Phys. Rev. Lett. **79**, 1289.
Ha, B.-Y., and A. J. Liu, 1998, Phys. Rev. E **58**, 6281.
Ha, B.-Y., and A. J. Liu, 1999a, Phys. Rev. E **60**, 803.
Ha, B.-Y., and A. J. Liu, 1999b, Phys. Rev. Lett. **83**, 2681.
Ha, B.-Y., and D. Thirumalai, 1996, J. Chem. Phys. **106**, 4243.
Ha, S. C., K. Lowenhaupt, A. Rich, Y. G. Kim, and K. K. Kim, 2005, Nature (London) **437**, 1183.
Hagerman, P. J., 1988, Annu. Rev. Biophys. Biophys. Chem. **17**, 265.
Hamelberg, D., L. D. Williams, and W. D. Wilson, 2001, J. Am. Chem. Soc. **123**, 7745.
Hansen, P. L., D. Svenšek, A. Parsegian, and R. Podgornik, 1999, Phys. Rev. E **60**, 1956.
Harned, H. S., and B. B. Owen, 1950, *The Physical Chemistry of Electrolytic Solutions*, 2nd ed. (Reinhold, New York).
Harreis, H. M., A. A. Kornyshev, C. N. Likos, H. Löwen, and G. Sutmann, 2002, Phys. Rev. Lett. **89**, 018303.
Harreis, H. M., C. N. Likos, and H. Löwen, 2003, Biophys. J. **84**, 3607.
Harris, R. H., and J. E. Hearst, 1969, J. Chem. Phys. **44**, 2595.
Harris, A. B., R. D. Kamien, and T. C. Lubensky, 1997, Phys. Rev. Lett. **78**, 1476.
Harris, A. B., R. D. Kamien, and T. C. Lubensky, 1999, Rev. Mod. Phys. **71**, 1745.

Heath, P. J., J. B. Clendenning, B. S. Fujimoto, and J. M. Schurr, 1996, J. Mol. Biol. **260**, 718.
Horowitz, D. S., and J. C. Wang, 1984, J. Mol. Biol. **173**, 75.
Hsieh, P., C. S. Camerini-Otero, and R. D. Camerini-Otero, 1992, Proc. Natl. Acad. Sci. U.S.A. **89**, 6492.
Hud, N. V., 1995, Biophys. J. **69**, 1355.
Hud, N. V., M. J. Allen, K. H. Downing, J. Lee, and R. Balhorn, 1993, Biochem. Biophys. Res. Commun. **193**, 1347.
Hud, N. V., and K. H. Downing, 2001, Proc. Natl. Acad. Sci. U.S.A. **98**, 14925.
Hud, N. V., K. H. Downing, and R. Balhorn, 1995, Proc. Natl. Acad. Sci. U.S.A. **92**, 3581.
Hud, N. V., and J. Feigon, 1997, J. Am. Chem. Soc. **119**, 5756.
Hud, N. V., V. Sklenar, and J. Feigon, 1999, J. Mol. Biol. **286**, 651.
Hud, N. V., and I. D. Vilfan, 2005, Annu. Rev. Biophys. Biomol. Struct. **34**, 295.
Hulmes, D. J. S., A. Miller, D. A. D. Parry, K. A. Piez, and J. Woodhead-Galloway, 1973, J. Mol. Biol. **79**, 137.
Inouye, H., 1994, Acta Crystallogr., Sect. A: Found. Crystallogr. **50**, 644.
Issaenko, S. A., and A. B. Harris, 2000, Phys. Rev. E **61**, 2777.
Issaenko, S. A., A. B. Harris, and T. C. Lubensky, 1999, Phys. Rev. E **60**, 578.
Ivanov, V. I., and D. Y. Krylov, 1992, in *Methods in Enzymology*, edited by D. M. J. Lilley and J. E. Dahlberg (Academic, San Diego).
Ivanov, V. I., L. E. Minchenkova, E. E. Minyat, M. D. Frank-Kamenetskii, and A. K. Schyolkina, 1974, J. Mol. Biol. **87**, 817.
Izyumov, Yu. A., and Yu. N. Skryabin, 1988, *Statistical Mechanics of Magnetically Ordered Systems* (Consultants Bureau, New York).
Jayaram, B., and D. L. Beveridge, 1996, Annu. Rev. Biophys. Biomol. Struct. **25**, 367.
Jayaram, B., D. Sprous, M. A. Young, and D. L. Beveridge, 1998, J. Am. Chem. Soc. **12**, 10629.
Jülicher, F., 1994, Phys. Rev. E **49**, 2429.
Kabsch, W., C. Sander, and E. N. Trifonov, 1982, Nucleic Acids Res. **10**, 1097.
Kamien, R. D., T. C. Lubensky, P. Nelson, and C. S. O'Hern, 1997, Europhys. Lett. **38**, 237.
Karlik, S. J., G. L. Eichorn, P. N. Lewis, and D. R. Crapper, 1980, Biochemistry **19**, 5991.
Kassapidou, K., W. Jesse, J. A. P. P. van Dijk, and J. R. C. van der Maarel, 1998, Biopolymers **46**, 31.
Katchalsky, A., 1971, Pure Appl. Chem. **26**, 327.
Kats, E. I., 1978, Sov. Phys. JETP **47**, 1205.
Kehrbaum, S., and J. H. Maddocks, 2000, in *Proceedings of the 16th IMACS World Congress 2000, Lausanne, Switzerland*, edited by M. Deville and R. Owens (IMACS, Lausanne).
Khan, S., T. L. Morton, and D. Ronis, 1987, Phys. Rev. A **35**, 4295.
Kielkopf, C. L., S. Ding, P. Kuhn, and D. C. Rees, 2000, J. Mol. Biol. **296**, 787.
Kirkwood, J. G., 1934, J. Chem. Phys. **2**, 767.
Kirkwood, J. G., and J. B. Schumaker, 1952, Proc. Natl. Acad. Sci. U.S.A. **38**, 863.
Kjellander, R., 1996, Ber, Bunsneges. Phys. Chem. **100**, 894.
Kjellander, R., and S. Marčelja, 1984, Chem. Phys. Lett. **112**, 49.
Kjellander, R., and S. Marčelja, 1986, Chem. Phys. Lett. **127**, 402.
Klug, A., F. H. C. Crick, and H. W. Wyckoff, 1958, Acta Crystallogr. **11**, 199.
Knoll, D. A., M. D. Fried, and V. A. Bloomfield, 1988, in *DNA and its Drug Complexes*, edited by R. H. Sarma and M. H. Sarma (Adenin, New York).
Kornyshev, A. A., 1981, Electrochim. Acta **26**, 1.
Kornyshev, A. A., 1985, in *The Chemical Physics of Solvation*, edited by R. R. Dogonadze, E. Kalman, A. A. Kornyshev, and J. Ulstrup (Elsevier, Amsterdam), Part A, p. 77.
Kornyshev, A. A., and A. M. Kuznetsov, 2006, Electrochem. Commun. **8**, 679.
Kornyshev, A. A., D. J. Lee, S. Leikin, A. Wynveen, and S. B. Zimmerman, 2005, Phys. Rev. Lett. **95**, 148102.
Kornyshev, A. A., and S. Leikin, 1989, Phys. Rev. A **40**, 6431.
Kornyshev, A. A., and S. Leikin, 1997, J. Chem. Phys. **107**, 3656.
Kornyshev, A. A., and S. Leikin, 1998a, Biophys. J. **75**, 2513.
Kornyshev, A. A., and S. Leikin, 1998b, Proc. Natl. Acad. Sci. U.S.A. **95**, 13579.
Kornyshev, A. A., and S. Leikin, 1999, Phys. Rev. Lett. **82**, 4138.
Kornyshev, A. A., and S. Leikin, 2000, Phys. Rev. E **62**, 2576.
Kornyshev, A. A., and S. Leikin, 2001, Phys. Rev. Lett. **86**, 3666.
Kornyshev, A. A., S. Leikin, and S. V. Malinin, 2002, Eur. Phys. J. E **7**, 83.
Kornyshev, A. A., E. Spohr, and M. A. Vorotyntsev, 2002, in *Encyclopaedia of Electrochemistry, Vol. 1: Thermodynamics and Electrified Interfaces*, edited by E. Gileadi and M. Urbakh, Chap. 2.1 (Wiley-VCH, Weinheim).
Kornyshev, A. A., and G. Sutmann, 1998, J. Electroanal. Chem. **450**, 143.
Kornyshev, A. A., and A. Wynveen, 2004, Phys. Rev. E **69**, 041905.
Korolev, N., A. P. Lyubartsev, A. Laaksonen, and L. Nordenskiöld, 2002, Biophys. J. **82**, 2860.
Korolev, N., A. P. Lyubartsev, L. Nordenskiöld, and A. Laaksonen, 2001, J. Mol. Biol. **308**, 907.
Kosikov, K. M., A. A. Gorin, V. B. Zhurkin, and W. K. Olson, 1999, J. Mol. Biol. **289**, 1301.
Kosterlitz, J. M., and D. J. Thouless, 1973, J. Phys. C **6**, 1181.
Kovac, J., and C. C. Crabb, 1982, Macromolecules **15**, 537.
Krasnow, M. A., and N. R. Cozzarelli, 1982, J. Biol. Chem. **257**, 2687.
Kratky, O., and C. Porod, 1949, Recl. Trav. Chim. Pays-Bas **68**, 1106.
Kuznetsova, N., D. C. Rau, V. A. Parsegian, and S. Leikin, 1997, Biophys. J. **72**, 353.
Laemmli, U. K., 1975, Proc. Natl. Acad. Sci. U.S.A. **72**, 4288.
Landau, L. D., and E. M. Lifshitz, 1969, *Statistical Physics* (Pergamon, Oxford).
Landau, L. D., and E. M. Lifshitz, 1982, *Electrodynamics of Continuous Media* (Pergamon, Oxford).
Lang, D., 1973, J. Mol. Biol. **78**, 247.
Lang, D., T. N. Taylor, D. C. Dobyan, and D. M. Gray, 1976, J. Mol. Biol. **106**, 97.
Langmuir, I., 1938, J. Chem. Phys. **6**, 873.
Langridge, R., H. R. Wilson, C. W. Hooper, M. H. F. Wilkins, and L. D. Hamilton, 1960, J. Mol. Biol. **2**, 19.
Lau, A. W. C., D. Levine, and P. Pincus, 2000, Phys. Rev. Lett. **84**, 4116.
Lau, A. W. C., and P. Pincus, 2002, Phys. Rev. E **66**, 041501.
Lau, A. W. C., P. Pincus, D. Levine, and H. A. Fertig, 2001,

Phys. Rev. E **63**, 051604.
Laughlin, R. B., D. Pines, J. Schmalian, B. P. Stojkovic, and P. Wolynes, 2000, Proc. Natl. Acad. Sci. U.S.A. **97**, 32.
Lavalle, N., S. A. Lee, and A. Rupprecht, 1990, Biopolymers **30**, 877.
Leach, D. R. F., 1996, *Genetic Recombination* (Blackwell Science, Oxford).
LeBret, M., 1984, Macromolecules **23**, 1835.
LeBret, M., and B. H. Zimm, 1984a, Biopolymers **23**, 271.
LeBret, M., and B. H. Zimm, 1984b, Biopolymers **23**, 287.
Lee, D. H., J. D. Joannopoulos, J. W. Negele, and D. P. Landau, 1986, Phys. Rev. B **33**, 450.
Lee, D. J., 2006, unpublished.
Lee, D. J., A. Wynveen, and A. A. Kornyshev, 2004, Phys. Rev. E **70**, 051913.
Lee, D. J., and A. Wynveen, 2006, J. Phys.: Condens. Matter **18**, 787.
Lee, K. C., I. Borukhov, W. M. Gelbart, A. J. Liu, and M. J. Stevens, 2004, Phys. Rev. Lett. **93**, 128101.
Leforestier, A., and F. Livolant, 1993, Biophys. J. **65**, 56.
Leikin, S., 1991, J. Chem. Phys. **95**, 5224.
Leikin, S., 1999, in *Hydration Processes in Biology*, edited by M.-C. Bellissent-Funel (IOS, Amsterdam), pp. 313–321.
Leikin, S., and V. A. Parsegian, 1994, Proteins: Struct., Funct., Genet. **19**, 73.
Leikin, S., V. A. Parsegian, D. C. Rau, and R. P. Rand, 1993, Annu. Rev. Phys. Chem. **44**, 369.
Leikin, S., V. A. Parsegian, W. H. Yang, and G. E. Walrafen, 1997, Proc. Natl. Acad. Sci. U.S.A. **94**, 11312.
Leikin, S., D. C. Rau, and V. A. Parsegian, 1991, Phys. Rev. A **44**, 5272.
Leikin, S., D. C. Rau, and V. A. Parsegian, 1994, Proc. Natl. Acad. Sci. U.S.A. **91**, 276.
Leikin, S., D. C. Rau, and V. A. Parsegian, 1995, Nat. Struct. Biol. **2**, 205.
Leonard, M., H. Hong, N. Easwar, and H. H. Strey, 2001, Polymer **42**, 5823.
Levin, Y., 2002, Rep. Prog. Phys. **65**, 1677.
Levin, Y., J. J. Arenzon, and J. F. Stilck, 1999, Phys. Rev. Lett. **83**, 2680.
Levitt, M., 1978, Proc. Natl. Acad. Sci. U.S.A. **75**, 640.
Lewin, B., 1997, *Genes VI* (Oxford University Press, Oxford).
Lifson, S., and A. Katchalsky, 1953, J. Polym. Sci. **13**, 43.
Likos, C. N., 2001, Phys. Rep. **348**, 267.
Livolant, F., 1984, Eur. J. Cell Biol. **33**, 300.
Livolant, F., 1991, Physica A **176**, 117.
Livolant, F., and A. Leforestier, 1996, Prog. Polym. Sci. **21**, 1115.
Lorman, V., R. Podgornik, and B. Žekš, 2001, Phys. Rev. Lett. **87**, 218101.
Löwen, H., P. A. Madden, and J. P. Hansen, 1993, J. Chem. Phys. **98**, 3275.
Ma, C., and V. A. Bloomfield, 1994, Biophys. J. **67**, 1678.
Mahanty, J., and B. W. Ninham, 1976, *Dispersion Forces* (Academic, London).
Mandel, M., 1992, J. Phys. Chem. **96**, 3934.
Manning, G. S., 1969, J. Chem. Phys. **51**, 924.
Manning, G. S., 1978, Q. Rev. Biophys. **11**, 179.
Manning, G. S., 1984, J. Chem. Phys. **88**, 6654.
Manning, R. S., J. H. Maddocks, and J. D. Kahn, 1996, J. Chem. Phys. **105**, 5626.
Marčelja, S., 1992, Biophys. J. **61**, 1117.
Marčelja, S., and N. Radic, 1976, Chem. Phys. Lett. **42**, 129.
Mariani, P., F. Ciuchi, and L. Saturni, 1998, Biophys. J. **74**, 430.
Mariani, P., and L. Saturni, 1996, Biophys. J. **70**, 2867.
Marko, J. F., 1997a, Phys. Rev. E **57**, 2134.
Marko, J. F., 1997b, Europhys. Lett. **38**, 183.
Marko, J. F., and E. D. Siggia, 1994, Macromolecules **27**, 981.
Marko, J. F., and E. D. Siggia, 1995, Macromolecules **28**, 8759.
Marquet, R., and C. Houssier, 1991, J. Biomol. Struct. Dyn. **9**, 159.
Marx, K. A., and G. C. Ruben, 1983, Nucleic Acids Res. **11**, 1839.
Mason, J. M., and K. M. Arndt, 2004, ChemBioChem **5**, 170.
Matulis, D., I. Rouzina, and V. A. Bloomfield, 2000, J. Mol. Biol. **296**, 1053.
McFail-Isom, L., X. Q. Shui, and L. D. Williams, 1998, Biochemistry **37**, 17105.
McFail-Isom, L., C. C. Sines, and L. D. Williams, 1999, Curr. Opin. Struct. Biol. **9**, 298.
Medina-Noyola, M., and D. A. McQuarrie, 1980, J. Chem. Phys. **73**, 6279.
Medvedev, I. G., 2004, Electrochim. Acta **49**, 207.
Mertz, E. L., 2005, J. Phys. Chem. A **109**, 44.
Mertz, E. L., and L. I. Krishtalik, 2000, Proc. Natl. Acad. Sci. U.S.A. **97**, 2081.
Millar, D. P., R. J. Robbins, and A. H. Zewail, 1980, Proc. Natl. Acad. Sci. U.S.A. **77**, 5593.
Minasov, G., V. Tereshko, and M. Egli, 1999, J. Mol. Biol. **291**, 83.
Misof, K., G. Rapp, and P. Fratzl, 1997, Biophys. J. **72**, 1376.
Misra, V. K., J. L. Hecht, A. S. Yang, and B. Honig, 1998, Biophys. J. **75**, 2262.
Mohammad-Rafiee, F., and R. Golestanian, 2004, Phys. Rev. E **69**, 061919.
Moldrheim, E., B. Anderson, N. A. Froystein, and E. Sletten, 1998, Inorg. Chim. Acta **273**, 41.
Moreira, A. G., and R. R. Netz, 2001, Phys. Rev. Lett. **87**, 078301.
Moreira, A. G., and R. R. Netz, 2002, Europhys. Lett. **57**, 911.
Moroz, J. D., and P. Nelson, 1998, Macromolecules **31**, 6333.
Mu, X.-Q., L. Makowski, and B. M. Fairchild, 1997, Acta Crystallogr., Sect. A: Found. Crystallogr. **53**, 55.
Murray, D., A. Arbuzova, G. Hangyas-Mihalyne, A. Gambhir, N. Ben-Tal, B. Honig, and S. McLaughlin, 1999, Biophys. J. **77**, 3176.
Naji, A., A. Arnold, C. Holm, and R. R. Netz, 2004, Europhys. Lett. **67**, 130.
Naji, A., S. Jungblut, A. G. Moreira, and R. R. Netz, 2005, Physica A **352**, 131.
Naji, A., and R. R. Netz, 2004, Eur. Phys. J. E **13**, 43.
Nelson, P., 1998, Phys. Rev. Lett. **80**, 5810.
Netz, R. R., and H. Orland, 2000, Eur. Phys. J. E **1**, 203.
Nguyen, T. T., A. Y. Grosberg, and B. I. Shklovskii, 2000a, J. Chem. Phys. **113**, 1110.
Nguyen, T. T., A. Y. Grosberg, and B. I. Shklovskii, 2000b, Phys. Rev. Lett. **85**, 1568.
Nguyen, T. T., I. Rouzina, and B. I. Shklovskii, 2000c, J. Chem. Phys. **112**, 2562.
Odijk, T., 1977, J. Polym. Sci., Polym. Phys. Ed. **15**, 477.
Odijk, T., 1993, Biophys. Chem. **46**, 69.
Odijk, T., 1995, Macromolecules **28**, 7016.
O'Hern, C. S., R. D. Kamien, T. C. Lubensky, and P. Nelson, 1998, Eur. Phys. J. B **1**, 95.
Oldman, K. B., and J. C. Myland, 1994, *Fundamentals of Electrochemical Science* (Academic, San Diego).

Olson, W. K., A. A. Gorin, X.-J. Lu, L. M. Hock, and V. B. Zhurkin, 1998, Proc. Natl. Acad. Sci. U.S.A. **95**, 11163.
Olson, W. K., N. L. Marky, R. L. Jernigan, and V. B. Zhurkin, 1993, J. Mol. Biol. **232**, 530.
Olson, W. K., and V. B. Zhurkin, 2000, Curr. Opin. Struct. Biol. **10**, 286.
Onsager, L., 1933, Chem. Rev. (Washington, D.C.) **13**, 73.
Onsager, L., 1949, Ann. N.Y. Acad. Sci. **51**, 627.
Oosawa, F., 1968, Biopolymers **6**, 134.
Oosawa, F., 1971, *Polyelectrolytes* (Dekker, New York).
Ouameur, A. A., and H. A. Tajmir-Riahi, 2004, J. Biol. Chem. **279**, 42041.
Overbeek, J. Th. G., 1956, Prog. Biophys. Biophys. Chem. **6**, 57.
Parsegian, V. A., 2005, *Van der Waals Forces, A Handbook for Biologists, Chemists, Engineers, and Physicists* (Cambridge University, New York).
Parsegian, V. A., R. P. Rand, N. L. Fuller, and D. C. Rau, 1986, Methods Enzymol. **127**, 400.
Parsegian, V. A., R. P. Rand, and D. C. Rau, 1987, in *Physics of Complex and Supermolecular Fluids*, edited by S. A. Safran and N. A. Clark (Wiley, New York), pp. 115–135.
Pauling, L., and R. B. Corey, 1951, Proc. Natl. Acad. Sci. U.S.A. **37**, 235.
Pelta, J., D. Durand, J. Doucet, and F. Livolant, 1996, Biophys. J. **71**, 48.
Pelta, J., F. Livolant, and J. L. Sikorav, 1996, J. Biol. Chem. **271**, 5656.
Perkins, T. T., D. E. Smith, R. G. Larson, and S. Chu, 1995, Science **268**, 83.
Podgornik, R., P. L. Hansen, and V. A. Parsegian, 2000, J. Chem. Phys. **113**, 9343.
Podgornik, R., and V. A. Parsegian, 1990, Macromolecules **23**, 2265.
Podgornik, R., D. C. Rau, and V. A. Parsegian, 1989, Macromolecules **22**, 1780.
Podgornik, R., D. C. Rau, and V. A. Parsegian, 1994, Biophys. J. **66**, 962.
Podgornik, R., H. H. Strey, K. Gawrisch, D. C. Rau, A. Rupprecht, and V. A. Parsegian, 1996, Proc. Natl. Acad. Sci. U.S.A. **93**, 4261.
Raspaud, E., I. Chaperon, A. Leforestier, and F. Livolant, 1999, Biophys. J. **77**, 1547.
Raspaud, E., D. Durand, and F. Livolant, 2005, Biophys. J. **88**, 392.
Raspaud, E., M. Olvera de la Cruz, J. L. Sikorav, and F. Livolant, 1998, Biophys. J. **74**, 381.
Rau, D. C., B. Lee, and V. A. Parsegian, 1984, Proc. Natl. Acad. Sci. U.S.A. **81**, 2621.
Rau, D. C., and V. A. Parsegian, 1990, Science **249**, 1278.
Rau, D. C., and V. A. Parsegian, 1992a, Biophys. J. **61**, 246.
Rau, D. C., and V. A. Parsegian, 1992b, Biophys. J. **61**, 260.
Rey, S., and J. H. Maddocks, 2000, in *Proceedings of the 16th IMACS World Congress 2000, Lausanne, Switzerland*, edited by M. Deville and R. Owens (IMACS, Lausanne).
Rhodes, D., and A. Klug, 1980, Nature (London) **286**, 573.
Rill, R. L., 1986, Proc. Natl. Acad. Sci. U.S.A. **83**, 342.
Rill, R. L., P. R. Hilliard, Jr., and G. C. Levy, 1983, J. Mol. Biol. **258**, 250.
Robinson, C., 1961, Tetrahedron **13**, 219.
Rouzina, I., and V. A. Bloomfield, 1996, J. Phys. Chem. **100**, 9977.
Royal Society Discussion, 2004, Philos. Trans. R. Soc. London, Ser. B **359**, 3.
Rozenberg, H., D. Rabinovich, F. Frolow, R. S. Hegde, and Z. Shakked, 1998, Proc. Natl. Acad. Sci. U.S.A. **95**, 15194.
Rubnitz, J., and S. Subramani, 1984, Mol. Cell. Biol. **4**, 2253.
Rudd, L., D. J. Lee, and A. A. Kornyshev, 2006, Phys. Chem. Chem. Phys. **8**, 4347.
Rudd, L., D. J. Lee, and A. A. Kornyshev, 2007, J. Phys.: Condens. Matter (to be published.
Rueda, M., E. Cubero, C. A. Laughton, and M. Orzco, 2004, Biophys. J. **87**, 800.
Ruff, I., and J. Liszi, 1985, in *The Chemical Physics of Solvation*, edited by R. R. Dogonadze, E. Kalman., A. A. Kornyshev, and J. Ulstrup (Elsevier, Amsterdam), Pt. A, p. 119.
Ruiz-Chica, J., M. A. Medina, F. Sánchez-Jiménez, and F. J. Ramirez, 2001a, Biophys. J. **80**, 443.
Ruiz-Chica, J., M. A. Medina, F. Sánchez-Jiménez, and F. J. Ramirez, 2001b, Biochem. Biophys. Res. Commun. **285**, 437.
Rupprecht, A., J. Piskur, J. Schultz, L. Nordenskiold, Z. Y. Song, and G. Lahajnar, 1994, Biopolymers **34**, 897.
Saenger, W., 1984, *Principles of Nucleic Acid Structure* (Springer-Verlag, New York).
Saminathan, M., T. Antony, A. Shirahata, L. H. Sigal, T. Thomas, and T. J. Thomas, 1999, Biochemistry **38**, 3821.
Schellman, J. A., and N. Parthasarathy, 1984, J. Mol. Biol. **175**, 313.
Schlick, T., 1995, Curr. Opin. Struct. Biol. **5**, 245.
Schmickler, W., 1996, *Interfacial Electochemistry* (Oxford University, New York).
Schnur, J. M., 1993, Science **262**, 1669.
Selinger, J. V., and R. F. Bruinsma, 1991, Phys. Rev. A **43**, 2922.
Selinger, J. V., F. C. MacKintosh, and J. M. Schnur, 1996, Phys. Rev. E **53**, 3804.
Sharp, K. A., and B. Honig, 1990, Annu. Rev. Biophys. Biophys. Chem. **19**, 301.
Shen, P., and H. V. Huang, 1986, Genetics **112**, 441.
Shklovskii, B. I., 1999a, Phys. Rev. Lett. **82**, 3268.
Shklovskii, B. I., 1999b, Phys. Rev. E **60**, 5802.
Shore, D., and R. L. Baldwin, 1983, J. Mol. Biol. **170**, 983.
Shui, X. Q., L. McFail-Isom, G. G. Hu, and L. D. Williams, 1998, Biochemistry **37**, 8341.
Shui, X. Q., C. C. Sines, L. McFail-Isom, D. VanDerveer, and L. D. Williams, 1998, Biochemistry **37**, 16887.
Sikorav, J. L., and G. M. Church, 1991, J. Mol. Biol. **222**, 1085.
Sikorav, J. L., J. Pelta, and F. Livolant, 1994, Biophys. J. **67**, 1387.
Singer, B. S., L. Gold, P. Gauss, and D. H. Doherty, 1982, Cell **31**, 25.
Sitko, J. C., E. M. Mateescu, and H. G. Hansma, 2003, Biophys. J. **84**, 419.
Skolnick, J., and M. Fixman, 1977, Macromolecules **10**, 945.
Smith, B., Y. V. Zastavker, and G. B. Benedek, 2001, Phys. Rev. Lett. **87**, 278101.
Smith, S. B., Y. J. Cui, and C. Bustamante, 1996, Science **271**, 5250.
Smith, S. B., Y. J. Cui, and C. Bustamante, 2003, Methods Enzymol. **361**, 134.
Smith, S. B., L. Finzi, and C. Bustamante, 1992, Science **258**, 1122.
Solis, F. J., and M. O. de la Cruz, 1999, Phys. Rev. E **60**, 4496.
Soumpasis, D., 1978, J. Chem. Phys. **69**, 3190.
Stanley, C. B., H. Hong, and H. H. Strey, 2005, Biophys. J. **89**, 2552.
Stanley, H. E., S. V. Buldyrev, A. L. Goldberger, S. Havlin, C.

K. Peng, and M. Simons, 1999, Physica A **273**, 1.
Stellwagen, N. C., S. Magnusdottir, C. Gelfi, and P. G. Righetti, 2001, J. Mol. Biol. **305**, 1025.
Stevens, M. J., 1995, J. Chem. Phys. **103**, 1669.
Stevens, M. J., 1999, Phys. Rev. Lett. **82**, 101.
Stevens, M. J., 2001, Biophys. J. **80**, 130.
Straley, J. P., 1976, Phys. Rev. A **14**, 1835.
Strey, H. H., V. A. Parsegian, and R. Podgornik, 1997, Phys. Rev. Lett. **78**, 895.
Strey, H. H., V. A. Parsegian, and R. Podgornik, 1999, Phys. Rev. E **59**, 999.
Strey, H. H., J. Wang, R. Podgornik, A. Rupprecht, L. Yu, V. A. Parsegian, and E. B. Sirota, 2000, Phys. Rev. Lett. **84**, 3105.
Strick, T. R., D. Bensimon, and V. Croquette, 1999, Genetica (The Hague, Neth.) **106**, 57.
Strogatz, H. S., 1994, *Nonlinear Dynamics and Chaos: with Applications to Physics, Biology, Chemistry and Engineering* (Addison-Wesley, Reading, MA).
Strzelecka, T. E., M. W. Davidson, and R. L. Rill, 1988, Nature (London) **331**, 457.
Strzelecka, T. E., and R. L. Rill, 1990, Biopolymers **30**, 57.
Tanaka, F., and H. Takahashi, 1985, J. Chem. Phys. **83**, 6017.
Taylor, W. H., and P. J. Hagerman, 1990, J. Mol. Biol. **212**, 363.
Tereshko, V., G. Minasov, and M. Egli, 1999, J. Am. Chem. Soc. **121**, 470.
Todd, B. A., V. A. Parsegian, A. Shirahata, T. J. Thomas, and D. C. Rau, 2007, unpublished.
Toulouse, G., 1977, Commun. Phys. (London) **2**, 115.
Tracy, C. A., and H. Widom, 1997, Physica A **244**, 402.
Travers, A. A., 2004, Philos. Trans. R. Soc. London, Ser. A **362**, 1423.
Trifonov, E. N., R. K.-Z. Tan, and S. C. Harvey, 1987, in *DNA Bending and Curvature*, edited by W. K. Olson, M. H. Sarma and M. Sundaralingam (Adenine, Schenectady, NY), p. 243.
Tsuru, H., and M. Wadati, 1986, Macromolecules **25**, 2083.
Ubbink, J., and T. Odijk, 1995, Biophys. J. **68**, 54.
Vaillant, C., B. Audit, C. Thermes, and A. Arneodo, 2003, Phys. Rev. E **67**, 032901.
Vainshtein, B. K., 1966, *Diffraction of X-rays by Chain Molecules* (Elsevier, Amsterdam).
Van der Meer, B. W., G. Vertogen, A. J. Dekker, and J. G. J. Ypma, 1976, J. Chem. Phys. **65**, 3935.
van Roij, R., and J. P. Hansen, 1999a, Phys. Rev. Lett. **79**, 3082.
van Roij, R., and J. P. Hansen, 1999b, Phys. Rev. E **59**, 2010.
van Steenwinkel, R., F. Campagnari, and M. Merlini, 1981, Biopolymers **20**, 915.
Van Winkle, D. H., M. V. Davidson, W.-X. Chen, and R. L. Rill, 1990, Macromolecules **23**, 4140.
Verwey, E. J. W., and J. T. Overbeek, 1948, *Theory of the Stability of Lyophobic Colloids* (Elsevier, Amsterdam).
Vijayanathan, V., T. Thomas, A. Shirahata, and T. J. Thomas, 2001, Biochemistry **40**, 13644.
Voet, D., J. G. Voet, and J. G., 1995, *Biochemistry*, 2nd ed. (Wiley, New York).
Volkov, A. G., D. W. Deamer, D. L. Tanelian, and V. S. Markin, 1998, *Liquid Interfaces in Chemistry and Biology* (Wiley, New York).
Vologodskii, A. V., and N. R. Cozzarelli, 1994, Annu. Rev. Biophys. Biomol. Struct. **23**, 609.
Wagner, K., E. Keyes, T. W. Kephart, and G. Edwards, 1997, Biophys. J. **73**, 21.
Wang, J. C., 1979, Proc. Natl. Acad. Sci. U.S.A. **76**, 200.
Watson, J. D., and F. H. C. Crick, 1953, Nature (London) **171**, 737.
Watt, V. M., C. J. Ingles, M. S. Urdea, and W. J. Rutter, 1985, Proc. Natl. Acad. Sci. U.S.A. **82**, 4768.
Weiner, B. M., and N. Kleckner, 1994, Cell **77**, 977.
Wenner, J. R., M. C. Williams, I. Rouzina, and V. A. Bloomfield, 2002, Biophys. J. **82**, 3160.
Wennerström, H., B. Jönsson, and P. Linse, 1982, J. Chem. Phys. **76**, 4665.
Widom, J., and R. L. Baldwin, 1980, J. Mol. Biol. **144**, 431.
Widom, J., and R. L. Baldwin, 1983, Biopolymers **22**, 1595.
Wilkins, M. H. F., A. R. Stokes, and H. R. Wilson, 1953, Nature (London) **171**, 738.
Wilson, R. W., and V. A. Bloomfield, 1979, Biochemistry **18**, 2192.
Woods, K. K., L. McFail-Isom, C. C. Sines, S. B. Howerton, R. K. Stephens, and L. D. Williams, 2000, J. Am. Chem. Soc. **122**, 1546.
Wynveen, A., D. J. Lee, and A. A. Kornyshev, 2005, Eur. Phys. J. E **16**, 303.
Yang, A. S., M. R. Gunner, R. Sampogna, K. Sharp, and B. Honig, 1993, Proteins: Struct., Funct., Genet. **15**, 252.
Yang, J., and D. C. Rau, 2005, Biophys. J. **89**, 1932.
Yang, L., and B. M. Pettit, 1995, J. Phys. Chem. **100**, 2564.
Young, M. A., B. Jayaram, and D. L. Beveridge, 1998, J. Phys. Chem. B **102**, 7666.
Zastavker, Y. V., N. Asherie, A. Lomakin, J. Pande, J. M. Donovan, J. M. Schnur, and G. B. Benedek, 1999, Proc. Natl. Acad. Sci. U.S.A. **96**, 7883.
Zastavker, Y. V., B. S. Tilley, and J. C. Pratt, 2005, in *Women in Physics: 2nd IUPAP International Conference on Women in Physics*, AIP Conference Proceedings No. 795, edited by B. K. Hartline and A. Michelman-Ribeiro (AIP, Melville, NY), p. 206.
Zimm, B. H., and M. LeBret, 1983, J. Biomol. Struct. Dyn. **1**, 461.
Zimmerman, S. B., and B. H. Pheiffer, 1979, Proc. Natl. Acad. Sci. U.S.A. **76**, 2703.
Zinchenko, A. A., V. G. Sergeyev, K. Yamabe, S. Murata, and K. Yoshikawa, 2004, ChemBioChem **5**, 360.
Zuccheri, G., A. Scipioni, V. Cavaliere, G. Gargiulo, P. De Santis, and B. Samori, 2001, Proc. Natl. Acad. Sci. U.S.A. **98**, 3074.
See EPAPS Document No. E-RMPHAT-79-010702 for additional derivations and formulas. For more information on EPAPS, see http://www.aip.org/pubservs/epaps.html.